Doctoral Thesis

Asha Kiran Maddali

University of Szeged

Doctoral School of Biology

"Lipids of autophagic membranes and their role in the recruitment of Syntaxin 17 to the autophagosomes"

PhD Thesis

Maddali Asha Kiran

Supervisor: Dr. Laczkó-Dobos Hajnalka

Doctoral School of Biology

HUN-REN Biological Research Centre, Szeged

Institute of Genetics

University of Szeged

Faculty of Natural Sciences and Informatics

Szeged

2024

Table of Contents

List of Abbreviations

ACR: Autophagic components recycling

AFM: Atomic Force Microscopy

ALR: Autophagic lysosome reformation

ATG proteins: Autophagy-related proteins

BECN1: Beclin1

BHT: Butylated hydroxytoluene

CMA: Chaperone-mediated autophagy

Drosophila: *Drosophila melanogaster*

DLS: Dynamic light scattering

DMEM: Dulbecco's modified eagle's medium

DTT: Dithiothreitol

E. coli: *Escherichia coli*

EDTA: Ethylenediamine tetraacetic acid

EPG5: Ectopic P-granules autophagy protein 5 homolog

ER: Endoplasmic reticulum

ESCRT: Endosomal sorting complex required for transport complex

FWD primer: Forward primer

GABARAP: Gamma-aminobutyric acid receptor-associated protein

GABARAPL2: Gamma-aminobutyric acid receptor-associated protein like 2

GFP: Green fluorescent protein

GUV: Giant unilamellar vesicle

HBSS: Hank's Balanced Salt Solution

HEK-293: Human Embryonic Kidney cells

HEPES: 4-(2-hydroxyethyl)-1-piperazineethanesulfonic acid

HOPS complex: Homotypic fusion and protein sorting complex

IRGM: Immunity-related GTPase family M protein

LC3: Light chain 3

LIR: LC3 interacting region

LUV: Large unilamellar vesicle

MAM: Mitochondria-associated membranes

mTORC1: mechanistic target of rapamycin complex 1

NRBF2: Nuclear receptor binding factor 2

PA: Phosphatidic acid

PAGE: Polyacrylamide gel electrophoresis

PBS: Phosphate buffered saline

PC: Phosphatidylcholine

PCR: Polymerase chain reaction

PE: Phosphatidylethanolamine

PIPs: Phosphatidylinositol phosphates

PI(3)P: Phosphatidylinositol 3-phosphate

$PI(3,5)P_2$: Phosphatidylinositol 3,5-bisphosphate

PI(4)P: Phosphatidylinositol 4-phosphate

PI: Phosphatidylinositol

PI3KC: PI3-kinase complex

PI3KC3-C1: Class III phosphatidylinositol 3-kinase complex1

PI4K2A: PI 4-phosphate kinase type II α

PKA: Protein kinase A

PLEKHM1: Pleckstrin homology domain-containing family member 1

PMSF: Phenylmethylsulfonyl fluoride

PS: Phosphatidylserine

REV primer: Reverse primer

RFP: Red fluorescent protein

R/K>A: Arginine and lysine replaced with an alanine residue

RT: Room temperature

SDS: Sodium dodecyl sulfate

SNARE: Soluble N-ethyl maleimide-sensitive factor attachment protein receptor

STX17: Human Syntaxin 17

SUV: Small unilamellar vesicle

Syx17: *Drosophila* Syntaxin 17

TMD: Transmembrane domains

TMEM41B: Transmembrane protein 41B

U2OS: Human osteosarcoma cells

ULK1: Unc-51-like kinase complex1

VAMP7/8: Vesicle-associated membrane protein7/8

VMP1: Vacuole membrane protein1

WIPI proteins: WD-repeat protein interacting with phosphoinositides

1. INTRODUCTION

1.1 Autophagy

The term "Autophagy" was coined by Christian De Duve, a Belgian cytologist and biochemist in 1963. Autophagy is a natural and comprehensive degradation process that is conserved among eukaryotes. It helps to dispose of obsolete cytoplasmic components such as damaged organelles, aggregated proteins, lipids, invading bacteria etc. to lysosomes to form autolysosomes or to endosomes to form the amphisomes. Eventually, the amphisomes fuse with lysosomes for their degradation and recycling processes (Juhasz & Neufeld, 2006; Nezis et al., 2014). This pathway acts as a survival mechanism, particularly at the times of cellular stress, such as nutrient deprivation, oxidative stress, or infection. By recycling cellular components, autophagy provides the necessary building blocks and energy to sustain cellular functions during periods of limited resources. The autophagy pathway is not only essential for cellular survival but also plays a role in various physiological processes, including cellular homeostasis, development, immunity, and aging. Misregulation of autophagy has been implicated in various diseases, such as neurodegenerative disorders, cancer, and metabolic conditions (Takáts & Juhász, 2013; Katheder et al., 2017; Bhattacharjee et al., 2019). Therefore, understanding the molecular mechanisms that govern autophagy has become vital in biomedical research, with the hope of developing therapeutic interventions that can modulate autophagy for the treatment of various diseases.

1.1.1. Types of Autophagy

Autophagy is divided into three types based on the mechanism of delivering cargo to lysosomes. They are i) microautophagy ii) chaperone-mediated autophagy (CMA), and iii) macroautophagy (Mizushima, 2007) (Fig. 1).

1.1.1.1 Microautophagy

Microautophagy involves direct membrane invagination, where the cytoplasmic entities destined for the degradation are taken up by the late endosomes or lysosomes (in *Drosophila* or mammals) or by the vacuoles (in plants or yeast) (Wang et al, 2023) (Fig. 1).

1.1.1.2 Chaperone-mediated autophagy

The process of CMA does not involve vesicles or direct membrane invaginations. Instead, it uses a "protein translocation complex" to carry cytosolic proteins to the lysosomal lumen for

degradation (Galluzzi et al., 2017). Specific proteins bearing a targeting motif, the KFERQ-like motif, are identified by chaperone proteins and delivered to lysosomes. The chaperone proteins guide the unfolded substrate proteins across the lysosomal lumen and are degraded by lysosomal enzymes (Fig. 1).

1.1.1.3 *Macroautophagy*

Macroautophagy is mediated by the *de novo* formation of unique double membrane organelles called "autophagosomes" that engulf the portion of cytoplasm cargo and deliver to lysosomes for degradation (Lőrincz & Juhász, 2020). Macroautophagy is categorized into non-selective (involves during starvation conditions) and selective (involves during fed conditions) types of autophagy (Martens *et al*., 2020) (Fig. 1).

1.1.1.3.1 Non-selective autophagy

When the cell is experiencing a nutrient deficiency, a process called non-selective autophagy is triggered. This process is known as the bulk degradation selective process involves randomly engulfing cytoplasmic components into autophagosomes, which are then delivered to the lysosomes for degradation to generate recycling building blocks, which serve as a survival mechanism for the cell (Susmita Kaushik et al., 2021) (Fig. 1).

1.1.1.3.2 Selective autophagy

During nutrient-rich conditions, the cell targets specific cargo such as damaged mitochondria, excess peroxisomes and aggregated proteins for lysosomal degradation to maintain cellular homeostasis (Susmita Kaushik et al., 2021) (Fig. 1). Selective autophagy plays a vital role in this process by recognizing specific cargo via autophagy receptors or adaptor proteins. These receptors facilitate the interaction between the cargo and autophagic machinery to selectively engulf and degrade the targeted material. The process is tightly regulated and varies depending on the cellular components to be eliminated.

Some examples of selective autophagy include: Mitophagy, a process that removes only damaged or dysfunctional mitochondria from cells. This process is essential to maintain cellular energy balance and prevent the release of harmful molecules. Pexophagy is another process that degrades peroxisomes, organelles that are involved in lipid metabolism and detoxification. This process is necessary to prevent the accumulation of damaged peroxisomes. Ribophagy is the process of degrading ribosomal components and recycling them for the synthesis of new proteins. Lipophagy

is a pathway that breaks down lipid droplets and releases fatty acids for energy production and metabolic processes. Nucleophagy involves sequestering and degrading nuclear material, which contributes to nuclear quality control. ER-phagy is a pathway that removes portions of the endoplasmic reticulum to maintain ER homeostasis in response to ER stress. Aggrephagy is the process of degrading misfolded or aggregated proteins to maintain protein quality control. Finally, Virophagy is a process that captures and degrades viral material, providing a defence mechanism against viral infections (Susmita Kaushik et al., 2021).

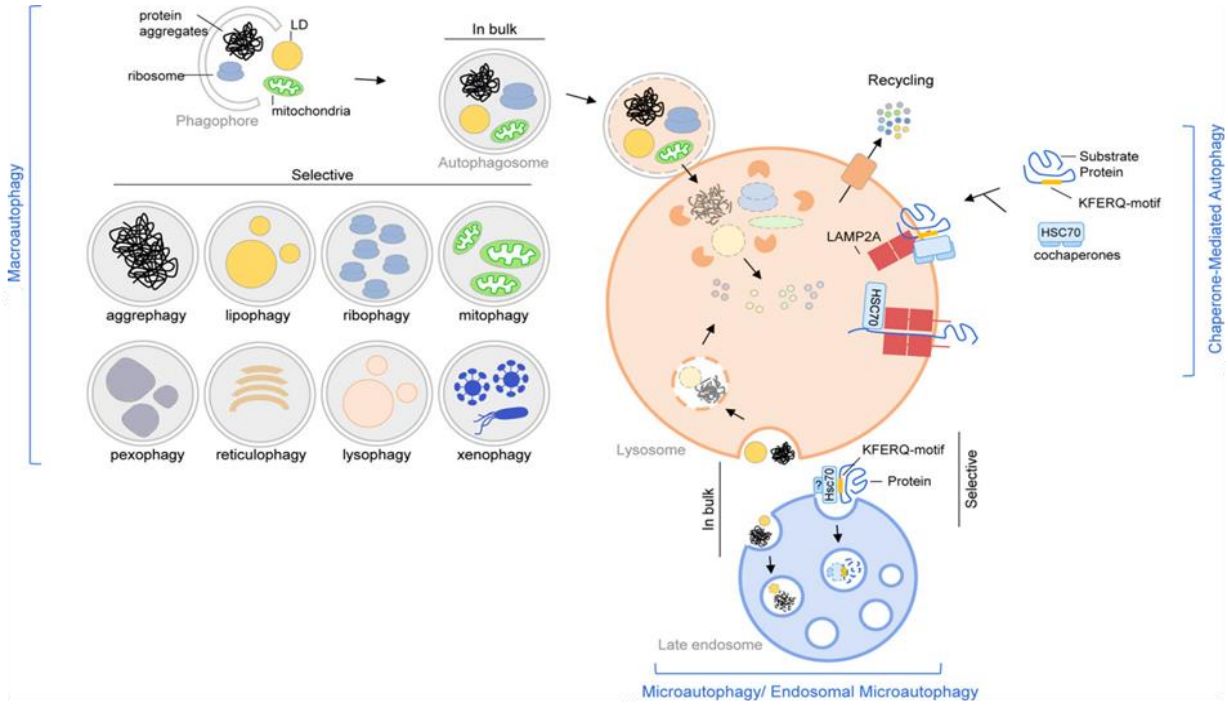

Figure 1: Various types of autophagy pathways.
The figure illustrates the 3 major types of autophagy based on the mechanism of cargo delivery to the lysosomes. i) Macroautophagy involves the sequestration of cargo inside double-membrane vesicles. ii) Microautophagy involves the direct engulfment of cytoplasmic cargo by lysosomal or endosomal membranes. These membrane protrusions pinch off as vesicles into the lysosomal lumen and eventually degrade by lysosomal hydrolases. iii) CMA involves the degradation of proteins containing the target motif by chaperons (Susmita Kaushik et al., 2021).

This study, mainly focused on 'Macroautophagy' (hereafter mentioned as only autophagy). Briefly, the pathway includes five steps— initiation, elongation, maturation, fusion and degradation. This pathway initiates with the nucleation of a cup-shaped isolation membrane surrounding cytoplasmic cargo called "phagophore", eventually, it can mature into a double membrane layered vesicle called an "autophagosome". As the final step the outer autophagosomal membranes fuse with the lysosome to form "autolysosomes" for the sequestered cargo degradation

by lysosomal acidic hydrolases (Lőrincz et al., 2017) (Fig. 2). This pathway relies on membrane surrounded organelles. Unlike other organelle membranes, autophagic structures are composed of more lipids and a few membrane proteins (Schütter et al, 2019; Schmitt et al, 2022). In mammals, the autophagosomes are formed throughout the cytoplasm. The membrane donor for the nucleation of phagophores is still under debate. However, based on the literature various sources are the following — endoplasmic reticulum (ER), the Golgi, mitochondria, plasma membrane, lipid droplets, and endosomes are suggested to dispense the lipids to isolation membrane (Axe et al., 2008; Hailey et al., 2010; Longatti & Tooze, 2012; Velázquez et al., 2016; Fernandez et al., 2017).

1.2 Initiation of autophagy

In mammalian cells, starvation-induced autophagy showed that the isolation membrane for phagophore nucleation is grown close to or at the ER domain (Hayashi-Nishino et al., 2009; Ylä-Anttila et al., 2009; Velázquez et al., 2016). The complete molecular mechanism underlying autophagosome formation still remains elusive. The initial steps of autophagosome biogenesis and formation are determined by three major complexes such as Unc-51-like kinase complex1 (ULK), Class III phosphatidylinositol 3-kinase complex1 (PI3KC3-C1), and ATG16L1–ATG5–ATG12 (Zhen & Stenmark, 2023). ULK complex, the central regulator during the autophagy initiation, is composed of FIP200, ATG13, ATG101, and the serine/threonine kinases ULK1 or ULK2. This complex is regulated by the mechanistic target of rapamycin complex 1 (mTORC1). Upon starvation, mTORC1 is inactivated and leads to the activation and assembly of the ULK complex at the ER premises where the downstream ATG proteins such as ATG9 vesicles are recruited and become seeds for the autophagosome formation (Yamamoto et al., 2023) (Fig. 2).

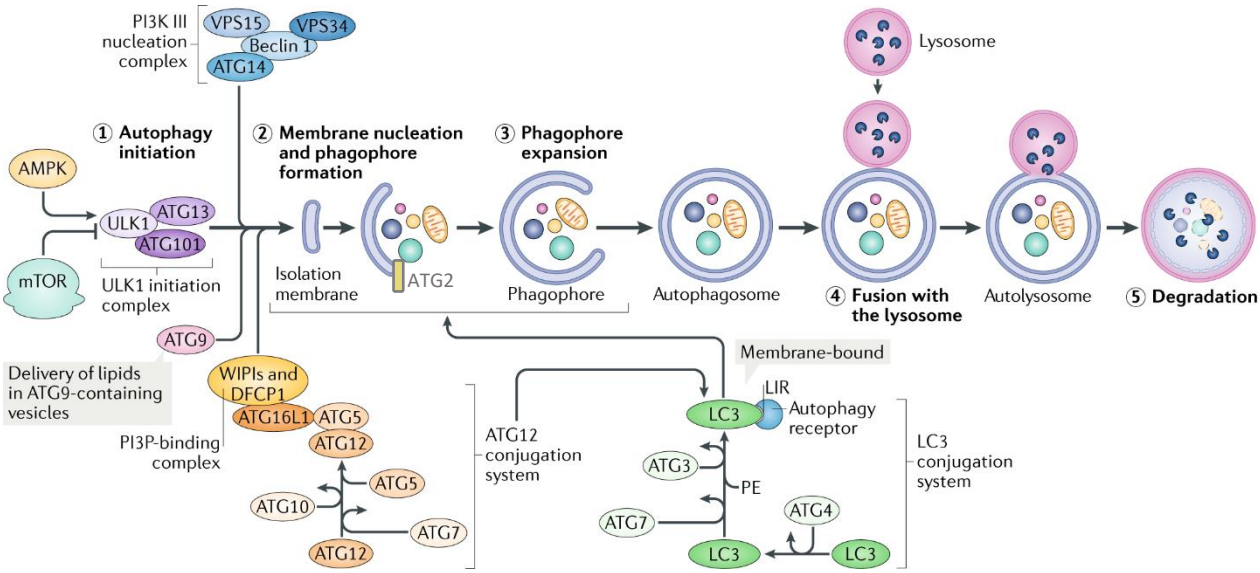

Figure 2: Autophagy pathways with involved regulatory machinery.
A schematic illustration that shows the main pathway and key regulatory machinery of autophagy. The main regulators, mTOR acts as an inhibitor and AMPK acts as an activator, consist of the formation of a cup-shaped phagophore that engulfs cytoplasmic material, sequestering it into double-membrane autophagosomes that fuse with lysosomes to form autolysosomes. The steps involved in the autophagy pathway are (1) initiation, (2) membrane nucleation and phagophore formation, (3) phagophore expansion, (4) fusion with the lysosome, and (5) degradation. The multi-step process of autophagy is governed by autophagy-related proteins (Hansen et al., 2018).

1.3 Membrane elongation

The ULK complex further recruits Class III PI3KC3–C1 to generate Phosphatidylinositol 3-phosphate (PI(3)P) on autophagic membranes. The PI3KC3–C1 is mainly a scaffold of five subunits such as VPS34, VPS15, Beclin1 (BECN1), ATG14, and nuclear receptor binding factor 2 (NRBF2). This complex binds to the membrane through ATG14, BECN1, and VPS34, after which VPS34 generates PI(3)P (Fig. 2) (Baskaran et al., 2014; Hurley & Young, 2017). PI(3)P binding proteins such as WD-repeat protein interacting with phosphoinositides proteins (WIPI) specifically WIPI2 recruit the ATG12–ATG5–ATG16L1 complex to promote LC3 lipidation (LC3-PE) on the phagophore membrane (Fig. 2) (Dooley et al., 2014). LC3 can further recruit ATG2. ATG2 functions as a lipid transfer protein and forms a rod-shaped structure by tether between ER with its N-terminal structure and autophagic membrane with its C-terminal tip to channel the phospholipids along with ATG9, vacuole membrane protein1 (VMP1), and transmembrane protein 41B (TMEM41B) for the phagophore membrane elongation (Fig. 3) (Zheng et al., 2017; Chowdhury et al., 2018; Maeda et al., 2019; Osawa et al., 2019; Valverde et

al., 2019). After ATG2 transfers phospholipids to the outer leaflet of the phagophore, ATG9 scrambles them to the inner leaflet (Ghanbarpour et al., 2021; Maeda et al., 2020; Matoba et al., 2020) (Fig. 3).

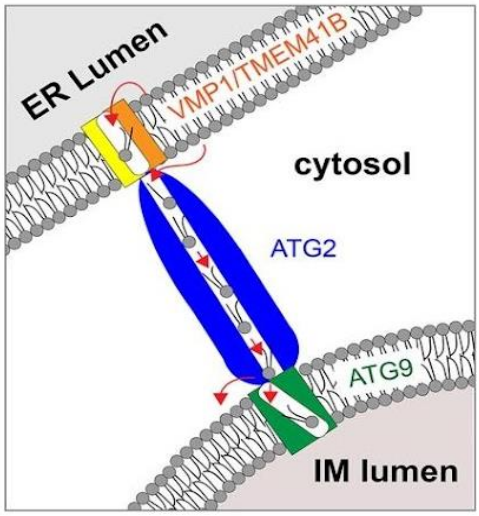

Figure 3: A model for ATG2 mediated lipid transport.
A model for ATG2, a lipid transporter protein transfers the lipids with the coordination of scramblase complex VMP1/TMEM41B at the ER lumen and the other side with the ATG9A in the nascent autophagosome for the elongation during autophagy (Ghanbarpour et al., 2021).

1.4 Autophagosome closure

Closure of autophagosomes is indeed an essential step that is topologically identical to membrane scission of the intraluminal vesicle in multi-vesicular bodies and virus budding formation at the plasma membrane. The Endosomal sorting complex required for transport complex (ESCRT complex) is essential for the scission of the autophagosome membrane, similar to the two processes mentioned above. (Takahashi et al., 2018; Zhou et al., 2019; Zhen et al., 2020). But how this complex is recruited to the open rim of the phagophore remains elusive.

1.5 Autophagosome-lysosome fusion

As the final step, the matured, closed autophagosome fuses with the lysosome to form an "autolysosome". In general, specific membrane fusion events are mediated by soluble N-ethyl maleimide-sensitive factor attachment protein receptor (SNARE) proteins thus forming a parallel four-helix bundle (containing Qa-, Qb-, Qc-, and R-SNAREs) to bridge two membranes (Hegedus et al., 2013). The fusion step is driven mainly by SNARE proteins namely, autophagosomal SNAREs – Syntaxin 17 (STX17 (human) /Syx17 (*Drosophila*)) and/or YKT6, cytosolic SNARE–

SNAP29, and lysosomal SNARE–VAMP7/VAMP8 (Vesicle-associated membrane protein7/8) (Itakura et al., 2012; Matsui et al., 2018) and by multiple tethering factors such as homotypic fusion and protein sorting complex (HOPS), pleckstrin homology domain-containing family member 1 (PLEKHM1), and Ectopic P-granules autophagy protein 5 homolog (EPG5) (Y. G. Zhao & Zhang, 2019). The functional differences between Syntaxin 17 and YKT6 are not well understood. Either of them, predominantly Syntaxin 17 recruits particularly to fully matured or closed autophagosomes but not to the phagophores thereby preventing premature autophagosome-lysosome fusion (Itakura et al., 2012). Along with the co-ordination of tethering factors, the YKT6 or STX17 (Qa-SNARE) form SNARE bundles with SNAP29 (Qbc-SNARE) and VAMP7/VAMP8 (R-SNARE) respectively for the successful membrane fusion (Hegedus et al., 2013; Takáts et al., 2013, 2014; Li et al., 2020) (Fig. 4). It is known that after fusion, lysosomal acidic hydrolases only degrade the inner autophagosomal membrane and its contents, but not the outer bilayer. This remains a mystery, even though both the inner and outer membranes originate from the same phagophore (C. Zhou et al., 2022). The membranes of autolysosomes contain components from lysosomes and autophagosomes and they are recycled through autophagic lysosome reformation (ALR) (L. Yu et al., 2018) and autophagosomal components recycling (ACR) (C. Zhou et al., 2022) respectively.

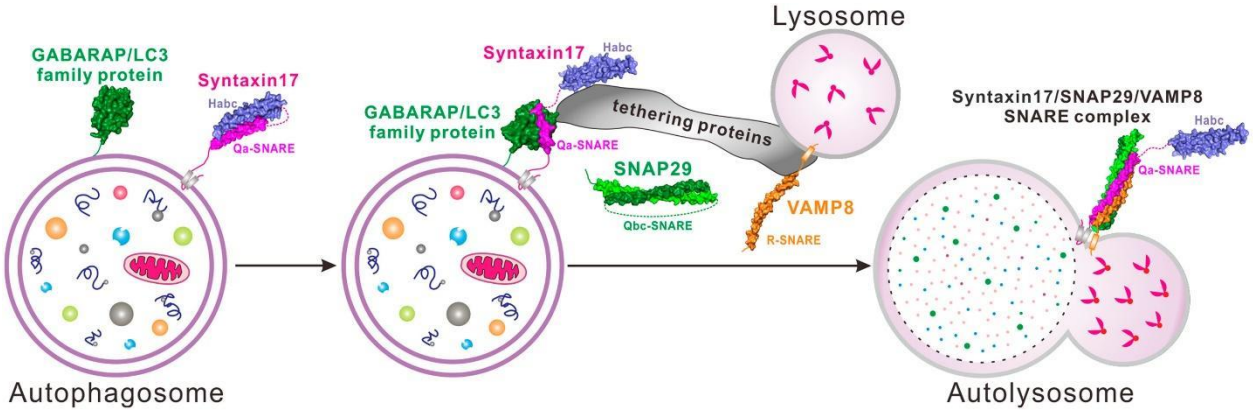

Figure 4: Autophagosome-lysosome fusion step facilitated by the SNAREs and tethering factors.
The schematic representation of autophagosome-lysosome fusion event. The potential working mode of Syntaxin 17 with the coordination of other fusion partners such as VAMP8, SNAP29, and, tethering factors to facilitate the fusion step during the autophagy process (Li et al., 2020).

The main focus of this study was on Syntaxin 17. Our research group and others have demonstrated the significant role of SNARE Syntaxin 17 during the fusion of autophagosomes and lysosomes

(Takáts et al., 2013; Itakura et al., 2012; Kato et al., 2021). Depletion of Syx17 using RNAi in *Drosophila* larvae caused a characteristic phenotype where Atg8a positive autophagosomes accumulated in the perinuclear region of fat body cells due to lack of autophagosome-lysosome fusion thus leading to a complete block of autophagy degradation (Takáts et al., 2013). The similar fusion defects are also observed in mammals and *Caenorhabditis elegans* suggesting an evolutionarily conserved role of autophagosomal SNARE Syntaxin 17 during autophagy (Itakura et al., 2012; Kato et al., 2021).

1.6 A key player, autophagosomal SNARE Syntaxin 17

The Syntaxin family proteins are one of the SNARE family proteins. They mainly participate as a Qa-SNARE during membrane fusion in eukaryotes (Jahn & Scheller, 2006). They are tail-anchored proteins and contain a SNARE motif with 60-70 amino acids length, flanked by a C-terminal transmembrane domain consisting of 17-24 hydrophobic amino acids and followed by a short C-terminal tail (Jahn & Scheller, 2006) (Fig. 5A).

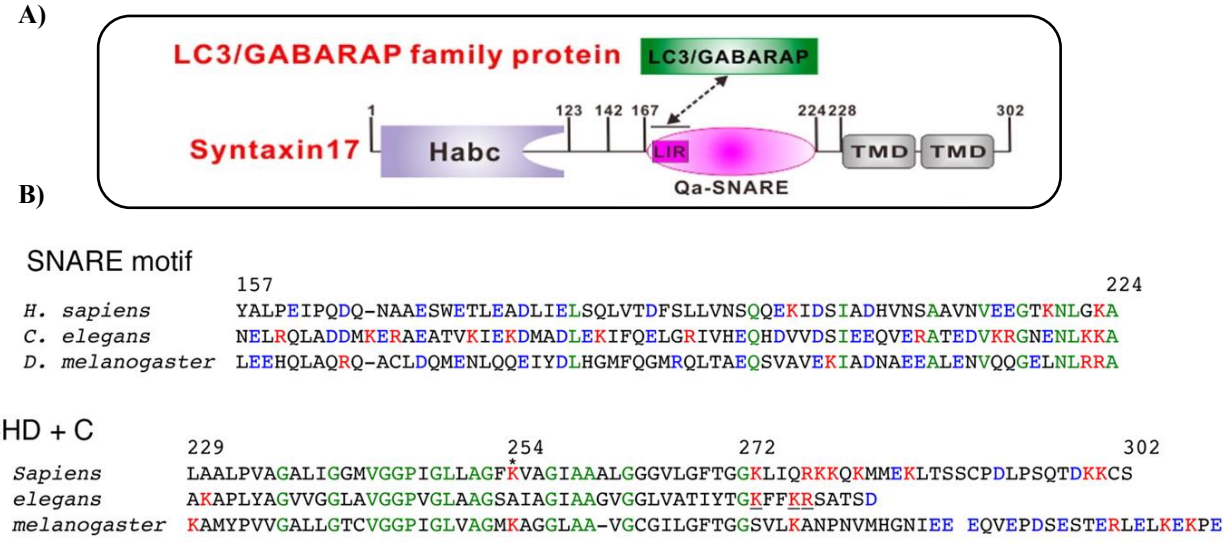

Figure 5: The structure of Syntaxin 17 and conserved SNARE motif and C-terminal region.

A) A model depicts the structure of SNARE Syntaxin 17 having N-terminal Habc domain followed by Qa-SNARE, and two transmembrane domains (Li et al., 2020). B) Comparison of the SNARE motif and C-terminal region of human, nematode and fly Syntaxin 17. Identical, basic and acidic amino acids are highlighted in green, red and blue, respectively (Kato et al., 2021).

Syntaxin 17 is one of the six ancients eukaryotic Qa SNARES but during evolution, it has been extinct in multiple lineages like in yeast. Interestingly, it is a unique SNARE protein consisting of

two-tandem, less hydrophobic transmembrane domains (TMDs) which are comprised of 44 amino acids separated by Lysine-254 exposing its C-terminus to the cytosol (Arasaki et al., 2015). The TMDs are highly conserved but the C-terminal tail varies among the organisms (Fig. 5B). Mammalian and nematode Syntaxin 17 is enriched with positive amino acids whereas *Drosophila* Syx17 possess negatively charged residues (Kato et al., 2021). Syntaxin 17 is pooled in various organelles like mitochondria, ER, and mitochondria-associated membranes (MAM). Interestingly, there is no consensus among the researchers regarding the localization of this protein. Some researchers showed that human STX17 can be both cytosolic and membrane-associated (Itakura et al., 2012) while the other group highlighted that human STX17 is mainly membrane-associated (Arasaki et al., 2015; Kato et al., 2021) while *Drosophila* Syx17 is mainly cytosolic in non-starved conditions and is translocated to membranes during starvation (Kato et al., 2021). Mizushima and colleagues showed human STX17 likely translocate from the cytosol to the matured autophagosome during the autophagosome-lysosome fusion step (Itakura et al., 2012). STX17 does not arise from the isolation membrane or phagophore but it is strictly recruited to the closed autophagosomes when it is needed (Itakura et al., 2012). The time-lapse event of green fluorescent protein (GFP)-STX17 left the impression that the STX17 is recruited into the autophagosomal membrane from the cytosol but not by any vesicle transport (Tsuboyama et al., 2016). The human STX17 inserts into the autophagosomal membrane by forming its two tandem transmembrane domains into hairpin-type tail-anchored structure via glycine-zipper motifs and leaving its C-terminal to the cytosol (Itakura et al., 2012) (Fig. 6). The localization of STX17 is determined by the C-terminal TMDs and a short tail region (Itakura et al., 2012; Kato et al., 2021). In addition, the light chain 3 (LC3) conjugation machinery can strongly influence the recruitment of STX17 to matured autophagosomes (Tsuboyama et al., 2016). The other study could reveal that recruitment of STX17 is promoted by small guanosine triphosphatase immunity-related GTPase family M protein (IRGM) and they both interact with mammalian ATG8 proteins which guide to autophagosomes (Kumar et al., 2018). However, STX17 recruitment is observed in ATG8 family protein-deficient cells (Nguyen et al., 2016) and ATG8 lipidation-deficient cells (Tsuboyama et al., 2016). *Drosophila* Syx17 lacks LC3 interacting region motifs (LIR motifs) and *Drosophila* has no IRGM homologs. Therefore, possibly the mechanism lying behind the Syntaxin 17 recruitment is likely independent of ATG8 family proteins and IRGM.

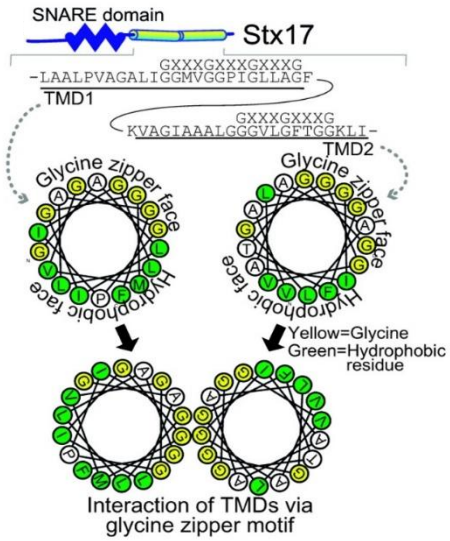

Figure 6: Syntaxin 17 forms a closely packed structure.

The two transmembrane domains of STX17 interact with each other via the glycine zipper-like motifs, exposing the hydrophobic faces to the hydrophobic part of the lipid bilayer. (Itakura & Mizushima, 2013).

Initially, Syntaxin 17 was discovered as SNARE which is abundantly expressed in steroidogenic cells that regulate the dynamics of smooth endoplasmic reticulum (Steegmaier et al., 2000). Later subsequent studies revealed it has multifunctional roles in addition to membrane fusion such as mitochondrial division, autophagosome formation, and lipid droplet biogenesis (Steegmaier et al., 2000; Kato et al., 2021). At the ER-mitochondria interface, this protein promotes mitochondrial fission in fed cells and autophagosome formation in starved cells by interacting with different partners. Under fed conditions, Syntaxin 17 interacts with Drp1 and prevents its protein kinase A (PKA) -mediated phosphorylation by competing with the AKAP protein Rab32 (Arasaki et al., 2015). Upon starvation, it dissociates from Drp1 and recruits the PI3KC to the MAM through interaction with the PI3-kinase subunit Atg14L. Drp1 is phosphorylated by PKA, leading to mitochondrial elongation (Arasaki et al., 2015) (Fig. 7). Mitsuo Tagaya and his group recently expressed fly and nematode Syntaxin 17 in HeLa cells and investigated their localization, roles in the mitochondrial division, autophagy, and lipid droplet formation (Kato et al., 2021). It is observed fly and nematode Syntaxin 17 expressed in HeLa cells predominantly localized in the cytosol and mitochondria. In contrast, mammalian STX17 is mostly membrane-associated such as ER, MAM, and autophagosomes (Kato et al., 2021). The expressed fly and nematode Syntaxin 17 exhibited either autophagic function or mitochondrial division function but not both. During evolution, Syntaxin 17 may have lost some of its functions, but it can compensate for the loss of

lipid droplet formation by interacting with ACSL3, which is responsible for the formation of lipid droplets. (Kato et al., 2021). As described above the structure of Syntaxin 17 in different species, Syntaxin 17 contains a commonly conserved SNARE motif but variable C-terminal tail, and possibly this is correlated with conserved roles and non-conserved multiple functions (Fig. 5B).

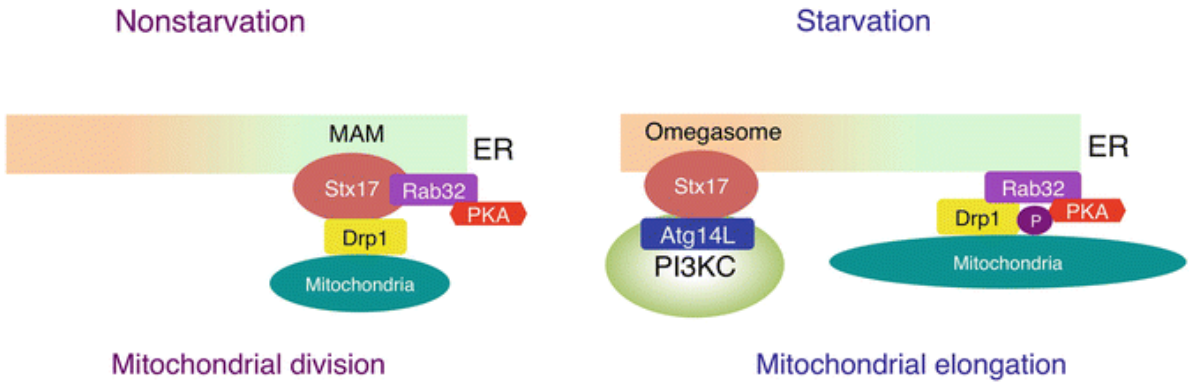

Figure 7: Starvation induces the redistribution of Syntaxin 17 and shifting binding partners.
A model that explains the function and localization of Syntaxin 17 during non-starved and starved conditions. Showing the different partners of Syntaxin 17 in both scenarios (Arasaki et al., 2015). Omegasome is another name for isolation membrane.

1.7 Lipids, the main components of autophagic membranes

Autophagy is a membrane-driven process hence it is heavily relying on membrane dynamics, membrane remodelling, and trafficking events (Dall'Armi et al., 2013). In eukaryotes, membranes are organized within lipid bilayers composed of thousands of lipids. Lipids are major structural components in a eukaryotic cell. They are mainly divided into triglycerides, sterols, and phospholipids. Triglycerides are tri-esters with glycerol bound to three fatty acid chains (Fahy et al., 2011). Principally they function as energy reservoirs in the cell (Fahy et al., 2011). Sterol molecules are complex structures that contain interlinking rings of carbon atoms with mostly no fatty acyl chains (Schade et al., 2020). Cholesterol is the best-known type of sterol. Cholesterol is present in the cell membrane of all body cells, and it has several essential functions in the body (Schade et al., 2020). Phospholipids are versatile amphipathic molecules and are structured with a hydrophilic head group, a phosphate group, a glycerol molecule, and two hydrophobic fatty acid chains (Vance, 2015) (Fig. 8).

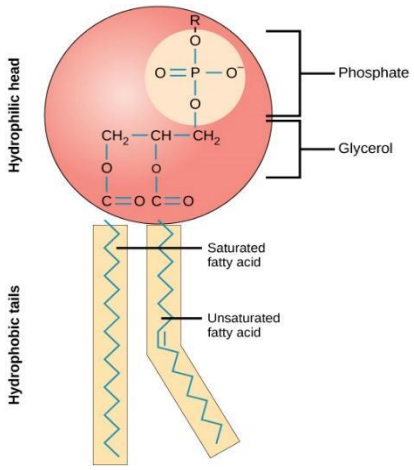

Figure 8: The structure of glycerophospholipid or phosphoglyceride.

The glycerol serves as a backbone that connects the phosphate group, polar head group (R) and two hydrophobic fatty acid chains. In the cell membrane, the polar head group orients to the hydrophilic side while the two fatty acid chains orient to the hydrophobic side (Vance, 2015).

This structure of lipids forms a bilayer in membranes with the polar head facing an aqueous environment whereas the tails are driven inward pointing to each other. These are the predominant structural lipids of eukaryotic cellular membranes that are distinguishable mainly by their head group — Phosphatidylcholine (PC), Phosphatidylethanolamine (PE), Phosphatidic acid (PA), Phosphatidylserine (PS), and Phosphatidylinositol (PI) (Vance, 2015) (Fig. 9).

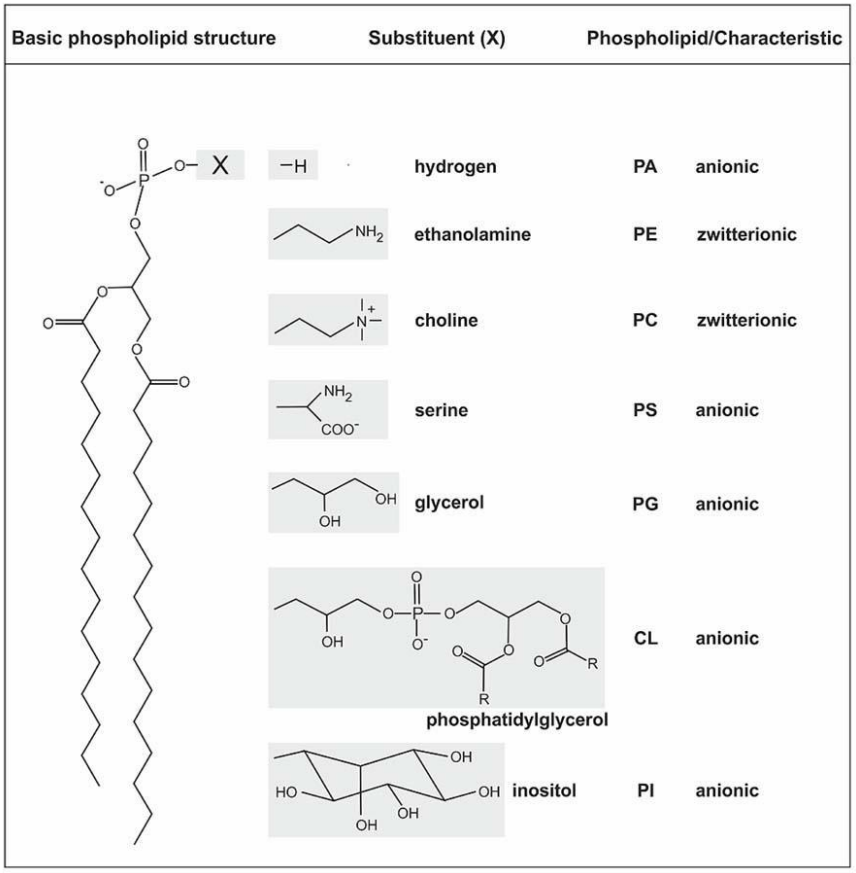

Figure 9: Various head groups of glycerophospholipids.

Types of common head groups of phospholipids. The names of head groups and charges are indicated. PA, phosphatidic acid; PE, phosphatidylethanolamine; PC, phosphatidylcholine; PS, phosphatidylserine; PG, phosphatidylglycerol; CL, cardiolipin; PI, phosphatidylinositol (Vance, 2015).

Lipids composing bilayers for different organelles are varied with their composition, fatty acid chain length (mainly 14 to 20 carbons), and degree of unsaturation. The hydrophobic tails can be saturated (no double bonds) or unsaturated (one or more double bonds). Based on their degree of saturation, the membranes can be tightly or loosely arranged. Interestingly, the shape of the lipid species can influence the geometry of membranes. PE with an unsaturated fatty acyl chain exhibits a conical geometry shape in the membrane because of its small head group whereas PC and PI impose cylindrical and inverted conical geometries respectively. The asymmetric distribution of PC and PE imposes a membrane curvature that accommodates downstream membrane proteins (Fig. 10). The differences in the lipidome determine the shape and physicochemical properties of the membrane such as fluidity, thickness, and plasticity (Rim Baccouch, et al., 2023). *Drosophila*

is a PE centric lipidome, while human lipidome is PC centric and PA, PS, PI are less abundant (Carvalho M, et al., 2012; Hammad L. A, et al., 2011; Guan X.L, et al., 2013).

After all, lipids are not only the backbone of organelle membranes but also essential signaling molecules during autophagy. Certain functional lipids that are present in autophagic membranes play an essential role in inducing and expanding phagophores and facilitating their fusion with lysosomes (Martens et al., 2016).

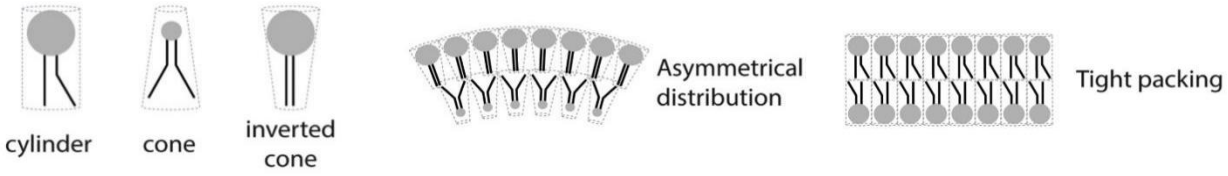

Figure 10: Geometry of phospholipids in the organelle membranes and influence on membrane shapes.

The lipid composition can influence the bilayers to form various membrane structures. For example: PE, the lipid molecule with a small head group can resemble the cone-shaped structure that leads the negative membrane curvature. PC, a cylindrical shape lipid molecule can form flat bilayers. The shape of lysophospholipids or polyphospholipids resembles the inverted cone structure that can form structures with positive membrane curvature (Sangeeta nath et al., 2014).

PI(3)P—The autophagy process depends on complex membrane remodelling and trafficking events. During phagophore assembly, the ULK1 complex through its subunit called FIP200 recruits to ER domain enriched with PI or PI(3)P followed by incorporation of a part of ATG9-containing vesicle. Then ULK1 complex translocates to the ATG9 vesicle to elongate the isolation membrane and further recruit ATG14 (Taki Nishimura et al., 2017) (Fig. 11). Notably, PI(3)P synergistically recruits various downstream ATG proteins. As mentioned above PI(3)P generated by class III PI(3)P complex 1 is critical not only for the formation of isolation membrane but is also likely to be indispensable for membrane elongation. WIPI family proteins such as WIPI2 can directly bind to the PI(3)P and PI(3,5)P_2 (Phosphatidylinositol 3,5-bisphosphate) on the autophagic membranes (Krick et al., 2012). WIPI2 complex with the ATG2A/B to expand the isolation membrane until the membrane closure (Kishi-Itakura et al., 2014; Obara et al., 2008; Velikkakath et al., 2012). Specific phosphatidylinositol phosphates (PIPs) generation on autophagosomes is critical for autophagosome-lysosome fusion too (Ogawa et al., 2011; H. Wang et al., 2015). TECPR1, a tethering factor, that complex with ATG12–ATG5, enabling binding to PI(3)P to facilitate the fusion step (Fig. 11) (Martens et al., 2016).

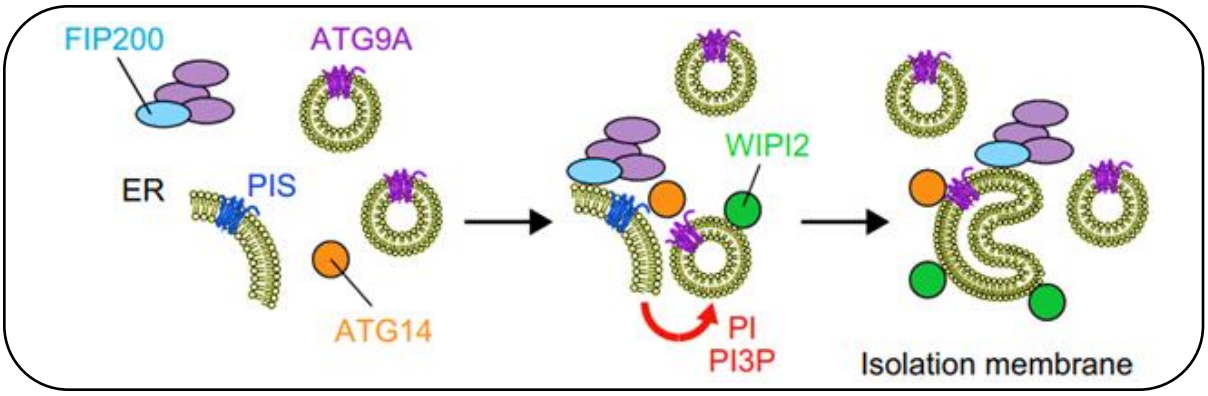

Figure 11: PI(3)P enriched membrane recruiting the downstream players during autophagosome biogenesis.
Illustrates FIP200 recruitment to the PI(3)P enriched ER domain induces recruitment of downstream players during the initial stages of autophagosome biogenesis, PIs enriched ER membrane supplies PI to Atg9A vesicles. (Taki Nishimura et al., 2017).

PI(4)P— PI 4-phosphate kinase type II α (PI4K2A) is an enzyme that generates Phosphatidylinositol 4-phosphate (PI(4)P) and is usually found in the perinuclear region and trans-Golgi network (TGN). Upon starvation, PI4K2A exits TGN and distributes in the cytoplasm and some co-localize with Gamma-aminobutyric acid receptor-associated protein (GABARAP) and Gamma-aminobutyric acid receptor-associated protein like 2 (GABARAPL2) (but not with LC3) on the autophagosomes in a palmitoylation-dependent manner (Wang et al., 2015; Martens et al., 2016) (Fig. 12). PI(4)P exhibits a similar pattern of distribution and depletion of PI4K2A reduces the PI(4)P abundance on autophagosomes. Depletion of GABARAP perturbs the localization of PI4K2A on autophagosomes but PI4K2A depletion does not affect GABARAP distribution. Knockdown of PI4K2A shows large autophagosomes and impaired autophagosome-lysosome fusion (Wang et al., 2015). However, the fusion defect is rescued by the PI(4)P introduction. The exact role of PI(4)P during fusion remains to be elucidated.

PI(3,5)P$_2$— Inositol polyphosphate-5 phosphatase E (INPP5E), a novel regulator in promoting the fusion step during autophagy (Hasegawa. R et al., 2016). Inhibition of INPP5E leads to the accumulation of autophagosomes due to the impairment of autophagosome-lysosome fusion. INPP5E protein is localized at the lysosomes that mediate the conversion of PI(3,5)P_2 to PI(3)P on the membrane, which in turn is crucial for the fusion with autophagosomes (Fig. 12). Also, other research has shown that the knockdown of the phosphoinositide kinase PIKfyve decreases the PI(3,5)P_2 levels on lysosomes and causes severe autophagy defects due to the loss of lysosomal

function (Lartigue et al., 2009). Therefore, proper levels of $PI(3,5)P_2$ in the lysosomal membrane seem to be indispensable to facilitate the fusion with autophagosomes during autophagy. INPP5E activity on lysosomes is ultimately required for the phosphorylation of cortactin/CTTN, which leads to actin polymerization followed by autophagosome-lysosome fusion. The abundance of $PI(3,5)P_2$ on lysosomal membranes influences the lysosomal acidity and function for the efficient autophagic cargo degradation by lysosomal hydrolases. The continuous process of autophagosome formation and degradation is maintained through the orchestrated actions of $PI(3,5)P_2$.

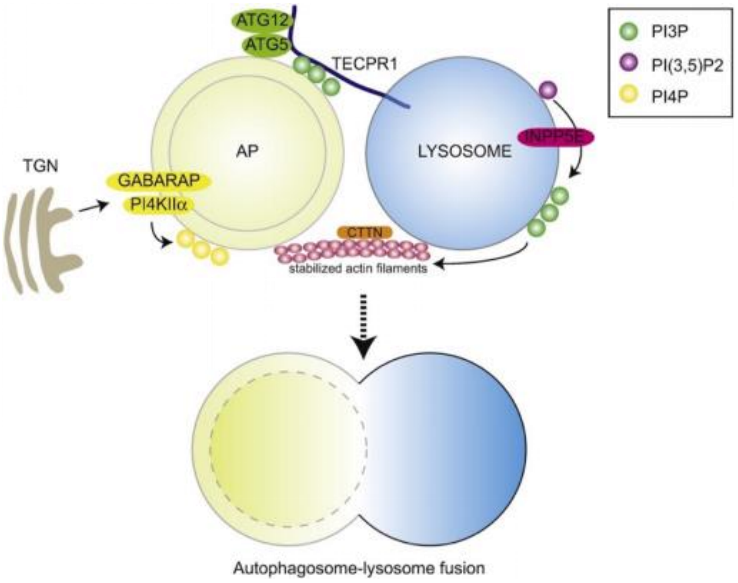

Figure 12: Role of phosphoinositides during autophagosome-lysosome fusion.
TECPR1, a tethering factor on the lysosome binds to the PI(3)P on the autophagosomes to interact with ATG12 and ATG5 to facilitate the autophagosome-lysosome fusion during autophagy. From the Trans Golgi Network (TGN), PI4K2A is recruited to the autophagosomes by GABARAP to generate PI(4)P. Phosphatase, inositol polyphosphate-5 phosphatase E (INPP5E) on the lysosomes converts $PI(3,5)P_2$ to PI(3)P activates cortactin/CTTN and stabilizes actin filaments that are required for the vesicle fusion (Martens et al., 2016). The sequential order of these events is not clear yet.

PE—PE plays a central role in autophagy by contributing to the formation and expansion of the autophagosomal membrane. LC3, a potential autophagic marker protein, undergoes a multi-step ubiquitin-like conjugation pathway with PE to form LC3-II. LC3-PE conjugation is essential for the association of LC3 with the autophagosomal membrane. The interaction between PE-conjugated LC3 and cargo receptors facilitates the selective recognition and sequestration of specific substrates. PE is actively involved in phagophore elongation, autophagosome maturation, and cargo sequestration (Dooley et al., 2014).

PA— Lipids can also influence the shape of autophagosome formation. The membrane curvature aids the insertion of hydrophobic regions of proteins into the lipid bilayer. Lipids with small head groups such as PA with or without bulky fatty acyl chains (cone-shape lipid) exhibit similar effects and promote insertion and binding of ATG3 and ATG12–ATG5-ATG16 complex during autophagosome formation (Dall'Armi et al., 2010). ATG3 and ATG12–ATG5-ATG16 complex prefers to bind highly curved membranes (Romanov et al., 2012; Nath et al., 2014). In mammals, PA is synthesized by phospholipase D1 (PLD1) which is found to be localized at the phagophore in a PI(3)P-dependent manner during its elongation. Therefore, local synthesis of PA is a prerequisite for autophagosome formation (Dall'Armi et al., 2010). As mentioned above, like PE, PA is a cone-shaped lipid molecule, and its presence may impose negative membrane curvature of the phagophore.

1.8 Lipid-protein interactions during autophagy

To consistently execute the autophagy process, interactions between membrane lipids and proteins must occur. Autophagosomes are unique compared to other vesicles due to their biogenesis, morphology, membrane lipid composition, and very few membrane proteins (Juhasz & Neufeld, 2006; Proikas-Cezanne & Robenek, 2011). Membrane lipids can interact with proteins in multiple ways such as i) through electrostatic or hydrophobic interaction– Basic amino acids of the protein domains form electrostatic interactions with the negatively charged lipids of the membrane. ii) Through specific structured PI binding domains– the structured domains have the membrane-deforming activity that is responsible for the formation of concave or convex membrane curvature mediated by membrane insertion. And, iii) through lipid binding domains that bind the membrane with no specificity– (Suetsugu et al., 2014) (Fig. 13). The insertion of amphipathic helix domains deforms the membrane through hydrophobic or electrostatic interactions. Whereas the proteins with BAR domains deform the membranes using their curved, positively charged surface. The protein with hydrophobic residue stretches can also form loop or wedge-shaped insertions into the membranes and cause membrane deformation (Suetsugu et al., 2014).

Remarkably, autophagosome formation happens very rapidly upon autophagy induction. This determines the tremendous demand and supply of lipids for autophagosome formation. The supply of structural lipids must be regulated in time and amplitude to implement the membrane remodelling events. It is known that phospholipids have significant roles at each step of autophagy.

Besides the profound involvement of structural lipids, the specific lipid composition of autophagosomal membranes may also implicate the autophagy pathway.

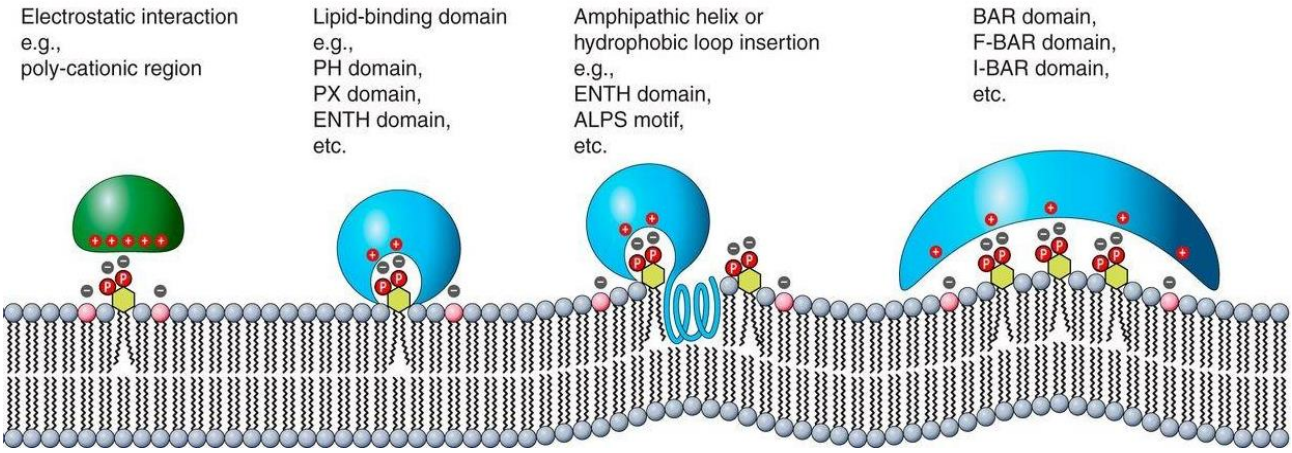

Figure 13: Varieties of lipid-protein interactions.

The lipid-protein interactions are classified into four categories based on protein domains that recognize and bind to lipids: 1) simple, charge-driven interactions without recognition of specific lipid species; 2) lipid species recognition by the protein structure; 3) membrane recognition and deformation with the insertion of an amphipathic helix or a hydrophobic loop; and 4) protein structure-based deformation of the membrane (e.g., BAR domains) (Suetsugu et al., 2014).

1.9 Model Systems

This study utilizes *Drosophila* starved adult flies (isolation of autophagosomes), mammalian cells like Human embryonic kidney cells (HEK-293) and human osteosarcoma cells (U2OS) (cell biology), and Escherichia coli (*E. coli*) (recombinant protein expression) as models. *Drosophila* is an ideal model to study autophagy in a whole organism because of its fast life cycle and relatively simple genetics. 60% of their genes are similar to the human genome, and 75% of human diseases associated with the genome exhibit homology with the genome of fruit flies (Reiter et al., 2001).

Mammalian cell cultures are another sophisticated tool to study the biology of cells from multicellular organisms. These techniques became robust by the 20th century. The immortalized cells are grown in certain conditions which consist of amino acids, carbohydrates, vitamins, minerals, growth factors, hormones, and gases (CO_2, O_2) along with a regulated physico-chemical environment. The most widely used immortalized cell line is the HEK-293 cell line which is derived from miscarried female fetus kidney cells (Graham *et al*., 1977). These cells are widely used in cell biology and biochemical experiments because of reliable growth and transfection efficiency. The other cell line is U2OS derived from the bone tissue of a human female suffering

from osteosarcoma in 1964. Although the propensity of transfection is not up to the HEK-293 cell type, the large cell size, larger cytoplasm and smaller nucleus than the other cell types are the biggest advantages of using U2OS for cell biology research and fluorescent microscopy visualization.

E. coli is the most reliable and popular model organism in the field of molecular biology and genetic engineering research fields because of its rapid growth and reproduction. DH5 alpha *E. coli* competent cells and BL3 variant of Rosetta *E. coli* competent cells are used for DNA cloning, recombinant protein expression, and purification respectively.

2. AIMS OF THE THESIS

Autophagy is spatiotemporally governed by a series of membrane-associated proteins, therefore it is essential to understand the interactions between membrane lipids and autophagy proteins. While several autophagy proteins that interact with autophagic membranes have been studied, there is no information available on the lipids involved in the recruitment of Syntaxin 17 to the autophagosomes. During the autophagosome-lysosome fusion step, Syntaxin 17 translocate from the cytosol to autophagosomes but not to the phagophores. However, the mechanism underlying the transient visit of Syntaxin 17 to the autophagosomes is not yet understood. One possibility is that *de novo* generated signaling lipids on the membrane, such as phosphoinositides PI(3)P, PI(4)P, or $PI(3,5)P_2$), can be the fundamental signal to recruit Syntaxin 17 to the matured autophagosomes. As known, lipids are not only for compartmentalization and energy storage but also function as relevant regulators in cellular signaling (Axe et al., 2008; Juhász et al., 2008; Dong et al., 2010; Wang et al., 2015; Martens et al., 2016). Therefore, our research aims to unravel the interacting lipids involved in the incorporation of Syntaxin 17 into the autophagosomal membrane.

Thus, the aims briefly:

✓ Investigate the role of lipids in facilitating the autophagosomal recruitment of Syntaxin 17 during autophagy *in vitro* and *in vivo*

- Establish a method for the isolation of intact autophagic vesicles from the *Drosophila*
- Decipher the lipid profiles of isolated autophagic structures

✓ Study the specific structural features of Syntaxin 17 that mediate lipid binding

✓ Confirm the significance of amino acids responsible for lipid-protein interactions

3. MATERIALS AND METHODS

3.1 *Drosophila* work

4 h starved homozygous control and Atg2^{-} (*Atg2*^{EP3697}) containing the *3xmCherry-Atg8a* autophagic reporter adult flies were generated by standard genetic methods and used to isolate autophagic membranes. The *Atg2*^{EP3697} EP element insertion line was purchased from Bloomington *Drosophila* Stock Center (BDSC) (FlyBase ID: FBal0123243) (Pircs et al., 2012; Scott et al., 2004). Earlier our lab generated the *3xmCherry-Atg8a* stock (Hegedus et al., 2016). The following lines were used for the PI(4)P co-localization studies: *y,w, hsFLP; Act>CD2>GAL4, UAS-GFP-Syx17, UAS-P4M-mCherry* (kind gift from Bing He), (Chen & He, 2022) and a genomic promoter-driven *3xmCherry-Atg8a* (Hegedus et al., 2016). Flies were maintained at 25 °C in vials containing a standard medium of cornmeal, sucrose, and yeast. After 4 h starvation the flies were collected, snap frozen, and stored at -80 °C until further use. Third instar larvae were washed in distilled water and dissected in 1x Phosphate buffered saline (PBS). The isolated larval fat bodies were moved to glass slides into a 1:1 glycerol-PBS mounting medium, covered with a coverslip, and sealed with nail polish.

The standard starvation protocols were applied from the literature. In the case of *Drosophila* adult flies, starvation was for 4 h. To induce starvation, adult flies were transferred to an empty vial (as they are more resistant to starvation by having a lot of reservoirs), while larvae were kept on 30% sucrose (to induce amino acid starvation, as they are more sensitive to starvation, being in active development).

3.2 Homogenization of flies

The control (400 mg) and Atg2^{-} (200 mg) flies were homogenized cryogenically using liquid nitrogen, mortar, and pestle. The double amount of control flies was used to acquire a sufficient quantity of membranes for further lipidomic analysis like in Atg2^{-} (accumulating autophagic structures). The obtained homogenized powder was resuspended to a final volume of 1 ml (in case of control 2 × 1 ml) with buffer containing 250 mM sucrose, 20 mM 4-(2-hydroxyethyl)-1-piperazineethanesulfonic acid (HEPES) 1 mM Ethylenediamine tetraacetic acid (EDTA), with freshly added protease inhibitors: 1 mM phenylmethylsulfonyl fluoride (PMSF), 1 mM Aprotinin and 1 mM Leupeptin. The resuspension mixture was centrifuged at 3000 g for 15 min at 4 °C to

get rid of the debris. The supernatant was collected and used further to isolate intact autophagic structures.

3.3 Isolation of autophagosomes by immunoprecipitation

The obtained supernatant after the last step of homogenization was used for the immunoprecipitation. 50 µl of the sample at each step was collected and used for further validation purposes. This isolation method is initiated by pre-clearing the lysate with pre-blocked beads (binding-control magnetic agarose beads, Chromotek, bab-20). 1 ml of homogenate was incubated with 25 µl of equilibrated pre-blocked magnetic beads on a rotator for 1 h at 4 °C. After incubation, the clear supernatant was separated from the binding-control magnetic beads using a magnetic separator (DynaMag –2).

3xmCherry-Atg8a autophagy reporter in the flies facilitated the use of the RFP-TRAP_AM beads for the isolation of autophagic membranes. 25 µl of equilibrated RFP-TRAP_AM beads (Chromotek, rtma-20) were used for the binding of 1 ml of pre-cleared supernatant on a rotator for 1 h at 4 °C. For the equilibration of any kind of mentioned beads, 3 × 500 µl of ice-cold dilution buffer (10 mM Tris/HCl pH 7.5, 150 mM NaCl, 0.5 mM EDTA) was used. After 1 h binding, the supernatant was discarded, and the beads were washed 5 times with dilution buffer. 50 µl of elution buffer (0.2 M glycine pH 2.5) was added and constantly pipetted up and down for 1 min and, cleared the eluted sample from beads using a magnetic separator and collected into a new sterile Eppendorf tube. Immediately pH of the eluted fraction was neutralized by 5 µl of 1 M Tris base (pH 10.4). The elution step was done two times, and these fractions were combined or used separately for further steps (such as Western, microscopy, and lipid isolation).

3.4 Immunoblot and Antibodies

The immunoprecipitated and TCA precipitated samples containing proteins were separated by sodium dodecyl sulfate-polyacrylamide gel electrophoresis (SDS-PAGE) (10 % or 15 % gels) and overnight or rapidly transferred to Immobilon-P PVDF FL membranes. The membranes were incubated with the appropriate primary antibodies diluted in 10 ml Odyssey PBS blocking buffer, containing 0.1 Tween-20 (2 h, RT or overnight at 4 °C). Membranes were washed 4 x 7 min with PBST, followed by incubation with Li-COR fluorescent secondary antibodies diluted in Odyssey buffer, containing 0.1 % Tween-20 and 0.01 % SDS (1 h, RT). Wash the membrane with 3 x 10 min, PBST, 1 x 10 min with PBS, few minutes with dH_2O and methanol. Then membranes (keep

away from light) were dried under a laminar airflow chamber for 20 min. The signal was detected with the Odyssey fluorescent scanner, using Li-COR Image studio software. Blots were incubated with the following primary antibodies: rabbit monoclonal anti-GABARAP ab109364 (Abcam) [1:2000], rabbit polyclonal anti-Atg5 A0856 (Sigma) [1:1000], mouse monoclonal anti-ATP5A ab14748 (Abcam) [1:5000], mouse monoclonal anti-Cnx99A 6–2-1 (DSHB) [1:2000], rabbit polyclonal anti-Rab5 ab31261 (Abcam) [1:1000], mouse monoclonal anti-Rab7 CG5915 (DSHB) [1:100], rabbit polyclonal anti-cathepsin L ab58991 (Abcam) [1:1000] and mouse monoclonal anti-α-Tubulin AA4.3 (DSHB) [1:2000], rabbit anti-*Drosophila* Syntaxin 17 [1:5000], rabbit polyclonal anti-human Syntaxin 17 (sigma, HPA001204) [1:1000], rabbit polyclonal anti - GST antibody (Invitrogen # 2362338) [1:3000], mouse monoclonal anti-α-Tubulin AA4.3 (DSHB) [1:2000]. Species-specific fluorescent secondary antibodies were used (Li-COR) [1:15000] for the detection on a Li-COR Odyssey CLx laser scanner.

3.5 Fluorescent Microscopy for validation of the autophagic structures

10 μl of the eluted fractions were pipetted onto a glass slide, mounted with a glass coverslip and immediately imaged in a Zeiss Axioimager M2 microscope equipped with Apotome 2 module and a Plan-Apochromat 100× 1.40 oil immersion objective. Raw images were processed in Zen 2 (Zeiss) software. Weak image deconvolution was performed to improve image sharpness from the 'Apotome' tab of Zen 2 and images were exported after adjusting brightness and contrast levels to remove noise. From these images, manual counting of the diameter of 3xmCherry-Atg8a positive structures (n=70) was performed in ImageJ (NIH) and statistics were performed in Graph Pad Prism. Statistical testing was performed by Mann-Whitney U test.

3.6 Atomic Force Microscopy (AFM)

All experiments were carried out with an MFP-3D atomic force microscope and controller (Asylum Research, Santa Barbara, CA; driving software IgorPro 6.32A, Wavemetrics). Aluminium backside-coated silicon cantilevers (Olympus, AC240) with a nominal spring constant of 2 N/m, and a resonant frequency of 70 kHz in air, were used. All cantilevers were calibrated prior to experiments with the help of the driving software of the instrument using the Sader method (Sader et al., 2012). Images were acquired using alternate-contact mode in a closed loop in an air medium at room temperature having 512 scan lines by 512 scan points. Background level correction and flattening were applied to each image to correct for eventual sample tilt. 5 μl of

eluted fraction was dropped onto a freshly cleaved mica surface, and then let dry. Salt depositions from the buffer were removed by gently washing with 200 µl of water, then dried again under high-purity air flow (RH < 5 %).

3.7 Lipid extraction

Total lipids were extracted from collected, eluted fractions of RFP-TRAP immunoprecipitated autophagic membranes, and snap-frozen samples such as *E. coli*, *Drosophila melanogaster*, mammalian cells (MCF7; cells collected from four 10 cm plates) by Folch (Folch et al., 1957) and Bligh and Dyer (BLIGH & DYER, 1959) with minor modifications. Briefly, 1 ml of aqueous solution was added and transferred to clean glass tubes containing a cap. Followed by the addition of chloroform: methanol (1:2), 0.01 % Butylated hydroxytoluene (BHT). BHT is added to protect the polyunsaturated lipids from oxidation. 1 ml chloroform and 1 ml water were added after the incubation of 30 min at RT. After phase separation, we collected the lower, lipid-containing phase. Subsequently, combined lipid extraction was performed by adding 1 ml chloroform to the sample (this step was repeated three times). The combined lower (chloroform) layers were washed with 0.5 ml of 1 M KCl and then with 0.5 ml of water. The solvent was evaporated under nitrogen gas using an MD200 sample concentrator and the lipid extract was dissolved in 0.5 ml chloroform/methanol (1:2), transferred to 2.0 ml clear glass vials with Teflon-lined screw cap and stored at −80 °C. In the case of mass spectrometry analysis of autophagic membranes, the solvent was evaporated before shipping the samples, and the glass tube was filled with inert nitrogen gas. The dried lipid extracts were measured by the gravimetric method.

3.8 Lipidome analysis for the lipids extracted from autophagic membranes

Lipidomic analysis (using tandem MS-based method) of the total lipid extracts from autophagic membranes was carried out. The 300 µl total volume of lipid extract was injected into the loop of the XEVOTQS#WAA627 mass spectrometer for analysis (Sparkes et al., 2010; Z. Zhou et al., 2011). The background subtraction used the standard in front of each set of replicates for the subtraction of contaminants. The reported amounts are expressed as normalized signals per milligram of protein. This means that the signals for the peaks in the sample are compared to the signals for peaks of internal standards that were added in known amounts and the resulting data is reported. So, the signal that is represented as 1 = the same signal as 1 nmol of internal standard (usually with an adjustment for variation in response with m/z). Thus, the numbers that we report

as normalized signal/mg protein for phospholipids can be considered to be equal to nmol/mg protein. To avoid many zeros, we report the data as picomol/mg protein. We also calculated the mol % of the lipids (the relative amount of that compound compared to other compounds in the sample). The mol % of lipid species are averages of three (control) and four (mutant) independent biological replicates. Double bond indices of different lipid classes were calculated similarly, as described in Falcone et al. 2004, using the following equation: [Σ (% of normalized signal intensity/mg protein of lipid species × no. of double bonds)] / 100.

3.9 Cloning and lentiviral transduction

The full-length *Drosophila* Syx17 and human STX17 and Atg3 encoding genes were used to generate pETARA-GST- Syx17, pETARA-GST-STX17, and pETARA-GST-Atg3. The source for gene encoding Syx17 and Atg3 was from *Drosophila* Gene Collection Release 1 library (DGCr1) (Stapleton et al., 2002) [Clone ID: GH06387, containing cDNA AY047555 in pOT2 vector (full-length *Drosophila* Syx17 cDNA)] [Clone ID: GH28859, containing cDNA AY119557 in pOT2 vector (full-length *Drosophila* Atg3 cDNA)] and STX17 was from Addgene # 45909 plasmid: pMRXIP GFP-STX17 WT (gift from Noboru Mizushima (Addgene plasmid # 45909; http://n2t.net/addgene:45909; RRID: Addgene_45909) (Itakura et al., 2012). The targets were amplified by polymerase chain reaction (PCR) using the primers mentioned in Table. 1. The amplified PCR products were purified (Thermo Scientific GeneJET Plasmid Purification Kit, K0701) and digested by restriction endonucleases (*Drosophila* Syx17 and Atg3 by BamHI (NEB#R3136S) and NotI (NEB#R3189L); human STX17 by SalI (NEB#R3138S) and NotI). Digested targets were ligated into similarly digested pETARA vectors. DH5alpha-competent *E. coli* cells were used for the cloning. The plasmid DNA was purified by a plasmid purification kit (Thermo Scientific GeneJET Plasmid Miniprep Kit, K0502).

Amino acid substitutions in the C-terminal region of pmRXIP Turquoise2-Syntaxin 17 (Addgene: #89938, Noboru Mizushima) (Tsuboyama et al., 2016) and pmRXIP Turquoise2-*Drosophila* Syx17 were performed by PCR amplifying two half-plasmid fragments from the wild-type template with the mutagenic primers spanning the C-terminal region and containing desired mutations (Table. 1). The PCR products were purified and assembled in a T5 exonuclease-dependent assembly (TEDA) reaction (Xia et al., 2019). The clones were verified by Sanger sequencing with the following primer: GTGGAGCATTTCATACTACTGAAGC. The

Drosophila Syx17 wt or the alanine substitutions in the C-terminal region constructs were swapped with the human STX17 sequence from pmRXIP Turquoise2-Syntaxin 17. The *Drosophila* Syx17 sequence was amplified from pETARA-GST-*Drosphila* Syx17 using the primers mentioned in Table. 1. Parallelly, the backbone was amplified from pmRXIP Turquoise2-Syntaxin 17. NEBuilder was used to assemble the backbone with the wild-type or the alanine substitution containing fragments of Syntaxin 17. Clones were verified by Sanger sequencing with the following primers: CCTCACATTGCCAAAAGACG and GAGCAAAGACCCCAACGAGA.

Table 1: Primers used in this study:

Primers for the plasmids of desired recombinant protein expression and purification		
pETARA-GST- Syx17	*FWD*AATAGGATCCATGACGCGCGATGAGAAACTG	*REV*TATTGCGGCCGCGGGTCATTCTGGCTTCT
pETARA-GST-STX17	*FWD*TATAGTCGACATGTCTGAAGATGAAGAAAAAGTG	*REV*GGTTGCGGCCGCTTAACTGCATTTCTTGTCAGTTTG
pETARA-GST-Atg3	*FWD* AACAGGATCCATGCAGAGTGTTCTCAACACC	*REV* TATTGCGGCCGCTGGCGGGTCTTAAGACATGT
Primers for the plasmids with Alanine substitutions at the C-terminal region of Syntaxin 17		
pmRXIP Turquoise2-STX 17 (R/K>A)	***Fragment 1***	
	*FWD*ACATTTCCCCGAAAAGTGCCACC	*REV*TGGACAGCTGGAAGTGAGCGCCTCCATCATGGCCTGTGCCGCGGCTTGTATCAATTTTCCACCTGTGAAGC
	Fragment 2	
	*FWD*GCGCTCACTTCCAGCTGTCCAGATCTTCCCAGCCAAACTGACGCTGCCTGCAGTTAAGGATCCCTCGAGCG	*REV*GGTGGCACTTTTCGGGGAAATGT
pmRXIP Turquoise2-Syx 17(Wild-type)	*FWD*ATGACGCGCGATGAGAAACTGCC	*REV*GACAGAAGCTTTCATTCTGGCTTCTCTTTTAGCTCCAGTCT
pmRXIP Turquoise2-Syx 17 (RRKK>A)	***Fragment 1***	
	*FWD*ATGACGCGCGATGAGAAACTGCC	*REV*GGCCGCTGCGTAGGTGAGCGCGGCAGCCAGATTCAATT CGCCCTGCTGGAC
	Fragment 2	
	*FWD*AATCTGGCTGCCGCGCTCACCTACGCAGCGGCCATGTACCCCGTAGTCGGA	*REV*GACAGAAGCTTTCATTCTGGCTTCTCTTTTAGCTCCAGTCT
The backbone for pmRXIP Turquoise2 plasmids	*FWD*CGGAGCTAAAAGAGAAGCCAGAATGAGGATCCCTCGAGCGGCCGCTACGTAA	
	*REV*AGTGGCAGTTTCTCATCGCGCGTCATCGGATCCGTTAACTCGCGAACGCGTG	

To generate stably expressing doxycycline-inducible shRNA for *PI4K2A*, the shRNA sequence from the Sigma Mission TRC collection: CCTCTTCCTGAGAACACTAAC (TRCN0000195396) was annealed and cloned between AgeI and EcoRI sites of tet-pLKO-puro (Addgene 21915, gift from Dmitri Wiederschain). Insertion was verified by Sanger sequencing with primer: GGCAGGGATATTCACCATTATCGTTTCAGA. The pLKO transfer plasmid along with 3rd generation helper plasmids (pMDLg: Addgene 12251, pMD2.G: Addgene 12259, pRSV-Rev: Addgene 12253; gifts from Didier Trono) were transfected in HEK-293T cells to produce lentivirus. Two days after transfection, the viral supernatant was filtered with a 0.45 µm filter,

supplemented with 8 μg/ml polybrene and added to target cells. Two days after transduction with lentivirus, puromycin selection was applied to establish stable cells expressing *shPI4K2A*. Knockdown was induced by adding doxycycline at 2 μg/ml for five days in culture medium. To validate knockdown, total RNA was extracted using a Direct-zol RNA Miniprep kit (Zymo Research, R2050) and quantitative real-time PCR was performed using PerfeCTa SYBR® Green FastMix (QuantaBio, 95072-250). Analysis was performed using the 2-ΔΔCT method against *GAPDH*. The following primers were used for qRT-PCR: *PI4K2A*: CGAGGCAATGACAACTGGCTGA and GCCACCTTGATAACAGGCTCCT; *GAPDH*: ATCCCATCACCATCTTCCAGG and CCTTCTCCATGGTGGTGAAGAC.

3.10 GST-Fusion proteins expression and purification

All our plasmid constructs contain N-terminal Glutathione S-transferase tags which are used for recombinant protein purification. Recombinant proteins were expressed in BL21 (DE3) Rosetta strain *E. coli* competent cells (Sigma-Aldrich). In the case of Syx17 and Atg3, the protein expression was induced by 0.1 mM isopropyl β-D-1-thiogalactopyranoside (IPTG) at 13 °C. The autoinduction medium was used for hSTX17 recombinant protein expression and incubated at 20 °C for two overnights. The harvested bacterial cell pellets (from 500 ml culture) were resuspended in 20 ml of lysis buffer (pH 7.5, 1x PBS, 1mM Dithiothreitol (DTT), Bug buster, and protease inhibitors) and lysed by a sonicator for 5 x 20 seconds. Then the lysate was transferred to clean centrifuge tubes and centrifuged at 20000 g for 30 min at 4 °C to acquire cytosolic fraction. Both proteins were purified by affinity chromatography using glutathione sepharose beads. Approximately 2 ml of Glutathione Sepharose High-Performance beads (GE Healthcare) were used for 500 ml volume culture with 1.9 OD to purify the expressed recombinant protein. The beads were equilibrated with wash buffer (1x PBS and 1mM DTT). At each step, the incubation of the beads was held on the rotator, at 4 °C, and they were pelleted by centrifugation at 3000 g for 15 min, 4 °C. The acquired cytosolic fraction was applied to bead binding for 1 hr. The beads were 2 times washed for 20 min with wash buffer. The beads were incubated with elution buffer (50 mM Tris HCl, 10 mM reduced glutathione, 5 mM DTT) for 20 min and eluted. The centricons (SIGMA; 30 KD pore size filter) were used to concentrate the eluted protein and to exchange the buffer (150 mM NaCl, 1 mM EDTA, 1 mM DTT, and 10 mM Tris-HCl) as this protein is stable in this protein for a long time. The protein concentration was quantified by Bradford's assay

(Thermo Scientific # XG343066) and the protein aliquots were stored at -80 °C. The purities and molecular masses of the proteins were validated by SDS-PAGE.

3.11 Protein and DNA content measurements

The protein content of the eluted immunoprecipitated fractions (ranging from 0.01683 mg to 0.0444 mg) and isolated plasmid DNA concentration was measured with a DeNovix DS-11FX spectrophotometer using the EasyApps software.

3.12 Liposome generation

Liposomes were generated from extracted natural total lipid mixtures and synthetic lipids (Avanti polar lipids). The organic solvents in the lipid mixture were removed by evaporation under an inert N_2 gas and vacuum desiccator. The dried lipids were dissolved to a 1 or 10 mg/ml concentration with liposome generation buffer (20 mM HEPES (pH 7.4) and 100 mM NaCl) and the emulsion was passed 11 times through a 100 nm or 50 nm in diameter pore size containing polycarbonate filter mounted in a mini extruder (Avanti polar lipids) to generate large unilamellar vesicles (LUVs) or small unilamellar vesicle (SUVs) (67 mol % PE + 17 mol % PC + 9 mol % PI + 2 mol % PS + 5 mol % PA). The combinations of lipids used to generate LUVs were as follows—*Drosophila* total lipid, MCF7 total lipid, 67 % PE+17 % PC+9 % PI+2 % PS+5 % PA, 55 % PE+35 % PC+10 % PI, 10 % POPE+90 % POPC, 10 % POPE+80 % POPC+10 % PI(3,5)P_2, 10 % POPE+80 % POPC+10 % PI(3)P, 10 % POPE+80 % POPC+10 % PI(4)P, 10 % PI+90 % POPC, 90 % PI+10 % POPC, 100 % PG, 100 % Cardiolipin (PE: 1-palmitoyl-2-oleoyl-sn-glycero-3-phosphoethanolamine; PC: 1-palmitoyl-2-oleoyl-glycero-3-phosphocholine; PI: L-α-phosphatidylinositol (Liver, Bovine); PS: 1-stearoyl-2-linoleoyl-sn-glycero-3-phospho-L-serine; PA: 1-palmitoyl-2-oleoyl-sn-glycero-3-phosphate; PI(3,5)P_2: 1,2-dioleoyl-sn-glycero-3-phospho-(1'-myo-inositol-3',5'-bisphosphate) PI(3)P: 1,2-dioleoyl-sn-glycero-3-phospho-(1'-myo-inositol-3'-phosphate); PI(4)P: 1,2-dioleoyl-sn-glycero-3-phospho-(1'-myo-inositol-4'-phosphate); PG: 1-palmitoyl-2-linoleoyl-sn-glycero-3-phospho-(1'-rac-glycerol); Cardiolipin: 1',3'-bis[1-palmitoyl-2-oleoyl-sn-glycero-3-phospho]-glycerol). The giant unilamellar vesicles (GUVs) with 1 µm in diameter were generated by the electro-formation method (using nan]i[on Vesicle Prep Pro). The vesicles formed using synthetic lipids for the *Drosophila* autophagosome mimetics (67 mol % PE + 17 mol % PC + 9 mol % PI + 2 mol % PS + 5 mol % PA). 10 µl of lipid mixture at 10 mg/ml was dropped within the greased rubber ring placed on the conductive side of ITO-coated plate and

quickly dried under vacuum approximately for 20 min. After the solvent evaporation, 250 µl of GUV generation buffer (1 M D (-) sorbitol, 1 mM EGTA, 2 mM HEPES - NaOH; pH - 7.4) (Nguyen Bao Quoc et al) was added to the dried lipid mixture. The electro-formation chamber was created by placing the second ITO slide facing the conductive side to the other. An electro-swelling was formed by using the following protocol, Initial (0 V, 5 Hz, 50 °C, 5 min); Start (4 V, 10 Hz, 50 °C, 10 min); Main (4 V, 10 Hz, 50 °C, 90 min); Fall (0 V, 10 Hz, 50 °C, 10 min); End (0 V, 10 Hz, 20 °C). Gently lifted and removed the ITO slide, eventually GUVs were collected by pipetting and stored at 4 °C.

3.13 **Liposome flotation assay**

Lipids were dissolved to a final total lipid concentration of 10 mg/ml in liposome generation buffer. Liposomes were generated as described above. Liposomes were used immediately for the assay. 50 µl of generated liposomes mixture was incubated with 50 pmol of *Drosophila* or human Syntaxin 17 or Atg3 or GST purified recombinant protein in 190 µl of binding buffer (50 mM HEPES/KOH, 150 mM potassium acetate, 1 mM magnesium acetate, 1 mM EDTA, and 1 mM DTT) (24056370). Followed by incubation on ice for 15 min. 40 µl of the sample was kept as input control. The remaining incubated mixture was added to 3 ml of binding buffer containing 70 % sucrose and added to the bottom of an SW40 polycarbonate tube. The sample was then covered with three cushions of 3 ml of binding buffer containing 50 %, 40 %, and 0 % sucrose. After centrifugation to equilibrium (70,000 g, 4 h, 4 °C) (Surespin Sorvall rotor), 12x1 ml fractions were harvested, precipitated by 100 % Trichloroacetic acid (TCA), and dissolved in 45 µl of 2x Laemmli buffer and boil for 5-10 min at 95 °C and validated by immunoblots (Genz et al., 2013). The flotation assays with each lipid composition were repeated at least 3 times.

3.14 **Dynamic light scattering (DLS) and zeta potential measurements**

The size and the zeta potential of the liposomes were characterized with Zetasizer Nano ZS (Malvern Instruments, UK). The size of the liposomes was measured as a quality control with DLS. The DLS describes the hydrodynamic radius and the polydispersity index (PDI) of the suspended particles. The charge of the liposomes was determined by zeta potential measurements. The surface charge of charged particles in a liquid suspension is not possible to measure directly, because counter-ions of the solution are attached to the surface of the particles, forming an electric double layer. Instead, the potential difference between the mobile fluid and the layer attached to

the surface can be measured, and this physical quantity is called the zeta potential. If an electric field is applied to the suspension, the charged particles start to move in the direction of the field. The speed of the charged particles is measured with laser-Doppler velocimetry and the zeta potential is calculated using the Smoluchowski equation:

$\zeta = 4\pi\mu\eta/\varepsilon$

Where μ is the electrophoretic mobility, η is the viscosity of the solvent and ε is the dielectric constant (Kincses et al., 2020). Three biological replicates were averaged; each replicate was the average of 5 measurements (11-15 runs in each measurement).

3.15 **Urea wash of liposomes**

For urea wash, the liposomes were incubated with *Drosophila* or human Syntaxin 17 proteins in a binding buffer. After incubation the liposomes were pelleted at 90,000 g using TH-641 Sorvall ultracentrifuge rotor. The supernatant was discarded, and the pellet was resuspended either in a binding buffer (serves as a control) or in 8M urea, pH 7-7.5 and incubated for 20 min at 4 °C (Zhao et al., 2004). The washed liposomes were pelleted again. After the ultracentrifugation, the supernatant was completely removed. The resuspended pellets (in binding buffer) together with the supernatant fractions were TCA precipitated and the proteins were detected by Western blotting, using specific antibodies against *Drosophila* and human Syntaxin 17 proteins.

3.16 **Cell culture, plasmids, and transfection**

HEK-293 and U2OS cells were cultured in Dulbecco's modified eagle's medium (DMEM) (high glucose) (Sigma # RNBL1426) supplemented with 10000 IU/ml penicillin, 10000 µg/ml streptomycin (Lonza # 9MB103), and 10 fetal calf serum (OPTI clone, Invitrogen). For starvation, the cells were washed 2 times with PBS and incubated 1 h with phenol red-free Hank's balanced salt solution (HBSS) (SIGMA). We applied standard cell culture starvation protocol from the literature, which means that after excessive washing steps, the cells are supplemented with an HBSS medium containing salts and glucose and free of phenol red and amino acids. I optimized starvation conditions for cell culture by testing different time frames such as 30 min, 45 min, and 1 h. The highest number of autophagic structures was observed in 1 h of starvation condition samples, so this was used for further experiments.

The following plasmids used for the transient transfection were purchased from Addgene—pmRFP-LC3 (21075): pMRXIP mTurquiose2-Syntaxin 17 (89938): pEGFP-2xFYVE (140047):

GFP P4M SidM (51471): mEGFP-PI(3,5)P_2 (92419): pEX-YFP-hLC3WT (24989): mCherry-P4M-SidM (51471). The cells were cultured on coverslips in 6 well cell culture dishes (600,000 cells / well) or confocal dishes (150,000 cells).

Transfection was done 24 – 48 h after cell seeding. 1 to 2 µg of plasmid DNA was used. Transfection was carried out at around 80 % confluency TransIT-LT1 transfection reagent (Mirus # 22084721) pursued by the manufacturer's instructions. 24 h post-transfection, cells were starved for 1 h with a phenol red-free HBSS (SIGMA). Cells were treated with chemical inhibitor 10 µM NC03 (PI4K2A inhibitor) (AOBIOUS; AOB17420) (30626625) for 10 min in the case of HEK cells and 20 min for U2OS followed by imaged immediately. For bafilomycin A1 treatment, 100 nm bafilomycin A1 (B1793, Sigma) was used in HBSS for 1.5 h. For the live imaging of U2OS cells, cultures were subjected to time-lapse microscopy starting from 30 min of starvation. For MitoTracker Green co-staining, transfected U2OS cells were incubated with 100 nM MitoTracker Green FM (Invitrogen, M7514) for 30 min at 37 °C.

3.17 **siRNA transfection**

HEK-293 cells were seeded in 6 well plates and grown up to 70 % confluence. Cells were transfected twice with 30 pmol siSTX17 (antisense: 5' AATTAAGTCCGCTTCTAAGGTTTCC 3', sense: 5' GGAAACCTTAGAAGCGGACTTAATT 3', Integrated DNA Technologies, with a four-day interval with the help of Lipofectamine RNAiMAX (Invitrogen, 13778). 3 days after final transfection, cells were either processed for validation of knockdown by western blotting or seeded in confocal dishes for transfection with rescue constructs.

3.18 **Immunoblotting for human cell samples**

HEK-293 cells as well as the shPI4K2A cells were grown in a 60 mm diameter plate. The cells were grown in normal growth media (as described above in Mammalian cell culture, plasmids, and transfection section) or starved in HBSS for 1 h before harvesting them. HEK-293 cells were treated or not with 10 µM of NC03 inhibitor for 20 min. shPI4K2A knockdown cells were induced or not by adding doxycycline (Sigma-Aldrich, D9891) at 2 µg/ml for five days in the culture medium. The cells were collected in PBS (Capricorn Scientific, PBS-1A) (centrifuged at 500 g, for 5 min, 4 °C) and lysed for 45 min (on ice) in 50 µl of RIPA buffer (NaCl 150 mM, Nonidet P-40 1 % [Sigma-Aldrich, H3375], SDS 0.1 % [Sigma-Aldrich, 151-21-3], Tris (pH 7.4) 50 mM [Sigma-Aldrich, 77-86-1]) containing protease inhibitor cocktail (Sigma- Aldrich, P8340). After

lysis, the cells were centrifuged at 15 000 g, 10 min at 4 °C. The supernatant was boiled for 10 min at 95 °C in an equal volume of 2x Laemmli buffer. The following antibodies were used: anti-STX17 antibody (Sigma, HPA001204) [1:1000] and TUBA/alpha-tubulin antibody (Thermo Fisher, 62204) [1:5000].

3.19 PI(4)P immunostaining

Cells were seeded in confocal dishes to 70 % confluence and starved with HBSS for 1 h. Afterwards, cells were fixed with 4 % paraformaldehyde (Avantor, 50-00-0) in PBS and immunostained for anti PI(4)P antibody (Echelon Biosciences, Z-P004) [1:500], anti-mouse Alexa Fluor 488 secondary antibody (Invitrogen, A-11001) [1:800] and mounted in Vectashield mounting solution (Vector Laboratories, H-1000-10). Cells were imaged in a confocal microscope as described in the microscopy section.

3.20 Microscopy

Cultured cells were imaged on a Zeiss Axio Observer.Z1 equipped with an LSM 800 confocal module using a Plan-Apochromat 63x/1.40 oil DIC M27 objective and appropriate excitation /emission settings for mTurquoise2, GFP and RFP. Equal acquisition settings were used for all samples/treatments/genotypes within an experiment. *Drosophila* adipose tissue was imaged on a Zeiss Axioimager M2 equipped with an Apotome2 module and an ORCA Flash 4.0 LT sCMOS camera (Hamamatsu) using Plan-Apochromat 63x/1.40 oil DIC M27 objective. Live imaging of U2OS cells was carried out on an Olympus IX83P1ZF widefield microscope equipped with an ORCA Fusion BT sCMOS camera (Hamamatsu) using UPLXAPO 60X/1.42 oil objective.

3.21 Quantification and statistical analysis

Images were processed with the Zeiss Zen Blue software to adjust histogram and to remove background. Puncta colocalization (e.g. fusion) was measured by first applying a 'Local Maxima' filter in ImageJ to isolate LC3+ structures (Cutoff=80), and this selection was restored in other channels. After auto thresholding, colocalized puncta number was counted after a size cutoff based on vesicle size (0.12-2.5 μm^2). Non-puncta, pixel-based colocalization (e.g. mitochondria vs. STX17) was performed by measurement of Pearson's colocalization coefficient by using the 'Coloc2' plugin in ImageJ. Data from microscopy experiments are representative of at least two independent replicates. GraphPad Prism v8 was used for statistical analyses of microscopy data. For pairwise comparisons, Shapiro-Wilk normality test was first performed on the dataset. If the

normality test passed (p<0.05), data were analyzed by Student's t-test; otherwise, Mann-Whitney test was used. Differences were counted as significant if p<0.05. Number of cells (N) measured for each plot are indicated in corresponding figure legends. Statistical data for western blot analysis were obtained by Li-COR ImageJ software. The signal intensity was measured for each fraction on the blot. Then the sum of the floated fractions was divided by the sum of 12 fractions. Finally, the percentages were calculated.

Lipid statistical analyses were carried out using Microsoft Excel, and OriginPro 8, and treated statistically by a t-test at a significance level of at least $p < 0.05$, defined by Microsoft Excel. Significance levels in figures are designated as *$p < 0.05$, **$p < 0.01$, ***$p < 0.005$.

3.22 **Bioinformatic analysis**

3.22.1. **Databases**

Amino acid sequences were downloaded from the UniProtKB database (Bateman et al., 2021). For homology searches the UniRef50 database (standalone, version 2020_06) (Suzek et al., 2015) was used as a comprehensive and non-redundant UniProtKB reference cluster (clustering UniRef90 seed sequences at least 50 % sequence identity and 80 % overlap with the longest sequence in the cluster).

3.22.2. **Software**

PSI-BLAST (Position-Specific Iterated-Basic Local Alignment Search Tool) (standalone, version 2.11.0+) (Altschul et al., 1997) was applied for homology search against the UniRef50 database. The searches were carried out with the following parameters: the substitution matrix was BLOSUM45, (Henikoff & Henikoff, 1992) threshold of E-value was 0.01, no filter of complexity region was applied, and the number of iterations was 5. Simultaneous prediction of secondary structures and trans-membrane spans was carried out by the artificial neural network technique, BCL:Jufo9D (standalone, version 4.0.0) (Leman et al., 2013).

3.22.3. **Data handling and analysis**

The amino acid sequences were used in fasta format for PSI-BLAST and BCL::Jufo9D. Sorting, selection and analysis of outputs were carried out with Igor Pro (Wave Metrics, Lake Oswego, Oregon 97035, USA).

3.22.4. **Structural models**

The C-terminus of human (a.a. 219-302) and *Drosophila* (a.a. 213-301) Syntaxin 17 was extracted from AlphaFold models AF-P56962-F1-model_v4.pdb and AF-Q9VZC9-F1-model_v4.pdb, respectively (Varadi et al., 2022). To generate alternative conformations, local AlphaFold runs using only these C-terminal sequences with full database option were performed as described earlier (Hegedűs et al., 2022). The structures with the highest pLDDT scores were used in MD simulations. The same C-terminal Arg and Lysine residues as in experiments were mutated in CHARMM-GUI to build the arginine and lysine replaced with an alanine residue (R/K>A) -STX17 constructs (Jo et al., 2017).

3.22.5. **Molecular dynamic simulations**

The simulation systems were prepared using CHARMM-GUI. The structural models of Syntaxin 17 C-terminus were oriented during the process manually and visually to be close to the membrane bilayer without lipid interactions and to minimize system size. The luminal and the cytosolic leaflet contained 90:10 POPC:POPE and 80:10:10 POPC:POPE:POPI14, respectively (POPC: 1-palmitoyl-2-oleoyl-sn-glycero-3-phosphocholine, POPE: l-palmitoyl-2-oleoyl-phosphatidylethanolamine, and POPI14/PI(4)P: 1-hexadecanoyl-2-(9Z-octadecenoyl)-sn-glycero-3-phospho-(1'-myo-inositol-4'-phosphate)). The N-terminus was patched with ACE (acetyl) groups. KCl at a concentration of 150 mM was used. Grid information for PME (Particle-Mesh Ewald) electrostatics was generated automatically, and the number of particles, pressure of 1 bar, and temperature of 303.15 K were constant. GROMACS 2022 with the CHARMM36m force field was used to run molecular dynamics simulations (Huang et al., 2017). Each system was energy minimized using the steepest descent integrator, which stopped when the largest force in the system became less than 500 kJ/mol/nm. To increase sampling, two simulations were forked for each energy-minimized system, with different random velocities. Equilibration was performed in six steps and each production run was run for 2 μs. The corresponding parameter files are also

available for download. The trajectories were analyzed using MDAnalysis (Michaud-Agrawal et al., 2011) and NumPy. Molecular visualization was performed using PyMOL (Schrödinger, LLC). Graphs were generated using Python and its matplotlib library [10.1109/MCSE.2007.55].

4. RESULTS

The lipid-protein investigations are an essential aspect of studying the role of lipids in the recruitment of Syntaxin 17 to autophagosomes. To achieve this, it is necessary to understand the lipid composition of autophagosomes to mimic an *in vivo* lipid environment. However, the lipid profile of autophagic membranes at different stages, such as phagophores, autophagosomes, and autolysosomes, is poorly characterized. Therefore, I initiated my PhD project with establishing a method to isolate intact autophagic membranes from *Drosophila* starved adult control flies (+/+; 3xmCherry-Atg8a; +/+) and Atg2^{-} flies, followed by deciphering their lipid profile.

4.1 Isolation of intact autophagic vesicles from *Drosophila*

The isolation of autophagic structures was performed using *3xmCherry-Atg8a* transgene carrying control and Atg2^{-} *Drosophila* 4 h starved adult flies. The autophagic structures were enriched during starvation. We could isolate autophagosomes and phagophores from the control flies while majorily phagophores from Atg2^{-} flies. Due to the absence of Atg2, autophagosomes are not formed, resulting in the accumulation of stalled phagophores. This phenomenon has been observed in *Caenorhabditis elegans*, in mammalian cells, as well as in *Drosophila* (Lu et al., 2011; Velikkakath et al., 2012; Nagy et al., 2013).

4.1.1. Immunopurification of autophagic structures by RFP-trap

The Red fluorescent protein-trap (RFP-trap) magnetic agarose beads were used to pull down intact autophagic structures from the cytosolic fractions. The cryohomogenized fly lysates were enriched with *3xmCherry-Atg8a* containing autophagic structures upon starvation. These structures are recognized by anti-RFP which is covalently linked to magnetic agarose beads. Pre-clearing of the lysates by binding control magnetic agarose beads was performed to avoid unspecific organelle membrane bindings. The intact autophagic vesicles were eluted from the RFP-trap magnetic agarose beads by pH shift and used for the characterization of their lipid composition (Fig. 14A).

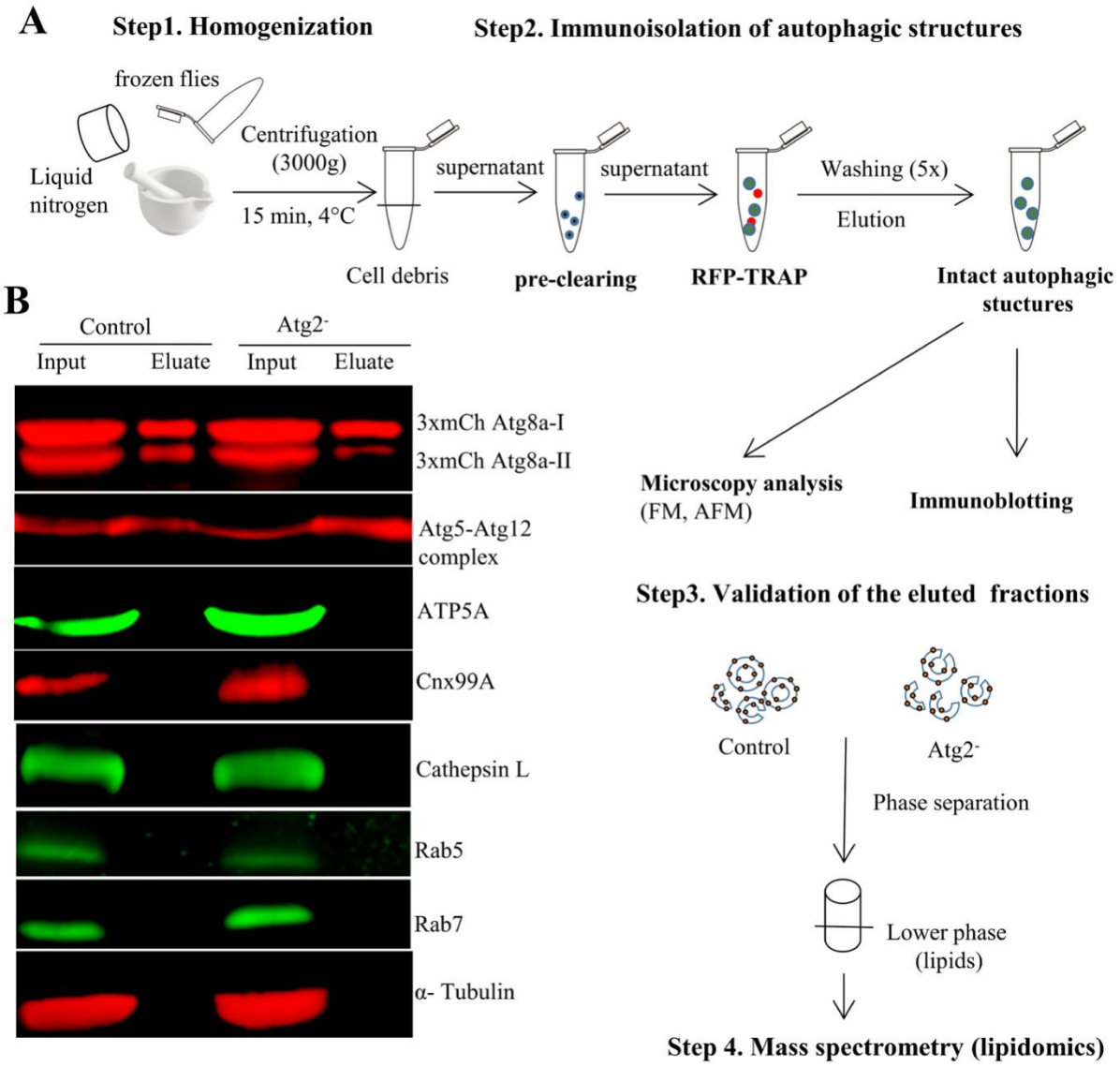

Figure 14: Illustration of an established method for the isolation of autophagic structures and their validation.
A) Schematic representation of the main steps of isolation of autophagic structures from control and Atg2⁻ starved adult flies. B) Western blots of inputs and eluted fractions screened for autophagy and other organelle markers.

4.1.2. Validation of isolated intact autophagic structures by western blot

The eluted fractions along with pre-cleared lysates were validated by western blot. The autophagy marker proteins such as 3xmCherry-Atg8a-I and II and the Atg5-Atg12 complex (a common marker for the early autophagic structures) were enriched in our eluted fractions (Fig. 14B). To ensure the high degree of purity of isolated membranes, western blots were performed for a wide

range of other organelle-specific marker proteins namely, mitochondria (ATP5A), ER (Cnx99A), lysosomes (Cathepsin-L), early (Rab5), and late endosomes (Rab7) (Fig 14B). All these markers are present in the lysates but not seen in the eluted fractions.

4.1.3. Validation of isolated intact autophagic structures by epifluorescence microscopy

Though western blot provides information that the eluted fractions are enriched with our interested autophagy marker proteins such as 3x mCherry-Atg8a, the eluted fractions were further validated by epifluorescence microscopy to ensure these proteins are associated with the vesicles. A big variety of 3xmCherry-Atg8a decorated autophagic vesicles with an average size of 400 nm to 600 nm from both control and Atg2^{-} eluted fractions are observed (Fig. 15A, B). Semi-circle (phagophores) and about to seal or sealed (autophagosomes) are seen in the control and predominantly phagophores with lower average size (approximately 400 nm in diameter) are seen in the Atg2^{-} eluted fractions.

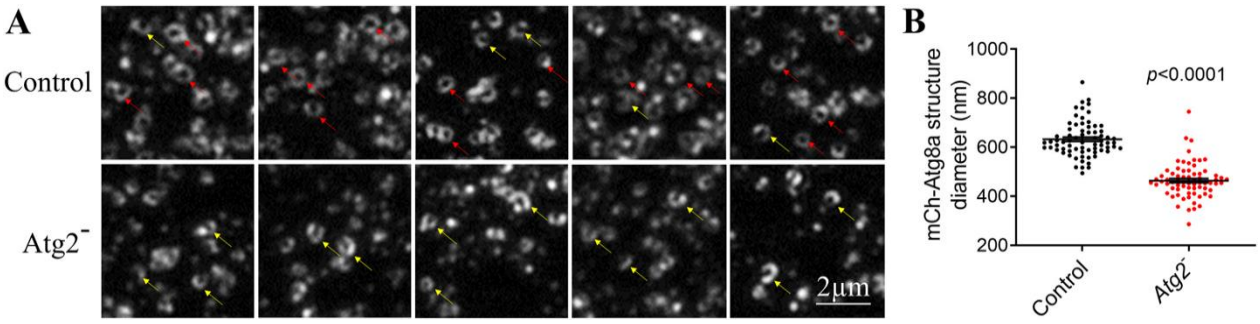

Figure 15: Visualization of isolated autophagic structures by fluorescent microscopy.
A) Visualization of immunoprecipitated autophagosomes, phagophores from the control and Atg2^{-} by fluorescent microscopy. Red arrows represent autophagosomes (closed or about to sealed vesicles) and yellow arrows represent semi-circle-like structures called phagophores. B) Diameter of mCherry-Atg8a structures (n = 70) isolated from control and Atg2^{-}. Statistical testing: Mann-Whitney U test.

4.1.4. Validation of isolated intact autophagic structures by Atomic Force Microscopy (AFM)

The eluted fractions were validated by AFM to confirm the presence of the double membrane containing vesicles. AFM is a useful technique to supplement the monitoring of vesicle-like structures. The instrument provides accurate three-dimensional data, simplifying the process of characterizing their size and volume, without the need for complicated post-processing. The eluted fractions from the control have shown the presence of round-shaped objects with a size of a few

hundred nanometres in diameter (Fig. 16A). The height of the flattened vesicles is slightly above 20 nm (Fig. 16B), which is roughly four-fold the thickness of a lipid bilayer (Szegletes et al., 2011).

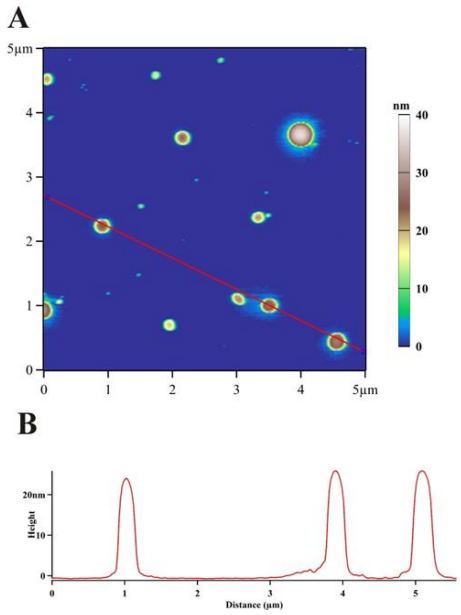

Figure 16: AFM confirmed the presence of double-membrane vesicles in eluted fractions.
A) Visualization of the presence of double-membrane vesicles in the eluted fractions by AFM. B) Peak showing the height of 20 nm in diameter of each vesicle.

4.2 Lipid profiles of autophagic membranes isolated from control and Atg2^{-} *Drosophila*

The lipids were extracted from the isolated autophagic vesicles from both control and Atg2^{-} flies after ensuring the presence of intact vesicles in the eluted fractions. The tandem mass spectrometry method was approached to identify the lipid composition of autophagic membranes. The amount of lipids was first normalized to the internal standards added in known amounts and secondly normalized to the protein content of the eluted fractions. The lipidomics data was carefully filtered and also excluded the possible overlapping species.

4.2.1. Phospholipids, the backbone of autophagic membranes

Based on the applied lipid isolation and lipidomic methods, around 70 phospholipid species that compose autophagic membranes were identified in both control and Atg2^{-}. The control lipidomics data showed 67 mol % of PE, followed by 16 mol % PC, 9 mol % of PI, 2 mol % of PS, and 5 mol

% of PA (Fig. 17A). In contrast Atg2⁻ structures showed a significant increase of PI, PS, and PI followed by PE lipid species. The level of PC lipid groups remained the same. The lipidomics data exhibited the presence of various fatty acid chain lengths containing lipid species ranging from 32 carbon atoms to 38 carbon atoms (Fig. 17B). The longer fatty acyl chains are abundant in Atg2⁻ whereas shorter fatty acyl chains are dominant in the control autophagic membranes (Fig. 17B).

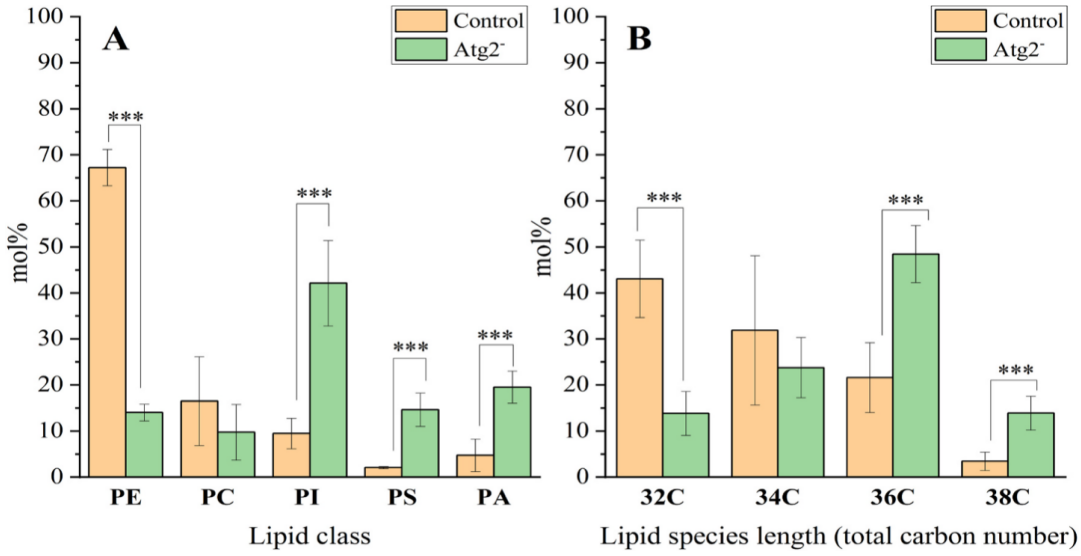

Figure 17: Phospholipid profiling of isolated autophagic membranes.
*A) The main lipid classes composing autophagic membranes from the control and Atg2⁻. B) Representing the fatty acid chain length of total lipid species belonging to various head groups. Mol % distribution data are means ± SD (n = 3 for control and n = 4 for Atg2⁻ flies). Statistically significant differences (based on t-tests) in figures are designated as *** for p < 0.005.*

4.2.2. **Detailed profile of specific phospholipid species of autophagic membranes**

The lipidomics data identified a wide variety of lipid species which is variable with their level of abundance, fatty acyl chain length, and the number of double bonds in each phospholipid class. PE, PC, and PS showed a big variety of lipid species than the PI and PA (Fig. 18A-E). The level of monounsaturated PE (32:1, 34:1) and polyunsaturated PE (32:2, 36:4) species was found significantly decreased in the Atg2⁻ compared to the control (Fig. 18A). The variety of lipid species belonging to PC did not show a significant increase or reduction but the following PC lipid species were missing: 36:0, 38:4, 38:3, 38:2 38:1 in Atg2⁻ (Fig. 18B) flies. In contrast, longer fatty acyl chain lengths containing PI species (36:3, 36:2, 36:1, 38: 2, 38:1) significantly increased but some PI species, such as 34:2 is reduced and 34:1 were missing in Atg2⁻ (Fig. 18C). Surprisingly

the negatively charged lipid species including PS (34:1, 36:5, 36:0) and PA (32:2, 32:1, 34:3, 34:1, 36:3) are also predominantly rich in Atg2⁻ lipidomics data compared to control (Fig. 18D and E).

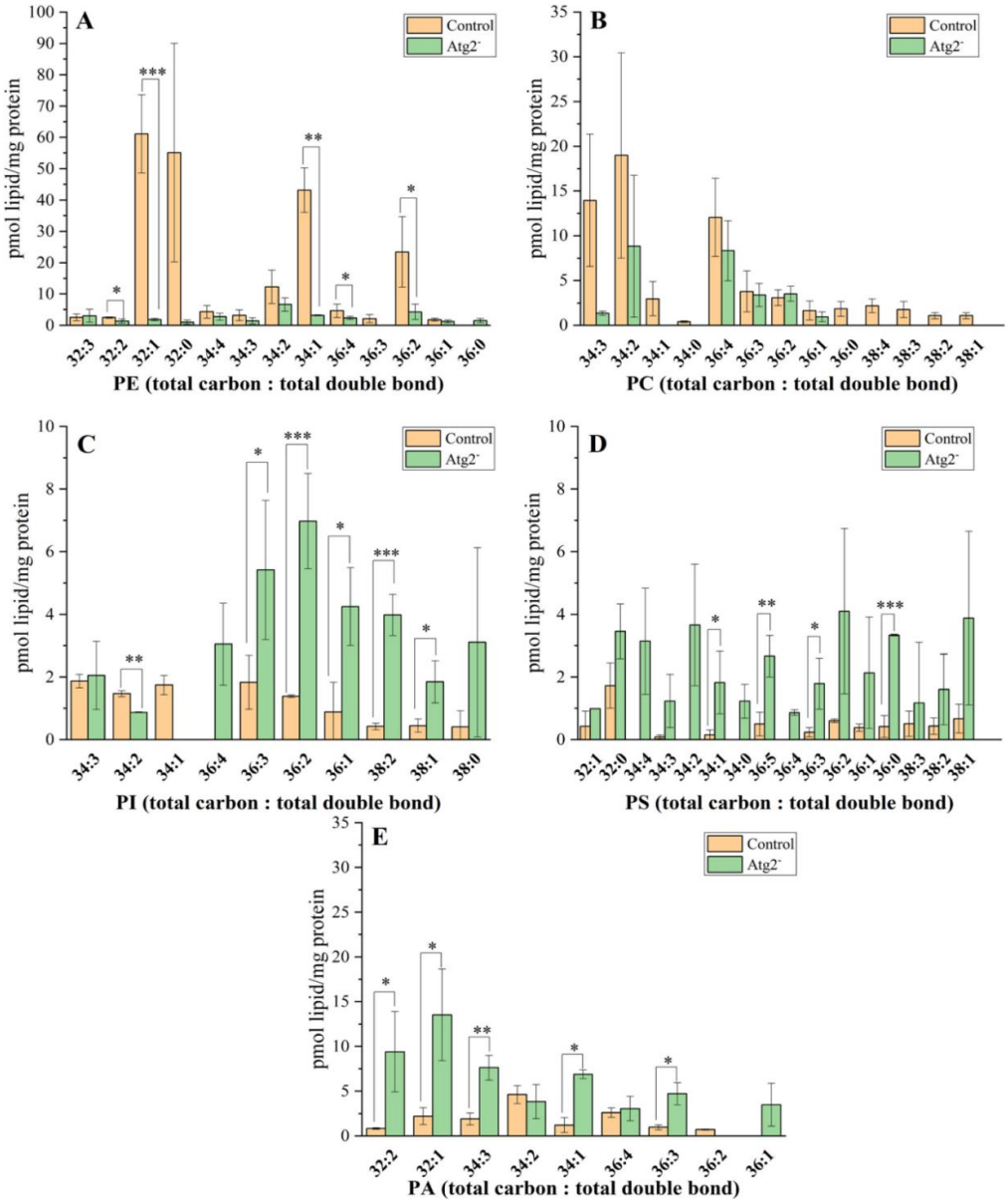

Figure 18: Detailed phospholipid species profiling of autophagosomes from *Drosophila*.

*Amount of lipid species belonging to PE (panel A), PC (panel B), PI (panel C), PS (panel D) and PA (panel E) lipid classes. Data are means ± SD (n = 3 for control and n = 4 for Atg2⁻). Absolute lipid amounts in pmol are normalized to the protein content of the eluted autophagy membrane fractions. Significance levels (t-test) in figures are designated as *p < 0.05, **p < 0.01, ***p < 0.005. Lipid species are denoted as total carbon number: total double bond. The identified lipid species belong to the following lipid classes: PE (phosphatidylethanolamine); PC (phosphatidylcholine); PI (phosphatidylinositol); PS (phosphatidylserine); PA (phosphatidic acid).*

4.2.3. **Autophagic membranes are highly unsaturated**

The degree of unsaturation of the autophagic membranes was investigated by calculating the mol % of lipid species belonging to saturated (no double bonds) and unsaturated (one or more double bonds) (Fig. 19A, B). The autophagic membranes from control flies consist of almost a third of unsaturated lipid species (63.4 %). Autophagic membranes from Atg2^{-} are comprised of even more highly unsaturated lipids (86 %) (Fig. 19A). The significant differences is shown also statistically in Fig. 19B.

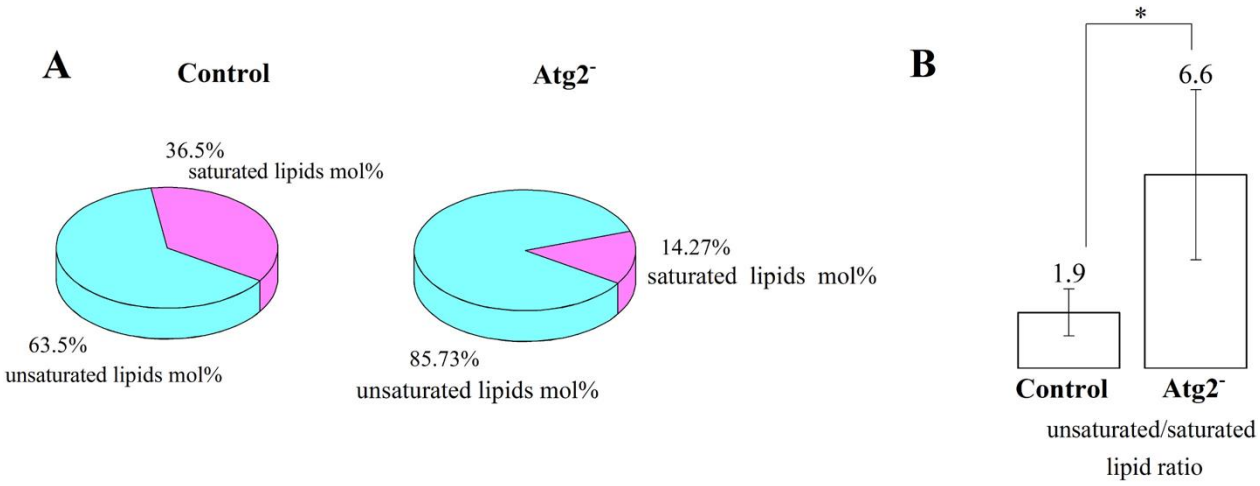

Figure 19: Autophagic membranes are highly unsaturated.
*A) The mol % distribution of saturated and unsaturated total lipids of isolated autophagic structures from control and Atg2^{-}, based on the average of three biological replicates. B) Unsaturated versus saturated lipid ratios were calculated from the total identified lipid species. Data are mean ± SD (n = 3 for control and n = 4 for Atg2^{-} flies). The significance level (t-test) is designated as *p < 0.05.*

4.3 Syntaxin 17 interacts with negative phospholipids *in vitro*

Knowing the lipid composition of the autophagosomes helped us to move on to one of the main objectives of this study, which is determining the functional role of lipids in the recruitment of Syntaxin 17 to the autophagosomes. To answer this, we primarily conducted the lipid-protein investigations *in vitro* using a liposome flotation assay method. To study the association of Syntaxin17 proteins with artificial membranes (liposomes), we cloned, expressed, and purified the wild-type, full-length *Drosophila* Syx17 and human STX17. The purified recombinant proteins and extruded liposomes were used to perform the liposome flotation assay, a reliable biochemical method that assesses protein-membrane association by their co-flotation during gradient centrifugation. To ensure the reliability of the results obtained by the liposome flotation assay

ATG3, a known membrane associating autophagy related protein (Nath et al., 2014) was used as a positive control and GST, a globular protein that does not associate with the membranes was used as a negative control (Fig. 20A). The *in vitro* spontaneous membrane binding ability of purified proteins was investigated with the liposomes composed of total lipids extracted from *Drosophila* adult flies and MCF7 cells. Both Syx17 and STX17 were detected in the liposome floated fractions 1-6 and 1-4 respectively, similar to the positive control (Fig. 20B). When the proteins alone were tested (without liposomes), they were found in the non-floated fractions as expected (Fig. 20A, B, No liposome (control)). To gain more information about specific interacting lipids, liposomes were generated using synthetic lipids with several combinations. The membrane loading of Syx17/STX17 was efficient when the molar ratios of negative lipids were increased (Fig. 20B). Subsequently, the negative charge of extruded liposomes was investigated by measuring the zeta potential values using a Zetasizer (Fig. 20C).

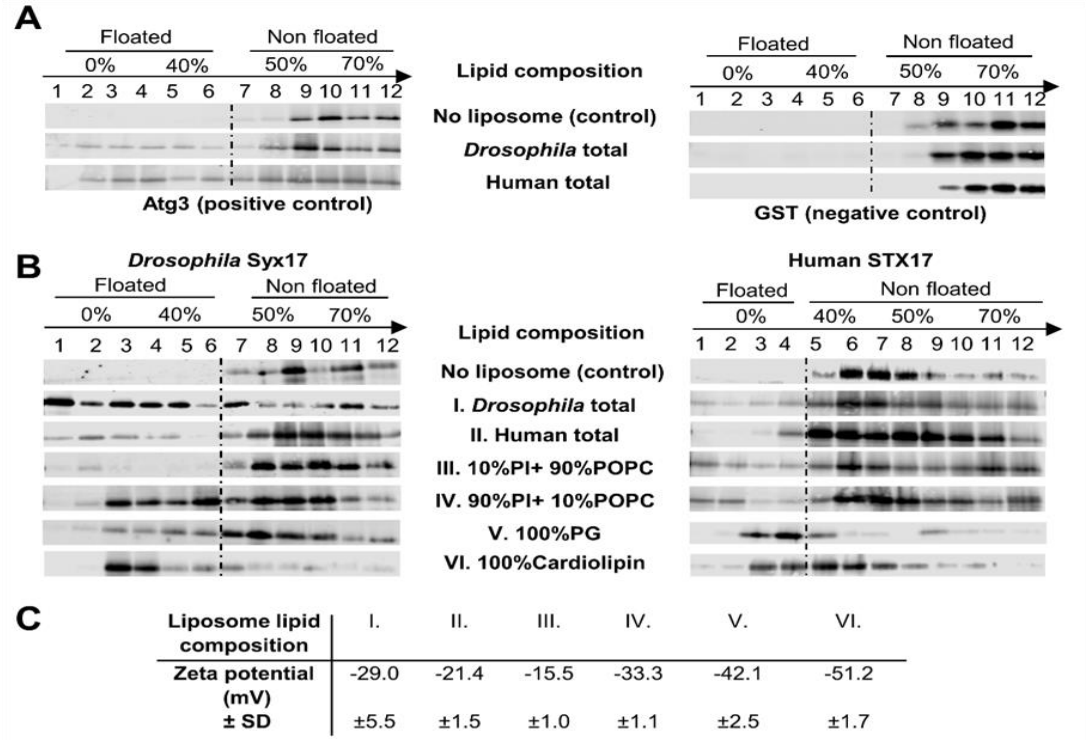

Liposome lipid composition	I.	II.	III.	IV.	V.	VI.
Zeta potential (mV)	-29.0	-21.4	-15.5	-33.3	-42.1	-51.2
± SD	±5.5	±1.5	±1.0	±1.1	±2.5	±1.7

Figure 20: Soluble Syx17/STX17 interacts with negative lipids.
A) Immunoblots for flotation experiments of positive and negative control. B) Soluble Syx17/STX17 associates with negatively charged lipids. C) Measured zeta potential values of extruded liposomes.

Having observed a preference for negatively charged lipids by both human and fly STX17, we were curious about their interaction with autophagosomal lipids. *In vitro* reconstitution

experiments represent a fundamental and widely used approach in molecular biology and biochemistry. These experiments are utilized to mimic biological processes outside of living organisms, typically in a controlled environment such as a test tube. The *in vitro* reconstitution autophagosome mimicking experiments were conducted based on our recently published wild-type autophagosome lipid profile data from *Drosophila* (Laczkó-Dobos et al., 2021). Both soluble Syx17 and STX17 show the membrane binding with the reconstituted autophagosomes (Fig. 21A).

The obtained *in vitro* data underscores the importance of negatively charged lipids for recruiting Syntaxin 17 to autophagosomes. This led to further exploration of the interactions between Syntaxin 17 and potentially relevant negatively charged signaling lipids that appear on autophagic structures, such as PI(3)P, PI(4)P, and PI(3,5)P_2. To answer this, initially, we prepared liposomes that were electrostatically neutral to study their interaction with Syntaxin 17 proteins. The results showed that the neutral liposomes did not associate with either of the Syntaxin 17 proteins (Fig. 21B). However, the recruitment of Syntaxin 17 occurred upon the addition of the above-mentioned PIPs to the neutral liposomes. Specifically, the presence of PI(3)P, PI(4)P, and PI(3,5)P_2 enhanced the membrane binding of STX17 (Fig. 21B), whereas Syx17 only interacted with PI(4)P and PI(3,5)P_2, but not PI(3)P (Fig. 21B). The negative charge of these liposomes is confirmed by their Zeta potential values (Fig. 21C). However, the association of Syntaxin 17 with vesicles containing PIP did not display a direct relationship with the vesicles' negative charge, as evidenced by the data presented in (Fig. 21B, C). This led to the conclusion that not only the general negative charge but also the specific lipid composition are crucial factors in the recruitment of STX17.

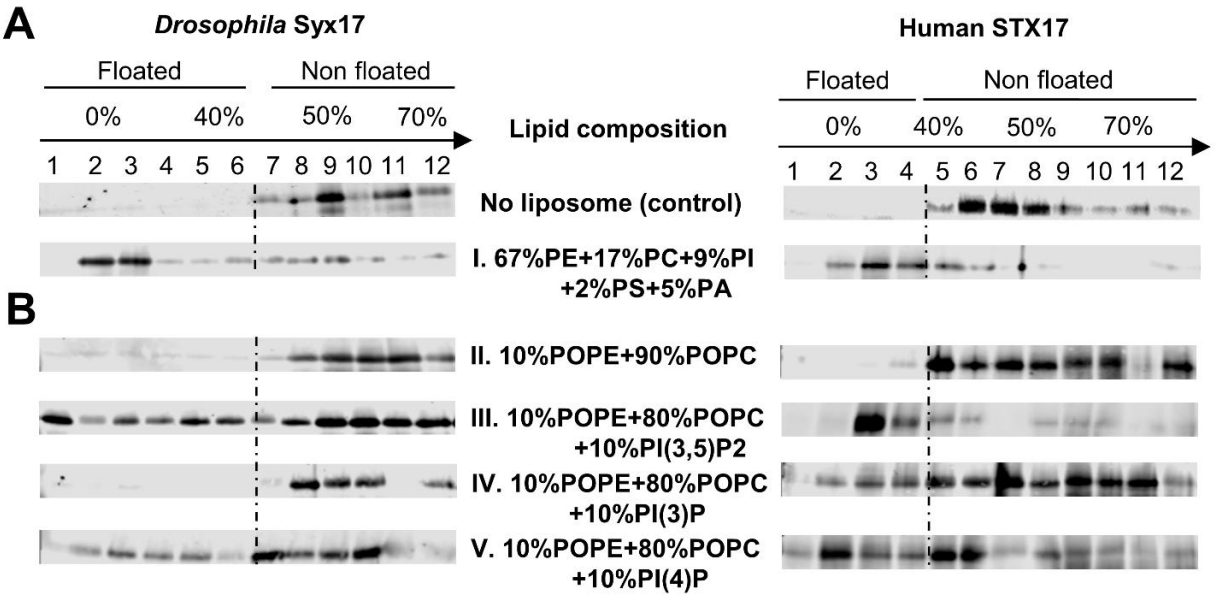

C

Liposome lipid composition	I.	II.	III.	IV.	V.
Zeta potential (mV)	-23.9	-1.4	-37.9	-30.0	-26.8
± SD	±0.9	±0.5	±4.3	±0.7	±1.8

Figure 21: PIPs promoting the recruitment of Syx17/STX17.
A) Immunoblots for autophagosome reconstitution experiments with Syx17/STX17. B) Syntaxin 17 proteins do not interact with neutral liposomes, while the addition of PI(3)P, PI(4)P or PI(3,5)P_2 results in clear protein recruitment (except for fly Syx17 and PI(3)P). (C) Liposome zeta potential values show the electrostatic charge of vesicles.

After confirming the significant role of PIPs during the Syntaxin 17 membrane association *in vitro*, we were curious about how deeply Syx17/STX17 proteins are integrated into the membrane. Therefore, we performed urea wash experiment, a reliable method used to strip peripheral membrane-associated proteins (Zhao et al., 2004). Urea is a chaotropic agent that can disrupt the weak interactions formed between peripheral proteins and lipid bilayer. Notably, the immunoblots of urea wash fractions show that Syx17/STX17 proteins remained in the liposomes even after such a harsh wash, suggesting that they are strongly associated with the membranes (Fig. 22A).

Further we aimed to determine whether a physiological parameter called membrane curvature plays a role in the recruitment of Syntaxin 17. Proteins can be recruited to membrane regions where curvature is naturally present, such as during vesicle formation, or they can actively induce curvature to create specialized membrane compartments for their function. To investigate this, our

approach involved performing flotation assays with generated liposomes of varying sizes (50 nm, 100 nm, 800 nm) and GUVs of 1 micron, under the premise that smaller liposomes exhibit higher membrane curvature. The analysis of the immunoblots from the flotation assay fractions revealed no discernible differences in the recruitment of STX17/Syx17 proteins across liposomes of different sizes (Fig. 22B). This finding indicates that the interaction between STX17/Syx17 proteins and membranes is predominantly influenced by electrostatic interactions, rather than membrane curvature.

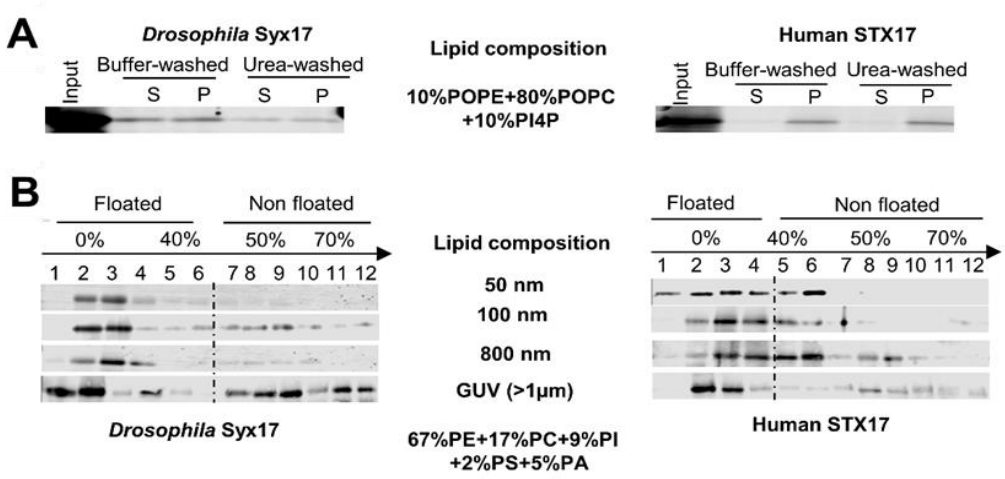

Figure 22: Syx17/STX17 autophagosomal recruitment is not membrane curvature dependent.
A) Immunoblots for urea wash experiments showing the integration of Syx17/STX17 into the liposomes. S-Supernatant and P-Pellet. B) Syx17/STX17 recruits in a membrane curvature non-dependent manner.

4.4 Co-localization of PIPs with LC3-STX17 positive structures in HEK-293 cells

After confirming that Syx17/STX17 binds spontaneously with liposomes containing PI(3)P, PI(4)P, and PI(3,5)P_2 *in vitro*, we decided to investigate their subcellular co-localization with LC3 and STX17 positive structures in mammalian cells. We used specific fluorescent reporters for the above-mentioned PIPs, LC3, and STX17 and followed their co-localizations upon starvation conditions. We found that PI(4)P reporter SidM is always co-localized with LC3 and STX17 positive structures in 1 h starved HEK-293 cells, while PI(3)P and PI(3,5)P_2 exhibited much lower co-localization (Fig. 23A, B). Based on our obtained subcellular co-localization findings and data

from the literature, we schematized the localization of PIPs on various stages of autophagic structures such as phagophores, autophagosomes as autolysosomes (Fig. 23C).

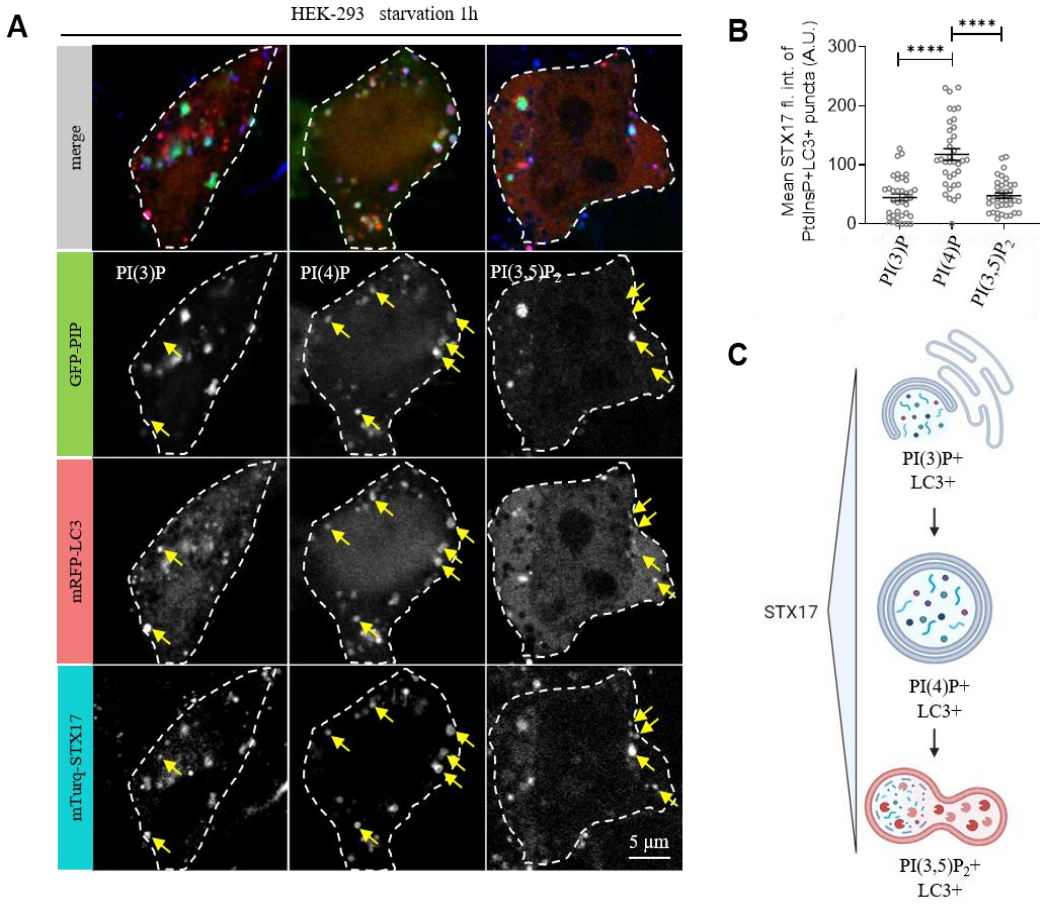

Figure 23: STX17 localization to PI(4)P positive autophagosomes.
*A) Co-localization analysis of mTurquoise-STX17 (cyan), RFP-LC3 (red) and selected phosphoinositides (green) using GFP-2xFYVE for PI(3)P, GFP-SidM for PI(4)P, and GFP-MLN1x2 for PI(3,5)P_2 in 1h-starved HEK-293 cells. Arrows point to the location of selected LC3+ dots in each channel. B) Background-subtracted fluorescence intensity of mTurquoise2 (for Syntaxin 17) on PIP-positive LC3 structures was quantified. N=37 for PI(3)P; N=36 for PI(4)P; N=38 for PI(3,5)P_2. ****p<0.0001. Error bars represent ± standard error of means. C) Diagram illustrates the stepwise maturation model of phospholipid content on LC3-positive autophagic structures. Syntaxin 17 fluorescence intensity on LC3-positive autophagic structures clearly corresponds to the presence of PI(4)P.*

Further, the live imaging in U2OS cells also supported the concomitant appearance of PI(4)P and STX17 on LC3 positive structures (Fig. 24A). Parallelly, the fat cells of starved *Drosophila* larvae exhibited the extensive co-localization of PI(4)P probes with Atg8a and Syx17 positive structures (Fig. 24B).

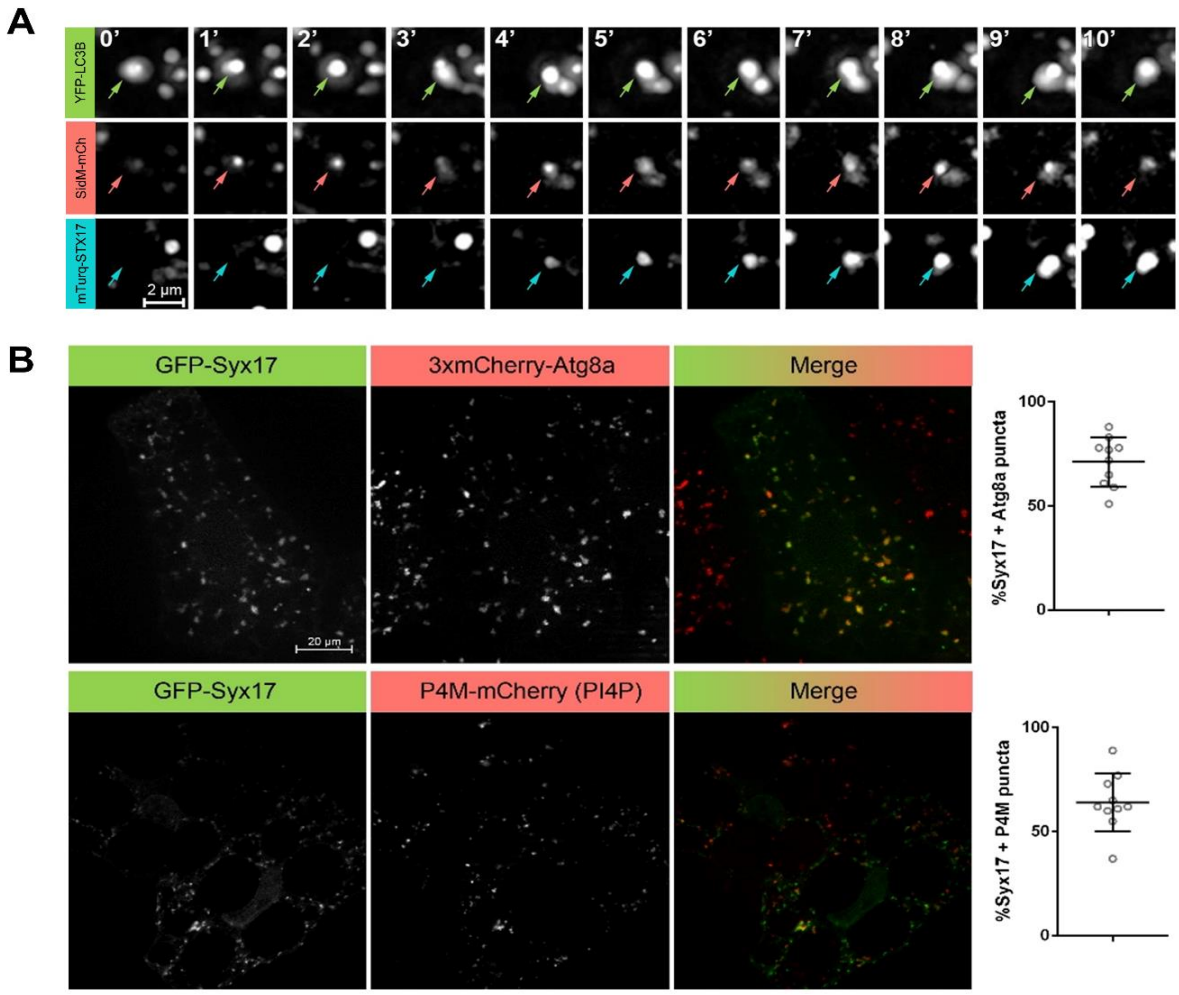

Figure 24: Live imaging of PI(4)P and Syntaxin 17 on autophagosomes in human cells and PI(4)P, Syx17, and Atg8 co-localization detection in *Drosophila*.
A) Live imaging of YFP-LC3 (autophagosome), SidM-mCherry for PI(4)P and mTurquoise-STX17 in 30 min starved U2OS cells. Panels show individual channels in 1 min intervals. Arrows indicate an autophagosome that first becomes positive for PI(4)P, followed by STX17. B) GFP-Syx17 and 3xmCherry-Atg8a reporters show clear overlap in fat cells of 3h-starved Drosophila larvae (top row, please note that the Syx17 reporter is only expressed in a single cell-clone while the endogenous promoter-driven Atg8a reporter is expressed in all cells). The majority of GFP-Syx17 dots are positive for the PI(4)P reporter P4M-mCherry in the adipose tissue of 3 h starved larvae (bottom row). Quantifications show the percentages of dots with overlapping reporters compared to all puncta per cell, N=10 cells. Error bars in panels represent ± standard error of means.

The co-localization analysis suggests PI(4)P might serve as the autophagosome maturation signal aiding in the recruitment of STX17 to fully formed autophagosomes. PI4K2A has been identified as the primary lipid kinase responsible for generating PI(4)P on mature autophagosomes, which promotes the fusion of autophagosomes with lysosomes during the autophagy pathway (Wang et

al., 2015). This led us to speculate that blocking the fusion step might result in PI(4)P accumulation on autophagosomes. To test this hypothesis, we inhibited the fusion between autophagosomes and lysosomes in HEK-293 cells using Bafilomycin A1, which resulted in the expected accumulation of autophagosomes. These accumulated LC3 positive structures showed co-localization with the PI(4)P marker SidM (Fig. 25A, B). Furthermore, we assessed the overall PI(4)P levels in HEK cells under starvation conditions and observed a significant elevation compared to cells that were not starved (Fig. 25C, D). The observed co-localization of PI(4)P with LC3-positive structures, coupled with its increased levels during starvation, strongly supports the notion that PI(4)P plays a crucial role in the recruitment of STX17 to autophagosomes.

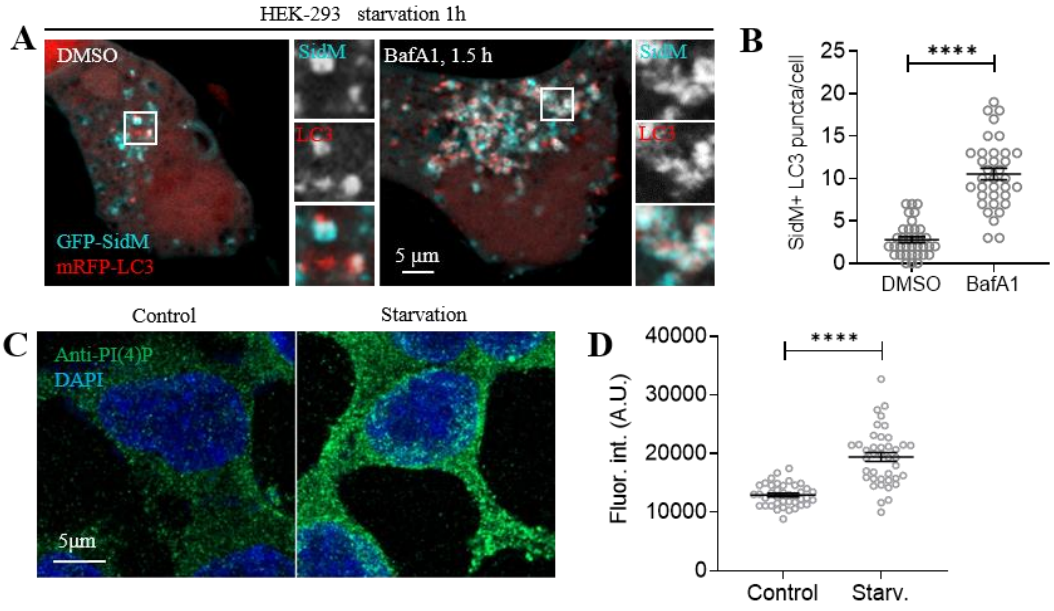

Figure 25: PI(4)P accumulates on autophagosomes.
*A) Blocking autophagosome-lysosome fusion with bafilomycin A1 treatment leads to the accumulation of mRFP-LC3+ autophagosomes, most of which contain PI(4)P (marked by GFP-SidM). B) Quantification of LC3+ SidM+ puncta per cell in control and BafA1-treated cells. N=35, DMSO; N=35, BafA1. C) Immunostaining of control and 1 h starved HEK-293 cells with an anti-PI(4)P antibody. D) Quantification of total cellular fluorescence of PI(4)P. N=40 for both. ****p<0.0001.*

4.5 Blocking PI(4)P synthesis on autophagosomes impaired STX17 recruitment

Further, we were curious how the PI(4)P depletion on autophagosomes influence STX17 recruitment to the autophagosomes. Previous studies had shown that silencing *PI4K2A* impaired the PI(4)P generation on autophagosomes (Wang et al., 2015; Sun et al., 2022). Therefore, we

generated the stable HEK-293 cells for inducible shRNA knockdown of PI4K2A and investigated. As expected, the long-term PI(4)P depletion on autophagosomes is indeed observed in stable PI4K2A knockdown HEK-293 cells compared to control cells (Fig. 26C). This reduction in PI(4)P adversely affected the fusion of autophagosomes with lysosomes, as evidenced by a significant decrease in co-localization of LC3 and STX17 (Fig. 26D). Consequently, we noted an accumulation of RFP-LC3 positive vesicles that lacked both STX17 and SidM markers (Fig. 26A). These findings indicate that the recruitment of STX17 to autophagosomes is significantly hindered by the depletion of PI(4)P, highlighting its crucial role in this process (Fig. 26A-D).

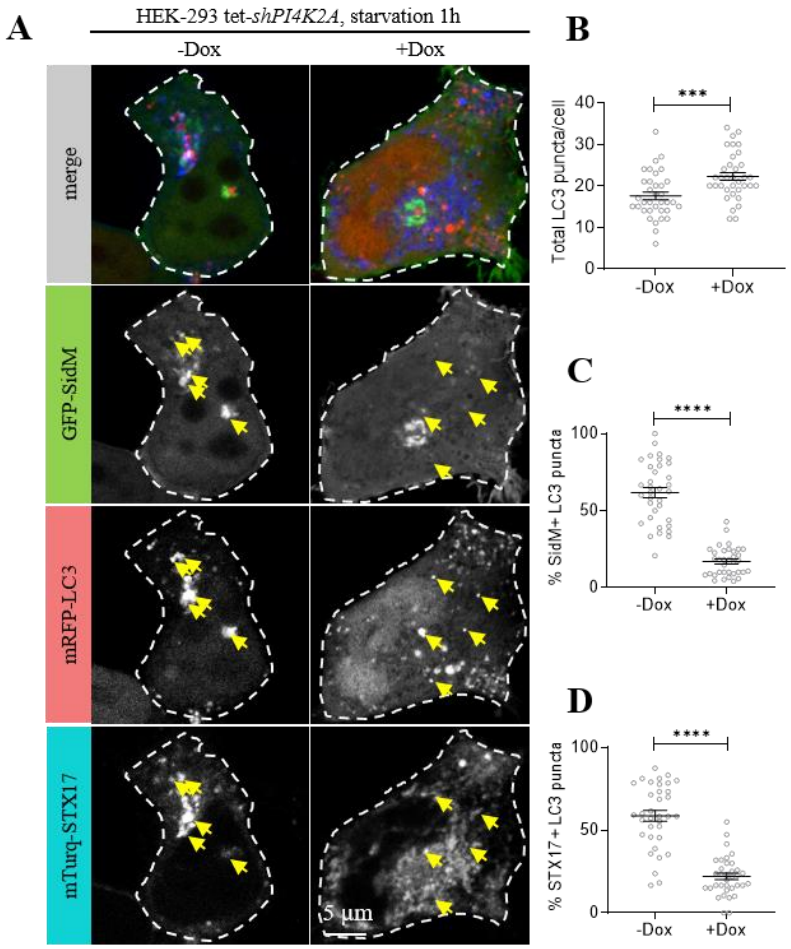

Figure 26: PI(4)P generated by PI4K2A promotes STX17 recruitment to autophagosomes.
*A) PI4K2A-silenced cells (+Dox) show impaired autophagosomal PI(4)P generation and Syntaxin 17 recruitment compared to control (-Dox) after 1 h starvation. Arrows point to the location of selected LC3+ dots in each channel. B) Quantification shows an increased number of LC3 puncta in shPI4K2A cells, consistent with an autophagosome-lysosome fusion defect. **p=0.0026. C) SidM+ LC3 puncta per cell. ****p<0.0001. D) STX17+ LC3 puncta per cell. ****p<0.0001. N=35, -Dox, N=35, +Dox for panels B-D.*

However, to prevent the complications caused by long-term PI(4)P depletion, we have employed a specific PI4K2A chemical inhibitor called NC03. This inhibitor can quickly deplete the PI(4)P pool specifically generated by PI4K2A (Sengupta et al., 2019). A 10-minute treatment of NC03 in HEK cells resulted in a noticeable decrease in autophagosomal PI(4)P levels without altering the abundance of LC3 puncta (Fig. 27A-C). Consequently, we observed a disruption in the recruitment of STX17 to autophagosomes (Fig. 27D), as evidenced by the reduced number of co-localizing puncta for STX17 and LC3 in cells treated with NC03 compared to the control group (Fig. 27A). These findings, whether through knockdown of PI4K2A or rapid chemical inhibition of PI(4)P, highlight the critical role of PI(4)P in recruiting STX17 to autophagosomes during the process of autophagy.

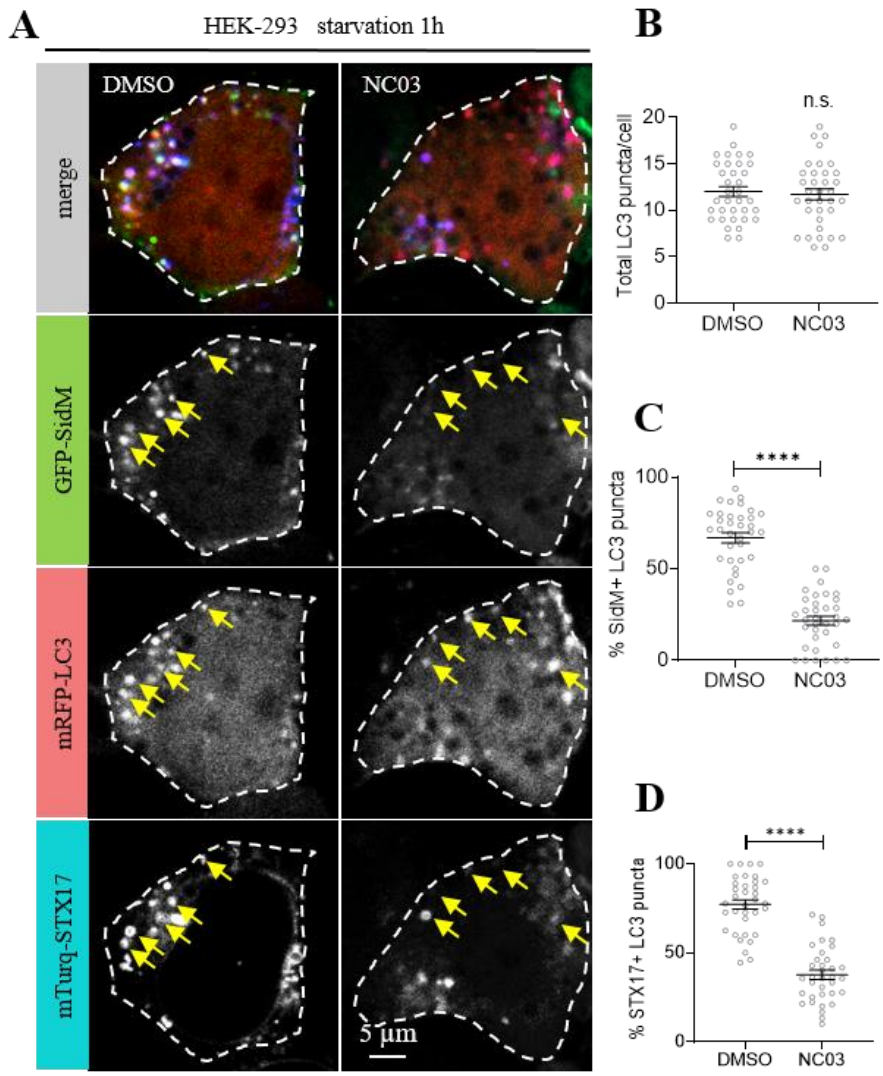

Figure 27: Autophagosomal PI(4)P is required for STX17 recruitment.
*A) Colocalization analysis of GFP-SidM for PI(4)P, mRFP-LC3 (autophagosome) and mTurquoise2-STX17 in 1 h-starved HEK-293 cells. 10 min treatment with the small-molecule PI4K2A inhibitor NC03 eliminates PI(4)P from autophagosomes and causes a concomitant defect in STX17 autophagosomal recruitment when compared to mock treated cells (DMSO). Arrows point to the location of selected LC3+ dots in each channel. B) Quantification of the total number of LC3-positive autophagic puncta. N=35 for DMSO and N=35 for NC03. C) Quantification of the percentage of PI(4)P-positive autophagosomes. N=35 for both. D) Quantification of the percentage of STX17-positive autophagosomes. N=35 for both. ****: $p<0.0001$, ns: $p>0.05$. Error bars represent ± standard error of means.*

The next question that raised was whether the PI(4)P depletion affects only autophagosomal STX17 recruitment or also its recruitment to the other pools, such as mitochondria. To answer this question, the investigation was carried out on U2OS cells to obtain the best visualization of the mitochondrial network. In 1 h starved U2OS cells, NC03 treatment showed a similar effect as in

HEK cells. However, the treatment of NC03 affected only the STX17 autophagosomal recruitment (Fig. 28B, C), but not the mitochondrial pool (Fig. 28A, D). This suggests that PI(4)P has a potential signaling role in the STX17 recruitment specifically to autophagosomes during autophagy

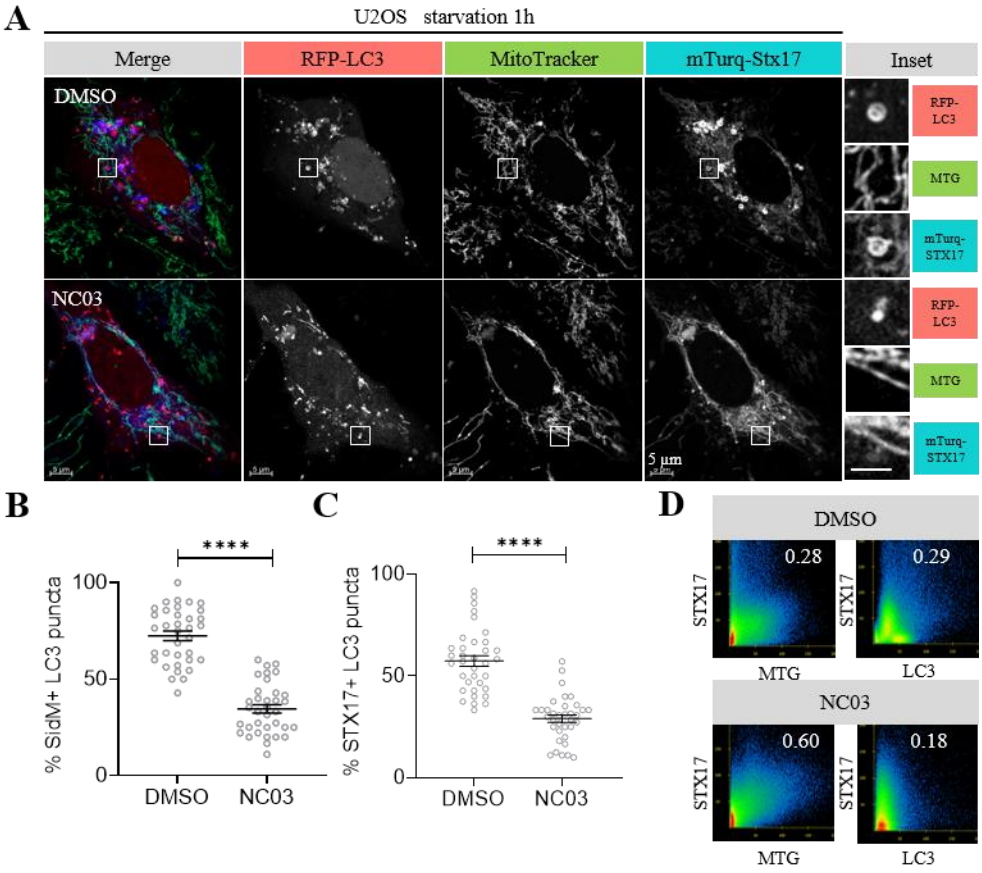

Figure 28: PI(4)P generated by PI4K2A is dispensable for STX17 recruitment to the mitochondria.

*A) STX17 co-localizes with both LC3-positive autophagic vesicles and Mitotracker Green (MTG)-positive mitochondria in mock treated (DMSO) 1 h starved U2OS cells. Only the autophagosomal pool of STX17 is affected by short-term (20 min) NC03 treatment, as its mitochondrial localization remains prominent. B) Quantification shows decreased PI(4)P localization to autophagic vesicles and C) a concomitant decrease of STX17-LC3 co-localization upon 20 min of NC03 treatment. N=35 for DMSO and N=35 for NC03. ****p<0.0001. Error bars in panels M, and N represent ± standard error of means. D) Pearson's correlation analysis of mitochondrial (MTG) or autophagosomal (LC3) versus Syntaxin 17 (STX17) fluorescence.*

We were further intrigued by the question of how PI(4)P depletion affects the total cellular levels (endogenous levels) of STX17. To answer this, the starved doxycycline-inducible shPI4K2A, NC03 treated, and control HEK-293 cells were analyzed by immunoblot. The results showed that neither of them affected the endogenous STX17 levels (Fig. 29).

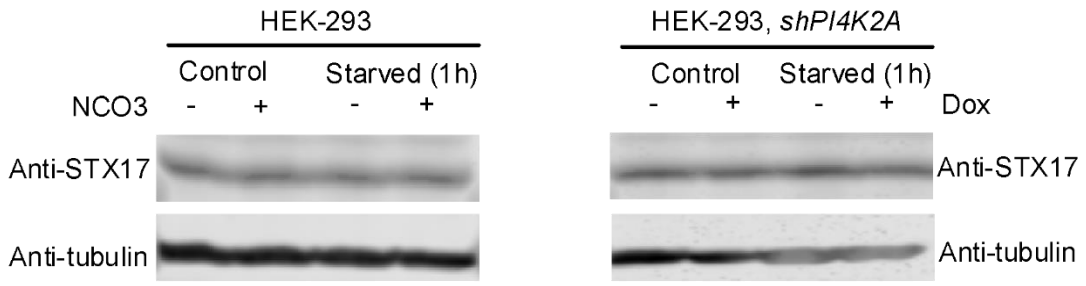

Figure 29: PI(4)P depletion has no impact on endogenous STX17 levels.
Endogenous Syntaxin 17 levels were monitored by western blot in HEK-293 cells treated with NC03 (PI4K2A inhibitor; 10 µM, 20 min), and doxycycline-inducible shPI4K2A cells.

4.6 Molecular dynamic simulations and mutagenesis

After confirming the role of PI(4)P in the STX17 autophagosomal recruitment, we were interested to know about the specific regions of Syntaxin 17 that mediate its PI(4)P binding of the autophagosomal bilayer. To answer this, we used both molecular simulation modelling and cellular mutagenesis methods. Molecular simulation studies are computational approaches that provide valuable insights into identifying lipid-binding sites on proteins, which helps to characterize the specificity and affinity of lipid-protein interactions. This information is crucial for understanding the molecular mechanisms that underlie lipid recognition and signalling processes.

The initial bioinformatics analysis were predicted the cytosolic versus membrane-binding parts of wild type full length fly and human Syntaxin 17 proteins contain the membrane-binding motif right after the two predicted transmembrane domains while the N-terminal domain and cytoplasmic tail are cytosolic (Fig. 30A). To gain an understanding of the specific amino acids that associate with the membrane, molecular dynamic simulations were ran only for the region that overlapping right after the SNARE domain until the end of the C-terminal region of the both Syntaxin 17 proteins (Fig. 30B). The model membranes using neutral lipid composition showed no interactions with STX17 (Fig. 30C). However, by the addition of PI(4)P to neutral model membranes enabled an electrostatic interaction with positively charged Lys and Arg residues present at the C-terminal parts of Syx17 (electrostatic interactions arised from the basic aminoacids located before the predicted TMDs) and STX17 (electrostatic interactions arised from the basic aminoacids located right after the predicted TMDs), especially when these were situated next to each other (highlighted in red in Fig. 30B, C). The obtained molecular simulation data points to

the importance of basic aminoacids that are present in the specific regions of Syntaxin 17 in its recruitment to the PI(4)P containing model membranes.

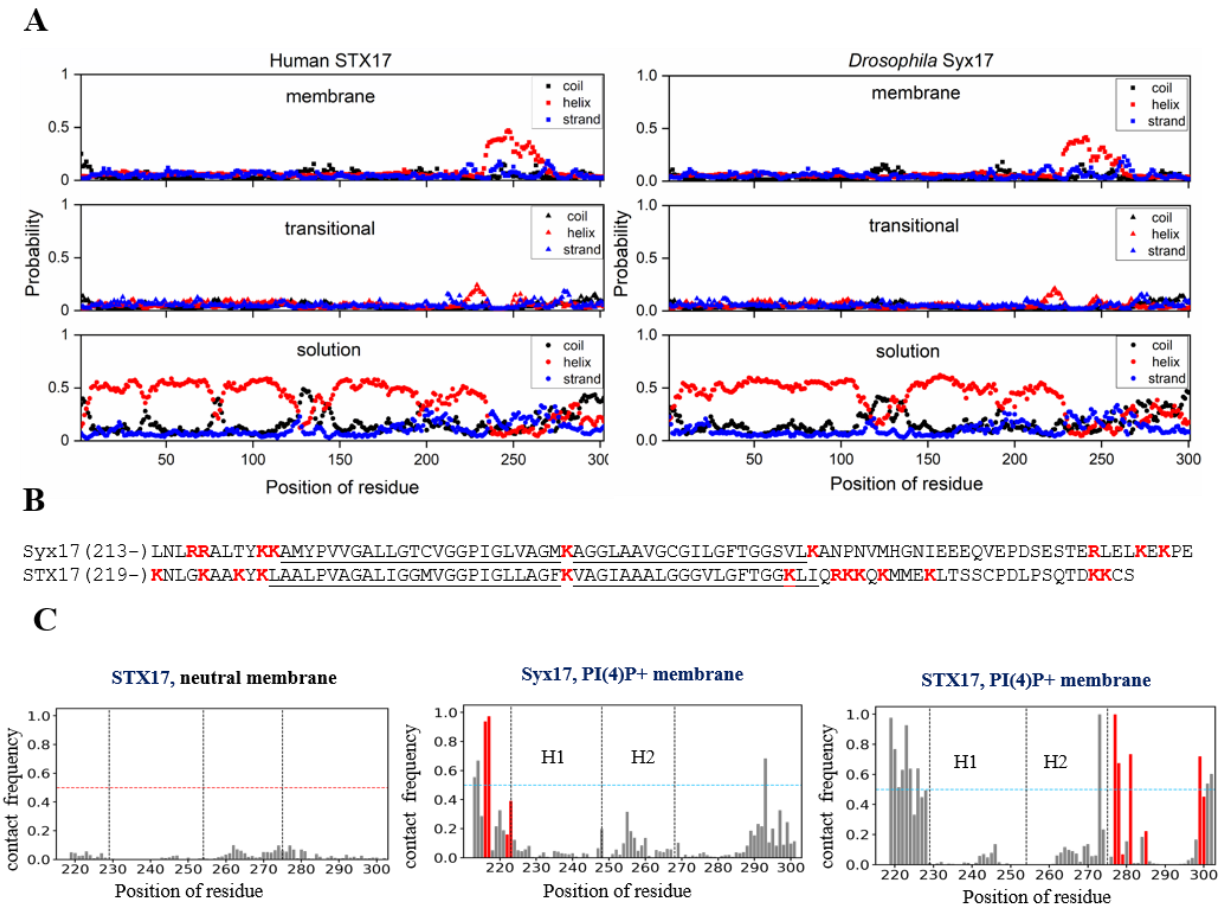

Figure 30: Predicted biochemical features of Syntaxin 17.

A) *Bioinformatic analysis shows the probabilities of secondary structure forms and environment (transmembrane, membrane cytosolic interface / transitional or cytosolic / solution) of full-length Syx17 and STX17 protein sequences. B) C-terminal sequences of Syntaxin 17 proteins that were used in molecular modeling. C) Predicted interactions of C-terminal parts of Drosophila (aa 213-301) and human (aa 219-302) Syntaxin 17 (extracted from AlphaFold AF-Q9VZC9-F1-model_v4.pdb and AF-56962-F1-model_v4.pdb, respectively) with lipid bilayers. STX17 shows no interaction with the membrane electrostatically neutral. Molecular modelling predicts which amino acid residues establish contact with PI(4)P-containing lipid bilayers. Positions of membrane binding involved residues in the STX17 and Syx17 are highlighted in red.*

We further aimed to test the contribution of above mentioned basic amino acids in Syntaxin 17 recruitment to the autophagosomes by cellular mutagenesis methods. Previous mutagenesis experiments revealed that deletion of either TMDs led to a complete cytosolic localization of STX17 while deleting either the first 5 or the last 2 positively charged residues in its C terminus did not prevent the autophagosomal localization of GFP-STX17 in cultured cells (Itakura et al.,

2012). These data motivated us to change all 7 positively charged residues to neutral Ala in the C-terminal part of human STX17 (R/K>A mutant). Briefly, the C-terminal part of human STX17 was mutated by replacing RKK and KK motifs, as well as two single K residues, with “A” (alanine). This led to impaired recruitment of STX17 to the autophagosomes and model membranes (Fig. 31A-C, G). Similarly, *Drosophila* Syx17 was mutated by replacing the RR and KK residues with “A” (alanine) that are present prior to the predicted transmembrane regions. These mutations impaired the protein’s recruitment to autophagosomes both in HEK-293 cells and model membranes (Fig. 31D-E, H). So far, the results confirmed the potential significance of positively charged amino acids in the Syntaxin 17 recruitment to the autophagosomes.

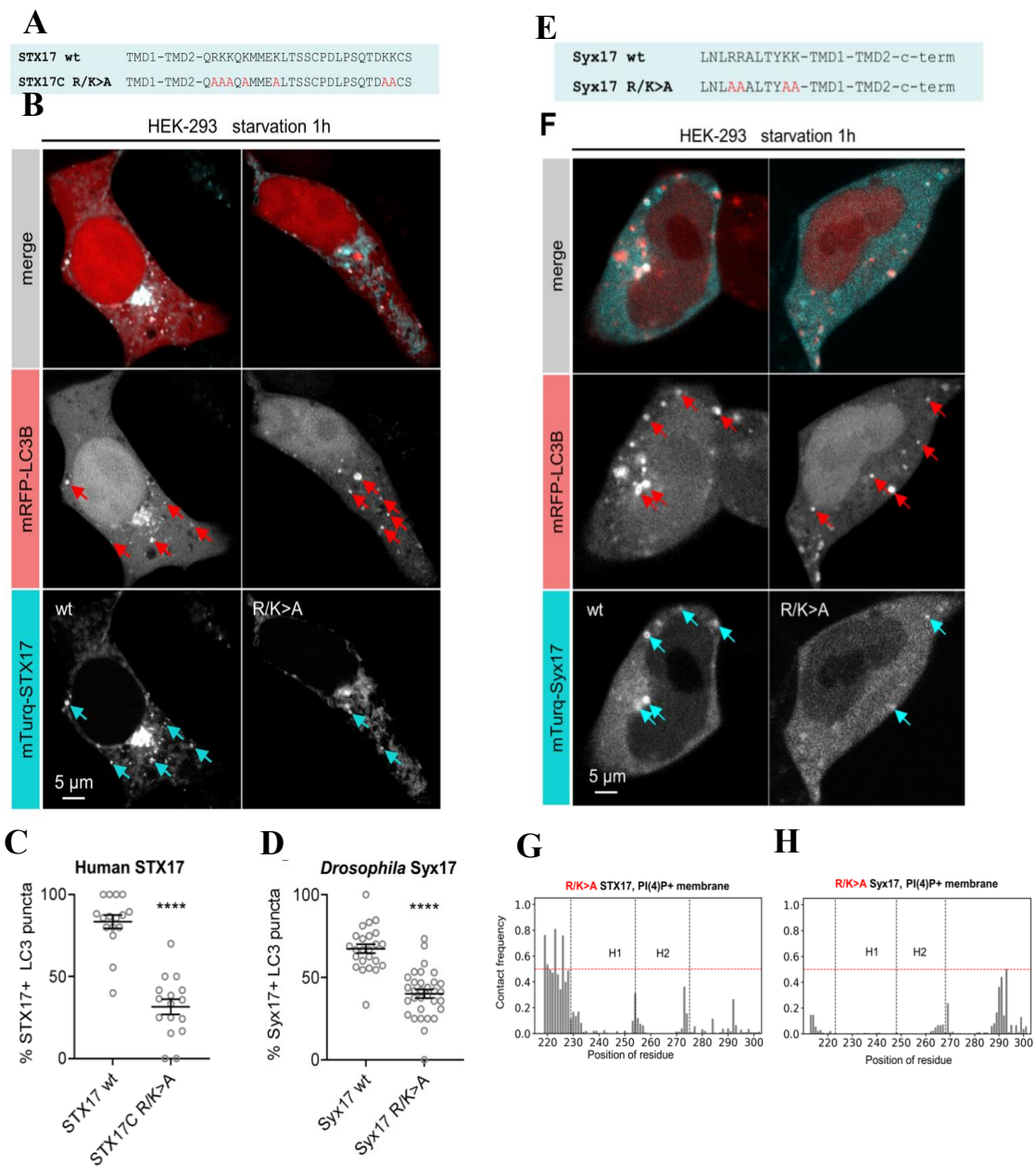

Figure 31: Ala substitution of positively charged amino acid residues near the transmembrane domains of Syntaxin 17 proteins impairs their autophagosomal recruitment.

*A), E) Location of R/K>A mutations following the TM domains in human STX17 and Drosophila Syx17. B) F) Ala substitutions of charged residues in the C-terminus of STX17 and Syx17 impair its recruitment to autophagosomes in 1h-starved HEK-293 cells respectively. Arrows point to LC3+ autophagosomes (red channel) and STX17/Syx17 (cyan channel) colocalizing with these. C) Quantification of the percentage of STX17-positive LC3+ puncta. N=16. **** p<0.0001. D) Quantification of the percentage of Syx17-positive LC3+ puncta. N=24, wt; N=32, Syx17$^{R/K>A}$. **** p<0.0001. Error bars in panels C, G represent ± standard error of means. G), H) Predicted interactions of C-terminal parts of human (aa 219-302) and Drosophila (aa 213-301) Syntaxin*

17 (extracted from AlphaFold AF-Q9VZC9-F1-model_v4.pdb and AF-P56962-F1-model_v4.pdb, respectively) with lipid bilayers. The simulations were prepared using CHARMM-GUI. The luminal and the cytosolic leaflets contained 90:10 POPC:POPE (neutral membrane) and 80:10:10 POPC:POPE:POPI14 (PI(4)P+ membrane), respectively.

Syntaxin17 being a wellknown fusion factor, to confirm the importance of above mentioned basic aminoacids in the fusion of autophagosomes with lysosomes we performed functional tests. To be able to follow the effect of mutated STX17 protein on the fusion process we knocked down the endogenous STX17 expression using a previously published siRNA protocol (Itakura et al., 2012), which resulted in reduced endogenous STX17 protein levels (Fig. 32C) and indeed exhibited the autophagosome-lysosome fusion defect based on decreased co-localization of LC3 and Lamp1 (lysosomal marker) punctae compared to control (Fig. 32A). Notably, the fusion defect of siRNA *STX17* was rescued by expression of siRNA-resistant WT STX17 but not R/K>A mutant STX17 (Fig. 32A, B). This results suggests the significance of basic residues involved in the autophagosomal recruitment of STX17 during autophagy.

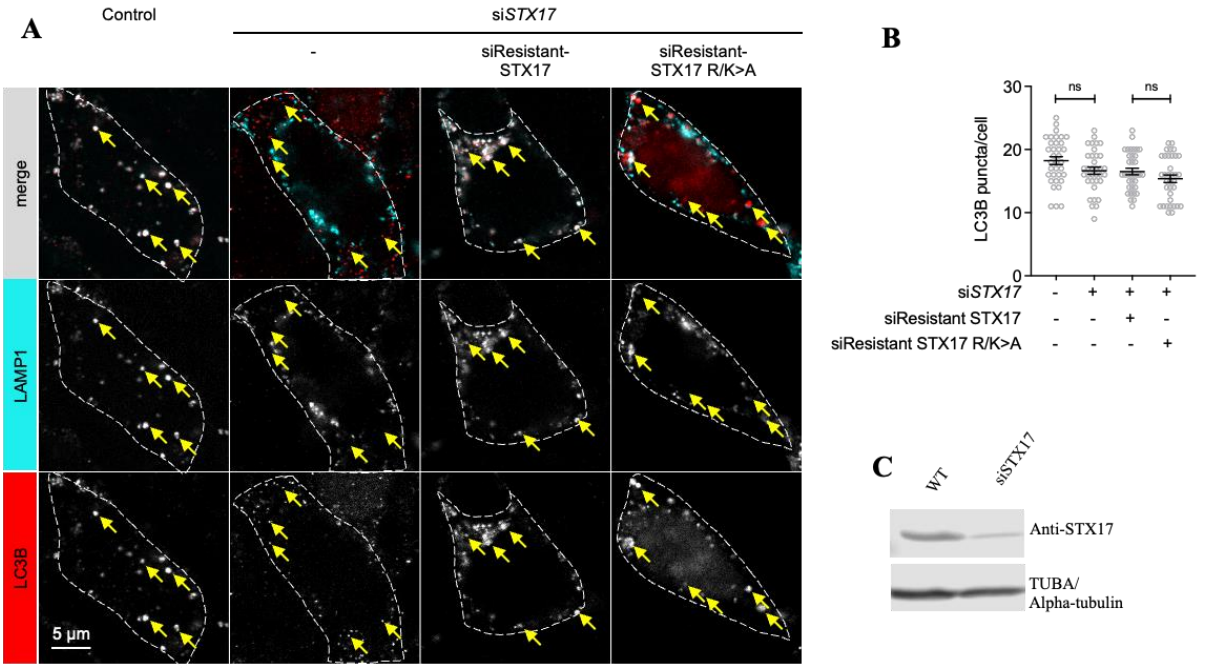

Figure 32: Fusion defect in STX17 C-terminal mutant.
*A) Cells were knocked down for STX17 and subsequently transfected with a siRNA-resistant form of STX17 wild-type or with desired mutations, and co-transfected with mRFP-LC3 and LAMP-mGFP to visualize autophagosome-lysosome fusion (arrows indicate LC3+ autophagosomes in both channels). B) Quantification of fusion between LC3+ autophagosomes and LAMP1+ lysosomes in STX17 knockdown cells, and siRNA-resistant rescue experiments with wild-type or R/K>A mutant constructs. N=36 for all samples. **** p<0.0001. C) Validation of endogenous STX17 knockdown efficiency by immunoblot in HEK-293 cells.*

5. DISCUSSION

Syntaxin17 is a SNARE protein playing an important role in the fusion step of autophagy pathway. Over the past decade, autophagy has been extensively studied, but the role of lipids and their interactions with proteins involved in this pathway have not been fully explored. This study aims to explore the role of lipids in the recruitment of SNARE Syntaxin 17 to the closed autophagosomes both *in vitro* and *in vivo*. To find specific lipid interactors of this protein it would be very useful to know the lipids composing these autophagic structures. However, the exact lipid composition of autophagic structures at different stages (phagophores, autophagosomes, and autolysosomes) remains poorly characterized, especially in flies. To successfully reconstitute autophagosomes *in vitro*, we need to understand their lipid composition. Therefore, this study initiated with establishing a fast, easy, and reliable method to immunoprecipitate autophagic membranes from control and Atg2^{-} starved adult flies and characterize their main phospholipid profile.

We exploited the anti-mCherry coated magnetic agarose beads to pull down the 3x mCherry-Atg8a-containing membranes from the cryo-homogenized control and Atg2^{-} adult starved *Drosophila* lysates. The control flies were used to isolate the various stages of autophagic membranes such as phagophores and autophagosomes, whereas Atg2^{-} flies were used to isolate enriched phagophores, because in the absence of this protein, autophagosomes are not closed resulting in the accumulation of phagophores (Lu et al., 2011; Velikkakath et al., 2012; Nagy et al., 2013;). Later, it was discovered that Atg2 is a lipid transporter protein from ER to the phagophores (Osawa et al., 2020; Ghanbarpour et al., 2021). Autophagy typically occurs at a basic level but can be significantly enhanced by starvation, which triggers the formation of additional autophagic structures. This increase can be monitored by tracking autophagy marker proteins. Conversely, employing chemical inhibitors of autophagy, such as bafilomycin A1, prevents the fusion of autophagosomes with lysosomes. This leads to the accumulation of autophagosomes, although it does not increase their total number. In this study, the flies were starved to enhance the autophagy thus leading to the enrichment of autophagic structures. The isolation protocol was initiated with pre-clearing lysate using control beads to get rid of the nonspecific binding. The successful purification of autophagic membranes in control and Atg2^{-} was ensured by western blot using a specific antibody that recognizes the mCherry-Atg8a. This protein is co-purified with an

early autophagic marker, the Atg5-Atg12 protein complex, which ensures the presence of isolated autophagic vesicles in the eluted fractions. As expected, the autophagy early marker complex is intensified in the Atg2^{-} than in the control eluted fractions demonstrating the enrichment of early autophagic structures (phagophores) (Fig. 14B). The phagophores are enriched in the mutant due to the lack of Atg2 protein whereas in the control different stages of autophagic structures are present. Before the fusion step, the Atg8 proteins are deconjugated from the autophagosomal outer membranes and that can prevent the extraction of autolysosomes and amphisomes (Z. Q. Yu et al., 2012). The high purity of isolated structures in the eluted fractions was confirmed by screening for the specific organelles that establish physical contact with autophagic structures such as ER, mitochondria, lysosomes, and endosomes (Molino et al., 2017) (Fig. 14B). Notably, no detergents were used during the isolation process. In line with this, a high degree of purity and integrity of the membranes were maintained during the isolation method.

Eluted fractions were visualized using fluorescent microscopy to confirm the presence of 3xmCherry-Atg8a positive intact vesicles (open or closed). The vesicles had an average size of 400-600 nm, which is consistent with literature data. Atg2^{-} fractions exhibited an enrichment of smaller vesicles (in the range of 400 nm). The previous *in vitro* studies showed that smaller liposomes are preferred by the Atg2 for its lipid transport activity (Osawa et al., 2019). Three-dimensional structures were visualized using AFM and their membrane heights corresponded to the double membrane nature vesicles.

The lipids were extracted after successful validation and visualization of autophagic structures from the eluted fractions of control and Atg2^{-}. This study focused on the phospholipid composition of phagophores and autophagosomes from adult flies to reduce the contaminants of triacylglycerols from the fat body tissues. The acquired lipid profile of autophagic structures from this study represents the average lipid composition originating from various tissues of the body. PE molecules are the most abundant in control samples (Fig. 17A). It is known that PE molecules are preferred by Atg8 proteins (Yu et al., 2012). During the autophagosome formation, Atg8 proteins form the covalent link that actively changes the membrane properties, and shape (Yu et al., 2012). The preferred fatty acid combinations of PE molecules are not known yet. However, in the control, PE species with 32C or 34C are the most dominant (Fig. 17B). The lipidome of the isolated autophagic structures is highly unsaturated, especially PE and PC has contributed to this high degree of unsaturation in reference to other biochemical methods such as imidazole-buffered

osmium tetroxide impregnation in mouse hepatocytes (Reunanen et al., 1985) and yeast autophagic membranes (Schütter et al., 2020).

Based on the lipidomics analysis, PI lipid class is the most dominant in Atg2^{-} whereas PE in the control (Fig. 17A). The PI is the precursor of PIPs (such as PI(3)P, PI(4)P, PI(3,5)P_2) that are present in autophagic membranes and mainly concerned functional lipids during autophagy. The increased proportions of PS and PA in the Atg2^{-} compared to control contributes to the negative charges of the phagophores in reference with another *in vitro* study that showed the presence of PS in the liposomes promoted the Atg2B lipid transporter activity (Osawa et al., 2020). The isolated membranes from Atg2^{-} are highly unsaturated than the control that mainly caused by the enrichment of polyunsaturated PS (36:5), PI (36:2, 36:3) and PA (34:3) species (Fig. 18). The membrane fluidity correlates with the degree of unsaturation. Double bonds in fatty acyl chains create kinks, resulting in loosely packed membranes and increased fluidity (Skowronska-Krawczyk & Budin, 2020). These properties of the membrane support to recruit downstream Atg proteins and fasten the reorganization of the membranes to enclose the cytoplasmic cargo (Hansen et al., 2018). The highly curved nature of the autophagic membranes in Atg2^{-} is shown by increased levels of PA (Fig. 17A). The PA has vital roles in the generation of membrane curvature due to its structure (Moon et al., 2020). Surprisingly, PE is reduced in Atg2^{-} compared to the control. This suggests that Atg2 may transports PE molecules from the ER to phagophores. This is in line with the latest published results showing the crystallized structure of PE with Atg2 (Osawa et al., 2019). The yeast Atg2A has the preference to bind mainly PE, and PC lipid molecules and less PI or PS (Valverde et al., 2019). Although there is no significant drop in PC levels due to the lack of Atg2 protein, some species of PC with 36:0, 38:4, 38:3 and 38:2 fatty acyl chains are missing in the Atg2^{-} compared to the control. All this information suggests the possible preferences of Atg2 protein in lipid transport roles *in vivo*. The longer fatty acyl chain containing lipid species is more abundant in the Atg2^{-} than in control flies indicating their distinct physiological properties. The autophagic structures from Atg2^{-} are 5-fold highly unsaturated than the autophagic structures isolated from the control (Fig. 19B). Fig. 33 illustrates the concept behind the isolation of these membranes and emphasises the benefits of using Atg2^{-} flies such as lipid composition is revealed for the enriched phagophores and could show the consequences of lack of Atg2 on the level of lipid composition. The distinctive differences in the lipid patterns indicate the potential role of the Atg2 protein, as well as the dynamic lipid characteristics that cause remodeling

effects during phagophores maturation and closure of autophagosomes. Overall lipidomics data reveals the phospholipid composition of different stages of autophagic structures (such as phagophores, and autophagosomes).

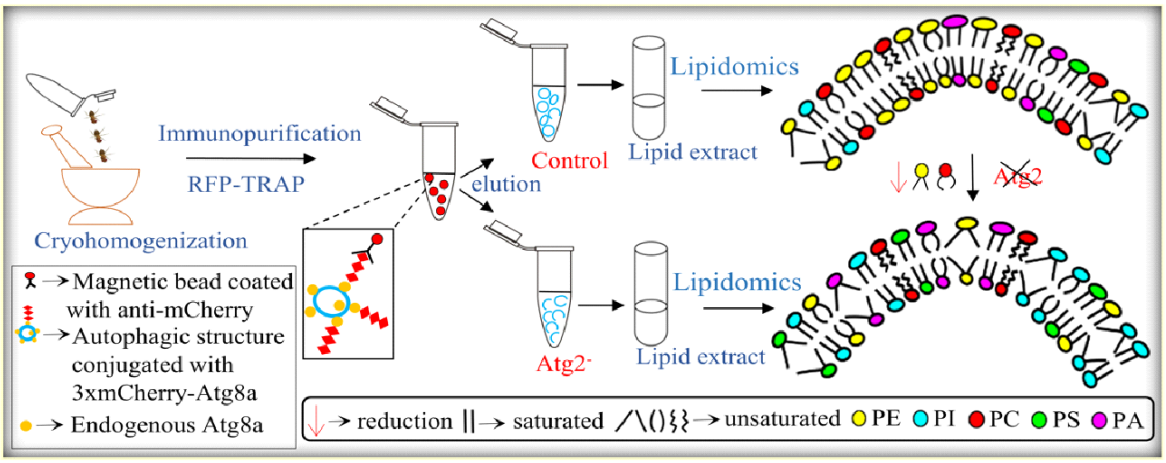

Figure 33: Graphical representation of an established method to isolate intact autophagy vesicles. *The illustration explains the logic behind immunoprecipitate of autophagy structures from wild type and Atg2⁻ flies. Emphasizing the basic phospholipid profile of isolated membranes and benefits of lack of Atg2 lipid transporter protein.*

To understand how lipids influence Syntaxin 17 recruitment to autophagosomes, we utilized our lipidomics data from purified control autophagic membranes to design synthetic lipid mixtures that mimic the composition of these membranes. The human STX17 and fly Syx17 proteins were expressed and purified from bacteria and studied their interaction with different types of liposomes by liposome flotation assay. The liposomes were made up of total lipids extracted from each protein's respective species, synthetic lipids, and autophagosome mimetics. In our flotation assay, which evaluates protein-lipid interactions, we selected Atg3, a protein well-documented for its involvement in autophagosome formation and membrane association, as a positive control. GST, known for its minimal interaction with lipids, was chosen as a negative control. These selections proved to be effective in our experiments (Fig. 20A). For the reference, the protein density of Atg3, GST, and STX17/Syx17 alone (incubated with no liposome) was established by demonstrating there presence in the non-floated fractions (Fig. 20A, B).

Primarily, the *in vitro* reconstitution experiments confirmed the direct binding of STX17/Syx17 proteins with autophagosomal mimetics (Fig. 21A, I). The Syx17 membrane binding seems to be species-specific since it preferred the liposomes generated from *Drosophila* total lipid extracts

compared to the human cell total lipid extracts (Fig. 20B, I). However, the STX17/Syx17 recruitment was not efficient with the human cell total lipid extracts or neutral lipids (Fig. 20B, II and Fig. 21B, II). Based on our lipidomics data it is known that autophagic membranes are negatively charged (Laczkó-Dobos et al., 2021). Following that several lipid compositions using synthetic negative lipids efficiently recruited the Syx17/STX17 proteins (Fig. 20B) and negative charge of generated liposomes was confirmed by Zeta potential measurements (Fig. 20C). So far, the lipid-protein investigation results pointed to the significance of negatively charged lipids in the Syntaxin 17 autophagosomal recruitment. It is also known that Syntaxin 17 recruits to the matured autophagosomes but not to the phagophores. Based on this observation, we propose that a crucial trigger for STX17/Syx17 association with autophagosomes *in vivo* could be a specific modification occurring during autophagosome maturation. The Atg8 family alone is unlikely because this protein is present even in the phagophores. Previous studies revealed that the binding of IRGM and Atg8/LC3 family proteins to the LIR motif of the STX17 SNARE domain is found to be involved in Syntaxin 17 recruitment to the autophagosomes (Kumar et al., 2018). However, the IRGM homolog is not present in *Drosophila* and unlike STX17, Syx17 does not contain the LIR binding motif. This points to the existence of an unexplored evolutionary conserved mechanism behind the recruitment of this protein to the autophagosomal bilayers. In accord with this, we hypothesize that negatively charged signaling lipids that generate during autophagosome maturation might facilitate the recruitment of Syntaxin 17 to the closed autophagosomal membrane. PI(3)P, PI(4)P, and PI(3,5)P_2 are the physiologically relevant functional lipids that are known to appear on autophagic structures (Rusten et al., 2007; Axe et al., 2008; Juhász et al., 2008; Wang et al., 2015). These PIPs present only 4-5 % in the cytosolic leaflet of the host membranes, despite this, even specific phospholipid-binding protein domains exhibit low affinity towards these lipids. (Carlton et al., 2005). We thus tested *in vitro*, whether these PIPs have a potential role in the Syntaxin 17 recruitment to the autophagosomes. STX17/Syx17 did not bind to liposomes containing only neutral lipids, but the addition of these PIPs shifted the charge of membranes from neutral to negative and concomitantly resulted in STX17/Syx17 recruitment (Fig. 21B) suggesting the potential role of PIPs in Syntaxin 17 membrane binding. However, the recruitment of Syntaxin 17 did not show a direct correlation with the negative charge of PIP-containing vesicles (Fig. 20B, C and Fig. 21B, C). Hence, eventually concluded that both the overall negative charge and the lipid specificity play a vital role in STX17 recruitment. Syx17/STX17 was found to be stably

integrated into the membranes as washing with 8M urea, a commonly used method to strip non-integral membrane proteins (Zhao et al., 2004), did not remove it from liposomes (Fig. 22A). Another essential physiological parameter in protein-membrane binding is membrane curvature which has proved no significant role in the Syntaxin 17 autophagosomal recruitment. Because there was no obvious significant difference in the efficiency of protein recruitment to different size liposomes (50 nm, 100 nm, 800 nm and GUVs) (Fig. 22B). Our findings suggest that the recruitment of STX17 to autophagosomes is primarily influenced by changes in the lipid composition that occur during maturation, rather than by the curvature of the autophagosomal membrane.

After confirming the spontaneous interaction of Syx17/STX17 with liposomes containing PI(3)P, PI(4)P, and PI(3,5)P_2 *in vitro*, we employed specific fluorescent markers to observe their co-localization with LC3 and STX17-positive autophagic structures in mammalian cells. Utilizing distinct fluorescent probes for each PIP, we observed that PI(4)P consistently marks STX17-positive autophagosomes, in contrast to PI(3)P and PI(3,5)P_2. (Fig. 23A-C). Elucidating that, PI4K2A generated PI(4)P during autophagosome maturation is indispensable for autophagosome-lysosome fusion (Wang et al., 2015). PI(3)P is generated by VPS34 lipid kinase (Axe et al., 2008; Juhász et al., 2008) and its dephosphorylation is the signal for the phagophore maturation (Cebollero et al., 2012). Lastly, PI(3,5)P_2 is present at a later stage, feasibly during or after lysosomal fusion (Rusten et al., 2007; Dong et al., 2010). The concomitant appearance of PI(4)P and STX17 on LC3 positive autophagosomes is evident by the live imaging conducted in U2OS cells (Fig. 24A). Similarly, fat cells of starved *Drosophila* larvae showed the Atg8a structures that are extensively co-localized with Syx17 and PI(4)P (Fig. 24B).

This observation prompted us to consider the possibility that inhibiting the autophagosome-lysosome fusion could lead to an increase in PI(4)P on autophagosomes. As expected the LC3 positive structures were accumulated, co-locaizing with PI(4)P reporter SidM in the bafilomycin A1 treated HEK-293 cells (Fig. 25 A, B). Additionally, the total PI(4)P levels in the starved HEK cells were increased compared to control non-starved cells (Fig. 25C, D). These findings provide a strong support for the hypothesis that PI(4)P plays an essential role in recruiting STX17 to autophagosomes, highlighting its critical importance in this process. However, it is interesting to note that PI(4)P plays different roles in autophagy depending on the kinase responsible for its synthesis. PI4KB/PI4KIIIβ generates PI(4)P and promotes autophagosome biogenesis (Judith et

al., 2019), while PI4K2A, which is recruited to autophagosomes through its interaction with ATG8 family proteins, generates PI(4)P to promote autophagosome-lysosome fusion (Wang et al., 2015). Notably, over expression of PI4KB/PI4KIIIβ fails to rescue the defective phenotype of PI4K2A, indicating a specific role of PI4K2A during autophagosome-lysosome fusion. Starved HEK cells treated with Bafilomycin A1 showed accumulation of autophagosomes positive for PI(4)P reporter SidM. (Fig. 25A, B).

The depletion of PI(4)P levels caused by doxycycline-inducible shRNA knockdown for PI4K2A successfully impaired the STX17 recruitment and autophagosome-lysosome fusion (Fig. 26A-D). To avoid potential complications arising from long-term perturbation of PI(4)P synthesis in cells, short-term PI(4)P depletion was carried out by treating the cells for 10 min with NC03 (a chemical inhibitor specifically for PI4K2A) that indeed reduced the PI(4)P levels on autophagosomes. We observed further impaired recruitment of STX17 to the autophagosomes, without affecting the total number of LC3-positive vesicles (Fig. 27A-D). Ultimately this short-term treatment perturbed only the autophagosomal STX17 recruitment but not the mitochondrial pool (Fig. 28A-D). However, neither long-term nor short-term PI(4)P depletion affected the endogenous STX17 levels (Fig. 29). Our findings demonstrate that PI(4)P is specifically required for STX17 autophagosomal recruitment during autophagy.

Later, we identified the specific characteristics of Syntaxin 17 proteins responsible for their binding to PI(4)P and subsequent recruitment to autophagosomes. The predicted molecular modelling approaches suggested the cytosolic versus membrane binding parts of full-length human and fly Syntaxin 17 proteins are lied to right after the predicted TMDs. The further molecular dynamics simulations ran only for C-terminal parts until the end of SNARE domains of Syntaxin 17 and *in silico* model membranes. STX17 showed no interaction with the membranes composed of neutral lipids correlating with *in vitro* results, while both the proteins remarkably bound to the negatively charged membranes containing PI(4)P as expected. The positively charged Lysine and Arginine residues, especially when they are situated next to each other have exhibited the highest affinity towards PI(4)P positive bilayers (electrostatic interactions). The mutation of RKK and KK motifs, as well as two single K residues to Alanine in the C-terminal part of human STX17 prevented the recruitment of STX17 to the autophagosomes in mammalian cells and *in silico* membranes to a similar extent as in the case of blocking PI(4)P synthesis. Similarly, for Syx17, RR and KK motifs that are located before the transmembrane regions are mutated to Alanine which

also impaired its recruitment to autophagosomes in mammalian cells and *in silico* lipid bilayers. The data acquired from molecular simulation and mutagenesis methods summarize that Syntaxin 17's basic residues play a significant role in binding to PI(4)P on autophagosomes during autophagosome-lysosome fusion.

During autophagy, PI(4)P has been identified as a rate-limiting factor in the final autophagosome-lysosome fusion step (Wang et al., 2015). However, the downstream mechanism has been poorly understood. The tethering complex HOPS is an indispensable player in the fusion of lysosomes with endosomes, autophagosomes, and secretory granules. Increased PI(4)P on endosomes and lysosomes is known to promote recruitment of HOPS complex, which facilitates the formation of SNARE complexes containing STX17, ultimately leading to enhanced autophagy (Juhász, 2016). ATG14 is involved in the assembly of the SNARE complex containing STX17 during the autophagosome-lysosome fusion step (Diao et al., 2015). Recent studies have shown that during autophagy, PI(4)P promotes ATG14 association with autophagosomes (Sun et al., 2022). These data are in line with the crucial role of PI(4)P in the autophagosomal recruitment of Syntaxin 17. While previous research has identified several protein-binding partners that play important roles in this process (Kumar et al., 2018, 2019; Rong et al., 2022; Zhou et al., 2022; Wang et al., 2023), this study is the first to demonstrate the key role of a specific lipid in recruiting Syntaxin 17 to mature autophagosomes. Phospholipid interactions with Syntaxin 17 are likely also important for various other cellular processes beyond autophagosome-lysosome fusion, including autophagy initiation (Hamasaki et al., 2013; Kumar et al., 2021), ER-mitochondria communication (Arasaki et al., 2017), mitochondrial division and mitophagy (Arasaki et al., 2015; McLelland et al., 2016), and lipid droplet formation (Kimura et al., 2018). Of note, both human and fly Syntaxin 17 could bind to PI(4)P and PI(3,5)P_2 on lysosomes, which may promote their necessary recycling after autophagosome-lysosome fusion (Zhou et al., 2022; Liu et al., 2023). The role of certain lipid species in these other trafficking scenarios does not necessarily involve the membrane recruitment of cytosolic Syntaxin 17, as lipid-protein interactions can as well regulate the sub-organellar targeting (e.g., to ER-mitochondria contact sites) or clustering (e.g., to subdomains of lysosomes where SNARE recycling takes place) of the transmembrane form of this protein.

The important relevant question arises—why is soluble STX17 not recruited to the Golgi (Itakura et al., 2012) that also contains PI(4)P (Judith et al., 2019)? Typically, phosphoinositide-binding proteins bind weakly and promiscuously to multiple related phosphoinositide species

(Carlton et al., 2005), yet have very specific localization. Weak interactions with proteins present on target membranes, along with phosphoinositide binding, ensure specific target localization (Genz et al., 2013). Considering the previously published Syntaxin 17 interacting partners, STX17 can be quickly and efficiently recruited to autophagosomes through simultaneous binding to ATG8 family proteins, HOPS, and newly generated PI(4)P (Takáts et al., 2014; Kumar et al., 2018). The binding of STX17 to specific factors and newly generated PI(4)P during autophagosome maturation serves as coincidence detection for the recruitment of STX17 to autophagosomes (Fig. 34). This pattern of multiple interactions also explains STX17 recruitment to abnormal autophagosomes in the absence of ATG8 proteins (Tsuboyama et al., 2016).

The research findings of this study conclude that electrostatic interactions between positively charged amino acid residues near the predicted transmembrane domains of STX17 and negatively charged PI(4)P are important for recruiting the soluble cytosolic form of Syntaxin 17 to the autophagosomes. During autophagosome maturation, PI4K2A generating PI(4)P is critical for the STX17 recruitment *in vivo*. This enables STX17 to fulfil its role as a competence factor for subsequent vesicle fusion and lysosomal cargo degradation.

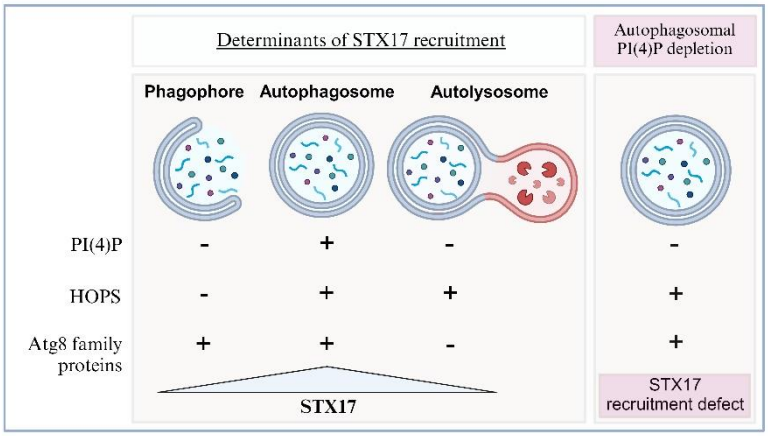

Fig. 34: A model for coincidences related to the recruitment of Syntaxin 17 to autophagosomes.
The model relies on vesicle-specific negatively charged PI(4)P, ATG8 family proteins, and likely also HOPS. When PI4K2A is inhibited, autophagosomal PI(4)P is depleted, that impairs the recruitment of STX17 to autophagosomes.

The novel research findings of this study are the following:

- Established a method to immunoprecipitate autophagic membranes from starved control and Atg2^{-} *Drosophila* adult flies and showed the validation of isolated intact vesicles by

western blot, fluorescent microscopy, AFM and screening of isolated fractions with various organelle markers confirming the high degree of purity.

- Characterized the phospholipid profile of isolated autophagic structures using mass spectrometry analysis.
- We initially demonstrated that Syntaxin 17 directly binds to *in vitro* autophagosome mimetics without requiring any additional cofactors.
- *In vitro* studies of lipid-protein interactions suggests that STX17 preferentially binds to negatively charged membranes, particularly PIPs like PI(3)P, PI(4)P, and PI(3,5)P_2) which might be important for its recruitment to autophagosomes.
- Western blots of liposome flotation assay fractions and Zeta potential measurements confirmed that the recruitment of STX17 is influenced not just by the overall negative charge but also by the lipid composition of the membranes.
- Recombinant Syntaxin 17 proteins are deeply integrated into the liposomes and this recruitment is not influenced by a physiological parameter called membrane curvature.
- Using specific fluorescent reporters in HEK-293 cells starved for 1 hour, our subcellular co-localization data revealed a greater degree of co-localization between STX17 and PI(4)P on autophagosomes compared to PI(3)P and PI(3,5)P2PI(3)P.
- PI(4)P, generated by PI4K2A on autophagosomes, is essential for the recruitment of STX17 to autophagosomes during the fusion with lysosomes. This hypothesis is specific to the pool of Syntaxin 17 associated with autophagosomes and does not apply to other Syntaxin 17 pools.
- Combined studies using molecular simulation and cellular mutagenesis revealed that specific basic amino acids at the C-terminus of Syntaxin 17 are critical for PI(4)P binding on autophagosomes.
- Functional assays corroborated the significance of the aforementioned positively charged amino acids in the STX17 C-terminus for autophagosomal recruitment.

Overall, our research suggests that electrostatic interactions between negatively charged lipids, particularly PI(4)P, on autophagosomes and positively charged amino acids at the C-terminus of Syntaxin 17 play a critical role in its autophagosomal recruitment during fusion step of autophagy.

6. ACKNOWLEDGEMENTS

I am immensely grateful to my PhD supervisor, Dr. Laczkó-Dobos-Hajnalka, for her unwavering support throughout my academic journey. Despite facing some of the toughest times of my life during my PhD, she believed in me and helped me to succeed. Hajni is not only an excellent mentor but also a compassionate person who always thinks ahead and is positive and helpful. I cannot express enough how thankful I am for the opportunity to work under her guidance and learn some of the most valuable skills from our interactions. Once again, thank you so much, Hajni.

Next, I would like to express my deepest gratitude to Prof. Juhász Gábor for his consistent support during my journey in his lab. He has consistently demonstrated a profound commitment to excellence, offering valuable insights and constructive feedback that significantly enriched the quality of this thesis. I would like to thank Dr. Arindam Bhattacharjee for his invaluable assistance with molecular and cell biology, and microscopy experiments throughout this project. A special thanks to Horváth Gábor for his valuable insights during the cloning and optimization of protein expression and Jipa András for providing *Drosophila* lines during autophagic membranes isolation. My extended thanks to the Kansas Lipidomics Research Center Analytical Laboratory, USA for the mass spectrometry analysis.

A special thanks to Erdődi Ildikó for always being there to share my feelings and for giving me loads of hugs. A big thanks to Szilvi, our lab assistant, for preparing reagents, litters of LB, and agar plates with a smile and immense patience. I am deeply grateful to András Dér and András Kincses from the Institute of Biophysics for their endless and tremendous efforts in measuring zeta potential values. I am thankful to Krisztina Sebők-Nagy, Tibor Páli, and Tamás Hegedűs for the molecular simulation studies. A big thanks to Gábor Csordás, Zsóka and Hussein Abuammar for their contribution to this project.

I would also like to thank all the current and past lab members that I've had some great times with. Whether it be brainstorming, retreat party, team gathering, or having a stimulating discussion about science, every interaction has helped me in some way to reach my goal and I'm happy to have met every one of you during my time here.

Last but not least, I am grateful to my family for their selfless support in every way they can throughout my PhD journey. Especially, I would like to dedicate this to my mother. I would like

to thank the Tempus Public Foundation and the University of Szeged for funding me the Stipendium Hungaricum PhD Scholarship. I am grateful to the Biological Research Centre for allowing me to join them and pursue my PhD. I am grateful to the University Grants Commission, India for nominating me for this scholarship and allowing me to become a better researcher.

7. REFERENCES

Altschul, S. F., Madden, T. L., Schäffer, A. A., Zhang, J., Zhang, Z., Miller, W., & Lipman, D. J. (1997). Gapped BLAST and PSI-BLAST: a new generation of protein database search programs. *Nucleic Acids Research*, *25*(17), 3389–3402. https://doi.org/10.1093/NAR/25.17.3389

Arasaki, K., Mikami, Y., Shames, S. R., Inoue, H., Wakana, Y., & Tagaya, M. (2017). Legionella effector Lpg1137 shuts down ER-mitochondria communication through cleavage of syntaxin 17. *Nature Communications*, *8*. https://doi.org/10.1038/NCOMMS15406

Arasaki, K., Shimizu, H., Mogari, H., Nishida, N., Hirota, N., Furuno, A., Kudo, Y., Baba, M., Baba, N., Cheng, J., Fujimoto, T., Ishihara, N., Ortiz-Sandoval, C., Barlow, L. D., Raturi, A., Dohmae, N., Wakana, Y., Inoue, H., Tani, K., & Tagaya, M. (2015). A role for the ancient SNARE syntaxin 17 in regulating mitochondrial division. *Developmental Cell*, *32*(3), 304–317. https://doi.org/10.1016/J.DEVCEL.2014.12.011

Axe, E. L., Walker, S. A., Manifava, M., Chandra, P., Roderick, H. L., Habermann, A., Griffiths, G., & Ktistakis, N. T. (2008). Autophagosome formation from membrane compartments enriched in phosphatidylinositol 3-phosphate and dynamically connected to the endoplasmic reticulum. *The Journal of Cell Biology*, *182*(4), 685–701. https://doi.org/10.1083/JCB.200803137

Baskaran, S., Carlson, L. A., Stjepanovic, G., Young, L. N., Kim, D. J. in, Grob, P., Stanley, R. E., Nogales, E., & Hurley, J. H. (2014). Architecture and dynamics of the autophagic phosphatidylinositol 3-kinase complex. *ELife*, *3*. https://doi.org/10.7554/ELIFE.05115

Bateman, A., Martin, M. J., Orchard, S., Magrane, M., Agivetova, R., Ahmad, S., Alpi, E., Bowler-Barnett, E. H., Britto, R., Bursteinas, B., Bye-A-Jee, H., Coetzee, R., Cukura, A., da Silva, A., Denny, P., Dogan, T., Ebenezer, T. G., Fan, J., Castro, L. G., & Teodoro, D. (2021). UniProt: the universal protein knowledgebase. *Nucleic Acids Research*, *49*(D1), 480–489. https://doi.org/10.1093/NAR/GKAA1100

Bhattacharjee, A., Szabó, Á., Csizmadia, T., Laczkó-Dobos, H., & Juhász, G. (2019). Understanding the importance of autophagy in human diseases using *Drosophila*. *Journal of Genetics and Genomics*, *46*(4), 157–169. https://doi.org/10.1016/J.JGG.2019.03.007

Bligh, E. G., & Dyer, W. J. (1959). A rapid method of total lipid extraction and purification. *Canadian Journal of Biochemistry and Physiology*, *37*(8), 911–917. https://doi.org/10.1139/O59-099

Carlton, J. G., & Cullen, P. J. (2005). Coincidence detection in phosphoinositide signaling. *Trends in Cell Biology*, *15*(10), 540-547. doi: 10.1016/j.tcb.2005.08.005

Carvalho, J.L., Sampaio, W., Palm, M., Brankatschk, S., & Eaton, A.S. (2012). Effects of diet and development on the *Drosophila* lipidome. *Molecular Systems Biology*, 8, 600. https://doi.org/10.1038/msb.2012.29

Cebollero, E., Van Der Vaart, A., Zhao, M., Rieter, E., Klionsky, D. J., Helms, J. B., & Reggiori, F. (2012). Phosphatidylinositol-3-phosphate clearance plays a key role in autophagosome completion. *Current Biology*, *22*(17), 1545–1553. https://doi.org/10.1016/J.CUB.2012.06.029

Chen, W., & He, B. (2022). Actomyosin activity-dependent apical targeting of Rab11 vesicles reinforces apical constriction. *The Journal of Cell Biology*, *221*(6). https://doi.org/10.1083/JCB.202103069

Chowdhury, S., Otomo, C., Leitner, A., Ohashi, K., Aebersold, R., Lander, G. C., & Otomo, T. (2018). Insights into autophagosome biogenesis from structural and biochemical analyses of the ATG2A-WIPI4 complex. *Proceedings of the National Academy of Sciences of the United States of America*, *115*(42), 9792–9801. https://doi.org/10.1073/PNAS.1811874115

Dall'Armi, C., Devereaux, K. A., & Di Paolo, G. (2013). The role of lipids in the control of autophagy. *Current Biology*, *23*(1). https://doi.org/10.1016/J.CUB.2012.10.041

Dall'Armi, C., Hurtado-Lorenzo, A., Tian, H., Morel, E., Nezu, A., Chan, R. B., Yu, W. H., Robinson, K. S., Yeku, O., Small, S. A., Duff, K., Frohman, M. A., Wenk, M. R., Yamamoto, A., & Di Paolo, G. (2010). The phospholipase D1 pathway modulates macroautophagy. *Nature Communications*, *1*(9). https://doi.org/10.1038/NCOMMS1144

Schmitt, D., Bozkurt, S., Henning-Domres, P., Huesmann, H., Eimer, S., Bindila, L., Behrends, C., Boyle, E., Wilfling, F., Tascher, G., Münch, C., Behl, C., & Kern, A. (2022). Lipid and protein content profiling of isolated native autophagic vesicles. *EMBO Reports*, *23*(12), 53065. https://doi: 10.15252/embr.202153065.

Diao, J., Liu, R., Rong, Y., Zhao, M., Zhang, J., Lai, Y., Zhou, Q., Wilz, L. M., Li, J., Vivona, S., Pfuetzner, R. A., Brunger, A. T., & Zhong, Q. (2015). ATG14 promotes membrane tethering and

fusion of autophagosomes to endolysosomes. *Nature*, *520*(7548), 563–566. https://doi.org/10.1038/NATURE14147

Dong, X. P., Shen, D., Wang, X., Dawson, T., Li, X., Zhang, Q., Cheng, X., Zhang, Y., Weisman, L. S., Delling, M., & Xu, H. (2010). PI(3,5)P(2) controls membrane trafficking by direct activation of mucolipin Ca(2+) release channels in the endolysosome. *Nature Communications*, *1*(4). https://doi.org/10.1038/NCOMMS1037

Dooley, H. C., Razi, M., Polson, H. E. J., Girardin, S. E., Wilson, M. I., & Tooze, S. A. (2014). WIPI2 links LC3 conjugation with PI(3)P, autophagosome formation, and pathogen clearance by recruiting Atg12-5-16L1. *Molecular Cell*, *55*(2), 238–252. https://doi.org/10.1016/J.MOLCEL.2014.05.021

Fahy, E., Cotter, D., Sud, M., & Subramaniam, S. (2011). Lipid classification, structures and tools. *Biochim Biophys Acta*, *1811*(11), 637–47. https://10.1016/j.bbalip.2011.06.009.

Falcone, D. L., Ogas, J. P., & Somerville, C. R. (2004). Regulation of membrane fatty acid composition by temperature in mutants of Arabidopsis with alterations in membrane lipid composition. *BMC Plant Biology*, *4*, 1–45. https://doi.org/10.1186/1471-2229-4-17

Fernandez-Fernandez, M. R., Ruiz-Garcia, D., Martin-Solana, E., Chichon, F. J., Carrascosa, J. L., & Fernandez, J. J. (2017). 3D electron tomography of brain tissue unveils distinct Golgi structures that sequester cytoplasmic contents in neurons. *Journal of Cell Science*, *130*(1), 83–89. https://doi.org/10.1242/JCS.188060

Folch, J., Lees, M., & Sloane, G. H. (1957). A simple method for the isolation and purification of total lipides from animal tissues. *Journal of Biological Chemistry*, *226*, 497–509. https://doi.org/10.1016/S0021-9258(18)64849-5

Fujita, N., Itoh, T., Omori, H., Fukuda, M., Noda, T., & Yoshimori, T. (2008). The Atg16L complex specifies the site of LC3 lipidation for membrane biogenesis in autophagy. *Molecular Biology of the Cell*, *19*(5), 2092–2100. https://doi.org/10.1091/MBC.E07-12-1257

Galluzzi, L., Baehrecke, E. H., Ballabio, A., Boya, P., Bravo-San Pedro, J. M., Cecconi, F., Choi, A. M., Chu, C. T., Codogno, P., Colombo, M. I., Cuervo, A. M., Debnath, J., Deretic, V., Dikic, I., Eskelinen, E., Fimia, G. M., Fulda, S., Gewirtz, D. A., Green, D. R., & Kroemer, G. (2017).

Molecular definitions of autophagy and related processes. *The EMBO Journal*, *36*(13), 1811–1836. https://doi.org/10.15252/EMBJ.201796697

Genz, C., Fundakowski, J., Hermesh, O., Schmid, M., & Jansen, R. P. (2013). Association of the yeast RNA-binding protein She2p with the tubular endoplasmic reticulum depends on membrane curvature. *The Journal of Biological Chemistry*, *288*(45), 32384–32393. https://doi.org/10.1074/JBC.M113.486431

Ghanbarpour, A., Valverde, D. P., Melia, T. J., & Reinisch, K. M. (2021). A model for a partnership of lipid transfer proteins and scramblases in membrane expansion and organelle biogenesis. *Proceedings of the National Academy of Sciences of the United States of America*, *118*(16). https://doi.org/10.1073/PNAS.2101562118

Graham, F. L., Smiley, J., Russell, W. C., & Nairn, R. (1977). Characteristics of a human cell line transformed by DNA from human adenovirus type 5. *The Journal of General Virology*, *36*(1), 59–72. https://doi.org/10.1099/0022-1317-36-1-59

Guan, X. L., Cestra, G., Shui, G., Kuhrs, A., Schittenhelm, R. B., Hafen, E., Van der Goot, F. G., Robinett, C. C., Gatti, M., Gonzalez-Gaitan, M., & Wenk, M.R. (2013). Biochemical membrane lipidomics during *Drosophila* development. *Devolepmental Cell*, *24*, 98–111. https://doi.org/10.1016/j.devcel.2012.11.012.

Gutierrez, M. G., Master, S. S., Singh, S. B., Taylor, G. A., Colombo, M. I., & Deretic, V. (2004). Autophagy is a defense mechanism inhibiting BCG and Mycobacterium tuberculosis survival in infected macrophages. *Cell*, *119*(6), 753–766. https://doi.org/10.1016/j.cell.2004.11.038

Hailey, D. W., Rambold, A. S., Satpute-Krishnan, P., Mitra, K., Sougrat, R., Kim, P. K., & Lippincott-Schwartz, J. (2010). Mitochondria supply membranes for autophagosome biogenesis during starvation. *Cell*, *141*(4), 656–667. https://doi.org/10.1016/J.CELL.2010.04.009

Hamasaki, M., Furuta, N., Matsuda, A., Nezu, A., Yamamoto, A., Fujita, N., Oomori, H., Noda, T., Haraguchi, T., Hiraoka, Y., Amano, A., & Yoshimori, T. (2013). Autophagosomes form at ER-mitochondria contact sites. *Nature*, *495*(7441), 389–393. https://doi.org/10.1038/NATURE11910

Hammad, L. A., Cooper, B. S., Fisher, N. P., Montooth, K. L., & Karty, J. A. (2011). Profiling and quantification of *Drosophila* melanogaster lipids using liquid chromatography/mass spectrometry. *Rapid Commun. Mass Spectrom*, *25*, 2959–2968. https://doi.org/10.1002/rcm.5187.

Hanada, T., Noda, N. N., Satomi, Y., Ichimura, Y., Fujioka, Y., Takao, T., Inagaki, F., & Ohsumi, Y. (2007). The Atg12-Atg5 conjugate has a novel E3-like activity for protein lipidation in autophagy. *The Journal of Biological Chemistry*, *282*(52), 37298–37302. https://doi.org/10.1074/JBC.C700195200

Hansen, M., Rubinsztein, D. C., & Walker, D. W. (2018). Autophagy as a promoter of longevity: insights from model organisms. *Nature Reviews. Molecular Cell Biology*, *19*(9), 579–593. https://doi.org/10.1038/S41580-018-0033-Y

Hasegawa, R., Iwamoto, T., Otomo, A., Nezu, M., Hamasaki, T., & Yoshimori. (2016). Autophagosome-lysosome fusion in neurons requires INPP5E, a protein associated with Joubert syndrome. *EMBO Journal*, 35, 1853-1867.

Hayashi-Nishino, M., Fujita, N., Noda, T., Yamaguchi, A., Yoshimori, T., & Yamamoto, A. (2009). A subdomain of the endoplasmic reticulum forms a cradle for autophagosome formation. *Nature Cell Biology*, *11*(12), 1433–1437. https://doi.org/10.1038/NCB1991

Hegedus, K., Takats, S., Boda, A., Jipa, A., Nagy, P., Varga, K., Kovacs, A. L., & Juhasz, G. (2016). The Ccz1-Mon1-Rab7 module and Rab5 control distinct steps of autophagy. *Molecular Biology of the Cell*, *27*(20), 3132–3142. https://doi.org/10.1091/MBC.E16-03-0205

Hegedus, K., Takats, S., Kovacs, A. L., & Juhasz, G. (2013). Evolutionarily conserved role and physiological relevance of a STX17/Syx17 (syntaxin 17)-containing SNARE complex in autophagosome fusion with endosomes and lysosomes. *Autophagy*, *9*(10), 1642–1646. https://doi.org/10.4161/AUTO.25684

Hegedűs, T., Geisler, M., Lukács, G. L., & Farkas, B. (2022). Ins and outs of AlphaFold2 transmembrane protein structure predictions. *Cellular and Molecular Life Sciences : CMLS*, *79*(1). https://doi.org/10.1007/S00018-021-04112-1

Henikoff, S., & Henikoff, J. G. (1992). Amino acid substitution matrices from protein blocks. *Proceedings of the National Academy of Sciences of the United States of America*, *89*(22), 10915–10919. https://doi.org/10.1073/PNAS.89.22.10915

Huang, J., Rauscher, S., Nawrocki, G., Ran, T., Feig, M., De Groot, B. L., Grubmüller, H., & MacKerell, A. D. (2017). CHARMM36m: an improved force field for folded and intrinsically disordered proteins. *Nature Methods*, *14*(1), 71–73. https://doi.org/10.1038/NMETH.4067

Hurley, J. H., & Young, L. N. (2017). Mechanisms of Autophagy Initiation. *Annual Review of Biochemistry*, *86*, 225–244. https://doi.org/10.1146/ANNUREV-BIOCHEM-061516-044820

Ichimura, Y., Imamura, Y., Emoto, K., Umeda, M., Noda, T., & Ohsumi, Y. (2004). In vivo and in vitro reconstitution of Atg8 conjugation essential for autophagy. *The Journal of Biological Chemistry*, *279*(39), 40584–40592. https://doi.org/10.1074/JBC.M405860200

Ichimura, Y., Kirisako, T., Takao, T., Satomi, Y., Shimonishi, Y., Ishihara, N., Mizushima, N., Tanida, I., Kominami, E., Ohsumi, M., Noda, T., & Ohsumi, Y. (2000). A ubiquitin-like system mediates protein lipidation. *Nature*, *408*(6811), 488–492. https://doi.org/10.1038/35044114

Itakura, E., Kishi-Itakura, C., & Mizushima, N. (2012). The hairpin-type tail-anchored SNARE syntaxin 17 targets to autophagosomes for fusion with endosomes/lysosomes. *Cell*, *151*(6), 1256–1269. https://doi.org/10.1016/J.CELL.2012.11.001

Itakura, E., & Mizushima, N. (2013). Syntaxin 17: the autophagosomal SNARE. *Autophagy*, *9*(6), 917–919. https://doi.org/10.4161/AUTO.24109

Jahn, R., & Scheller, R. H. (2006). SNAREs--engines for membrane fusion. *Nature Reviews. Molecular Cell Biology*, *7*(9), 631–643. https://doi.org/10.1038/NRM2002

Jo, S., Cheng, X., Lee, J., Kim, S., Park, S. J., Patel, D. S., Beaven, A. H., Lee, K. Il, Rui, H., Park, S., Lee, H. S., Roux, B., MacKerell, A. D., Klauda, J. B., Qi, Y., & Im, W. (2017). CHARMM-GUI 10 years for biomolecular modeling and simulation. *Journal of Computational Chemistry*, *38*(15), 1114–1124. https://doi.org/10.1002/JCC.24660

Judith, D., Jefferies, H. B. J., Boeing, S., Frith, D., Snijders, P. A., & Tooze, A. S. (2019). ATG9A shapes the forming autophagosome through Arfaptin 2 and phosphatidylinositol 4-kinase IIIβ. The *Journal of Cell Biology*, *218*(5), 1634-1652. https://doi: 10.1083/jcb.201901115

Juhász, G. (2016). A mitochondrial-derived vesicle HOPS to endolysosomes using Syntaxin-17. *The Journal of Cell Biology*, *214*(3), 241–243. https://doi.org/10.1083/JCB.201607024

Juhász, G., Hill, J. H., Yan, Y., Sass, M., Baehrecke, E. H., Backer, J. M., & Neufeld, T. P. (2008). The class III PI(3)K Vps34 promotes autophagy and endocytosis but not TOR signaling in *Drosophila*. *The Journal of Cell Biology*, *181*(4), 655–666. https://doi.org/10.1083/JCB.200712051

Juhasz, G., & Neufeld, T. P. (2006). Autophagy: a forty-year search for a missing membrane source. *PLoS Biology*, *4*(2), 161–164. https://doi.org/10.1371/JOURNAL.PBIO.0040036

Kabeya, Y., Mizushima, N., Ueno, T., Yamamoto, A., Kirisako, T., Noda, T., Kominami, E., Ohsumi, Y., & Yoshimori, T. (2000). LC3, a mammalian homologue of yeast Apg8p, is localized in autophagosome membranes after processing. *The EMBO Journal*, *19*(21), 5720–5728. https://doi.org/10.1093/EMBOJ/19.21.5720

Katheder, N. S., Khezri, R., O'Farrell, F., Schultz, S. W., Jain, A., Schink, M. K. O., Theodossiou, T. A., Johansen, T., Juhász, G., Bilder, D., Brech, A., Stenmark, H., & Rusten, T. E. (2017). Microenvironmental autophagy promotes tumour growth. *Nature*, *541*(7637), 417–420. https://doi.org/10.1038/NATURE20815

Kato, S., Arasaki, K., Tokutomi, N., Imai, Y., Inoshita, T., Hattori, N., Sasaki, T., Sato, M., Wakana, Y., Inoue, H., & Tagaya, M. (2021). Syntaxin 17, an ancient SNARE paralog, plays different and conserved roles in different organisms. *Journal of Cell Science*, *134*(22). https://doi.org/10.1242/JCS.258699

Kimura, H., Arasaki, K., Ohsaki, Y., Fujimoto, T., Ohtomo, T., Yamada, J., & Tagaya, M. (2018). Syntaxin 17 promotes lipid droplet formation by regulating the distribution of acyl-CoA synthetase 3. *Journal of Lipid Research*, *59*(5), 805–819. https://doi.org/10.1194/JLR.M081679

Kincses, A., Santa-Maria, A. R., Walter, F. R., Dér, L., Horányi, N., Lipka, D. V., Valkai, S., Deli, M. A., & Dér, A. (2020). A chip device to determine surface charge properties of confluent cell monolayers by measuring streaming potential. *Lab on a Chip*, *20*(20), 3792–3805. https://doi.org/10.1039/D0LC00558D

Kirisako, T., Ichimura, Y., Okada, H., Kabeya, Y., Mizushima, N., Yoshimori, T., Ohsumi, M., Takao, T., Noda, T., & Ohsumi, Y. (2000). The reversible modification regulates the membrane-binding state of Apg8/Aut7 essential for autophagy and the cytoplasm to vacuole targeting pathway. *The Journal of Cell Biology*, *151*(2), 263–275. https://doi.org/10.1083/JCB.151.2.263

Kishi-Itakura, C., Koyama-Honda, I., Itakura, E., & Mizushima, N. (2014). Ultrastructural analysis of autophagosome organization using mammalian autophagy-deficient cells. *Journal of Cell Science*, *127*(Pt 18), 4089–4102. https://doi.org/10.1242/JCS.156034

Krick, R., Busse, R. A., Scacioc, A., Stephan, M., Janshoff, A., Thumm, M., & Kühnel, K. (2012). Structural and functional characterization of the two phosphoinositide binding sites of PROPPINs, a β-propeller protein family. *Proceedings of the National Academy of Sciences of the United States of America*, *109*(30). https://doi.org/10.1073/PNAS.1205128109.

Kumar, S., Gu, Y., Abudu, Y. P., Bruun, J. A., Jain, A., Farzam, F., Mudd, M., Anonsen, J. H., Rusten, T. E., Kasof, G., Ktistakis, N., Lidke, K. A., Johansen, T., & Deretic, V. (2019). Phosphorylation of Syntaxin 17 by TBK1 Controls Autophagy Initiation. *Developmental Cell*, *49*(1), 130-144.e6. https://doi.org/10.1016/J.DEVCEL.2019.01.027

Kumar, S., Jain, A., Farzam, F., Jia, J., Gu, Y., Choi, S. W., Mudd, M. H., Claude-Taupin, A., Wester, M. J., Lidke, K. A., Rusten, T. E., & Deretic, V. (2018). Mechanism of Stx17 recruitment to autophagosomes via IRGM and mammalian Atg8 proteins. *The Journal of Cell Biology*, *217*(3), 997–1013. https://doi.org/10.1083/JCB.201708039

Kumar, S., Javed, R., Mudd, M., Pallikkuth, S., Lidke, K. A., Jain, A., Tangavelou, K., Gudmundsson, S. R., Ye, C., Rusten, T. E., Anonsen, J. H., Lystad, A. H., Claude-Taupin, A., Simonsen, A., Salemi, M., Phinney, B., Li, J., Guo, L. W., Bradfute, S. B., … Deretic, V. (2021). Mammalian hybrid pre-autophagosomal structure HyPAS generates autophagosomes. *Cell*, *184*(24), 5950-5969.e22. https://doi.org/10.1016/J.CELL.2021.10.017

Laczkó-Dobos, H., Maddali, A. K., Jipa, A., Bhattacharjee, A., Végh, A. G., & Juhász, G. (2021). Lipid profiles of autophagic structures isolated from wild type and Atg2 mutant *Drosophila*. *Biochimica et Biophysica Acta. Molecular and Cell Biology of Lipids*, *1866*(3). https://doi.org/10.1016/J.BBALIP.2020.158868

Lartigue, J. de., Polson, H., Feldman, M., Shokat, K., Tooze, S. A., Urbe, S., Clague, M.J. (2009). PIKfyve regulation of endosome-linked pathways. *Traffic*, *10*, 883-893.

Laurinyecz, B., Peter, M., Vedelek, V., Kovacs, A. L., Juhasz, G., Maroy, P., Vigh, L., Balogh, G., Sinka, R. (2016). Reduced expression of CDP-DAG synthase changes lipid composition and leads to male sterility in *Drosophila*. *Open Biology*, *6*, 50169. https://doi.org/10.1098/rsob.150169.

Leman, J. K., Mueller, R., Karakas, M., Woetzel, N., & Meiler, J. (2013). Simultaneous prediction of protein secondary structure and transmembrane spans. *Proteins*, *81*(7), 1127–1140. https://doi.org/10.1002/PROT.24258

Li, Y., Cheng, X., Li, M., Wang, Y., Fu, T., Zhou, Z., Wang, Y., Gong, X., Xu, X., Liu, J., & Pan, L. (2020). Decoding three distinct states of the Syntaxin 17 SNARE motif in mediating autophagosome-lysosome fusion. *Proceedings of the National Academy of Sciences of the United States of America*, *117*(35), 21391–21402. https://doi.org/10.1073/PNAS.2006997117

Liu, H., Shao, W., Liu, W., Shang, W., Liu, J. P., Wang, L., & Tong, C. (2023). PI(4)P exchange at endoplasmic reticulum-autolysosome contacts is essential for autophagy and neuronal homeostasis. *Autophagy*. https://doi.org/10.1080/15548627.2023.2222556

Longatti, A., & Tooze, S. A. (2012). Recycling endosomes contribute to autophagosome formation. *Autophagy*, *8*(11), 1682–1683. https://doi.org/10.4161/AUTO.21486

Lőrincz, P., & Juhász, G. (2020). Autophagosome-Lysosome Fusion. *Journal of Molecular Biology*, *432*(8), 2462–2482. https://doi.org/10.1016/J.JMB.2019.10.028

Lőrincz, P., Mauvezin, C., & Juhász, G. (2017). Exploring Autophagy in *Drosophila*. *Cells*, *6*(3). https://doi.org/10.3390/CELLS6030022

Lu, Q., Yang, P., Huang, X., Hu, W., Guo, B., Wu, F., Lin, L., Kovács, L. A., Yu, L., & Zhang, H. (2011). The WD40 Repeat PI(3)P-Binding Protein EPG-6 Regulates Progression of Omegasomes to Autophagosomes. *Developmental Cell*, *21*(2), 343-357. https://doi.org/10.1016/j.devcel.2011.06.024

Schütter, M., Giavalisco, P., Brodesser, S., & Graef, M. (2019). Local fatty acid channeling into phospholipid synthesis drives phagophore expansion during autophagy. *Cell*, *180*(1), 135-149. https://doi.org/10.1016/j.cell.2019.12.005

Maeda, S., Otomo, C., & Otomo, T. (2019). The autophagic membrane tether ATG2A transfers lipids between membranes. *ELife*, *8*. https://doi.org/10.7554/ELIFE.45777

Maeda, S., Yamamoto, H., Kinch, L. N., Garza, C. M., Takahashi, S., Otomo, C., Grishin, N. V., Forli, S., Mizushima, N., & Otomo, T. (2020). Structure, lipid scrambling activity and role in autophagosome formation of ATG9A. *Nature Structural & Molecular Biology*, *27*(12), 1194–1201. https://doi.org/10.1038/S41594-020-00520-2

Martens, S., Nakamura, S., & Yoshimori, T. (2016). Phospholipids in Autophagosome Formation and Fusion. *Journal of Molecular Biology*, *428*(24 Pt A), 4819–4827. https://doi.org/10.1016/J.JMB.2016.10.029

Matoba, K., Kotani, T., Tsutsumi, A., Tsuji, T., Mori, T., Noshiro, D., Sugita, Y., Nomura, N., Iwata, S., Ohsumi, Y., Fujimoto, T., Nakatogawa, H., Kikkawa, M., & Noda, N. N. (2020). Atg9 is a lipid scramblase that mediates autophagosomal membrane expansion. *Nature Structural & Molecular Biology*, *27*(12), 1185–1193. https://doi.org/10.1038/S41594-020-00518-W

Matsui, T., Jiang, P., Nakano, S., Sakamaki, Y., Yamamoto, H., & Mizushima, N. (2018). Autophagosomal YKT6 is required for fusion with lysosomes independently of syntaxin 17. *The Journal of Cell Biology*, *217*(8), 2633–2645. https://doi.org/10.1083/JCB.201712058

McLelland, G. L., Lee, S. A., McBride, H. M., & Fon, E. A. (2016). Syntaxin-17 delivers PINK1/parkin-dependent mitochondrial vesicles to the endolysosomal system. *The Journal of Cell Biology*, *214*(3), 275–291. https://doi.org/10.1083/JCB.201603105

Michaud-Agrawal, N., Denning, E. J., Woolf, T. B., & Beckstein, O. (2011). MDAnalysis: a toolkit for the analysis of molecular dynamics simulations. *Journal of Computational Chemistry*, *32*(10), 2319–2327. https://doi.org/10.1002/JCC.21787

Mizushima, N. (2007). Autophagy: process and function. *Genes & Development*, *21*(22), 2861–2873. https://doi.org/10.1101/GAD.1599207

Mizushima, N., & Komatsu, M. (2011). Autophagy: renovation of cells and tissues. *Cell*, *147*(4), 728–741. https://doi.org/10.1016/J.CELL.2011.10.026

Mizushima, N., Noda, T., Yoshimori, T., Tanaka, Y., Ishii, T., George, M. D., Klionsky, D. J., Ohsumi, M., & Ohsumi, Y. (1998). A protein conjugation system essential for autophagy. *Nature*, *395*(6700), 395–398. https://doi.org/10.1038/26506

Molino, D., Nascimbeni, A. C., Giordano, F., Codogno, P., & Morel, E. (2017). ER-driven membrane contact sites: Evolutionary conserved machineries for stress response and autophagy regulation? *Communicative & Integrative Biology*, *10*(5–6). https://doi.org/10.1080/19420889.2017.1401699

Moon, Y., Jun, Y. (2020). The effects of regulatory lipids on intracellular membrane fusion mediated by dynamin-Like GTPases. *Frontiers in Cell and Developmental Biology*, *8*(518). https://doi: 10.3389/fcell.2020.00518

Nagy, P., Hegedűs, K., Pircs, K., Varga, Á., & Juhász, G (2013). Different effects of Atg2 and Atg18 mutations on Atg8a and Atg9 trafficking during starvation in *Drosophila*. *FEBS Letters*, *588*(3), 408–413. https://doi.org/10.1016/j.febslet.2013.12.012

Narendra, D., Tanaka, A., Suen, D. F., & Youle, R. J. (2008). Parkin is recruited selectively to impaired mitochondria and promotes their autophagy. *The Journal of Cell Biology*, *183*(5), 795–803. https://doi.org/10.1083/JCB.200809125

Nath, S., Dancourt, J., Shteyn, V., Puente, G., Fong, W. M., Nag, S., Bewersdorf, J., Yamamoto, A., Antonny, B., & Melia, T. J. (2014). Lipidation of the LC3/GABARAP family of autophagy proteins relies on a membrane-curvature-sensing domain in Atg3. *Nature Cell Biology*, *16*(5), 415–424. https://doi.org/10.1038/NCB2940

Nezis, I. P., Vaccaro, M. I., Devenish, R. J., & Juhász, G. (2014). Autophagy in development, cell differentiation, and homeodynamics: from molecular mechanisms to diseases and pathophysiology. *BioMed Research International*, *2014*. https://doi.org/10.1155/2014/349623

Nguyen, T. N., Padman, B. S., Usher, J., Oorschot, V., Ramm, G., & Lazarou, M. (2016). Atg8 family LC3/GABARAP proteins are crucial for autophagosome-lysosome fusion but not autophagosome formation during PINK1/Parkin mitophagy and starvation. *The Journal of Cell Biology*, *215*(6), 857–874. https://doi.org/10.1083/JCB.201607039

Nishimura, T., Tooze A. S. (2020). Emerging roles of ATG proteins and membrane lipids in autophagosome formation. Cell Discovery, 6(32). https://doi: 10.1038/s41421-020-0161-3

Obara, K., Sekito, T., Niimi, K., & Ohsumi, Y. (2008). The Atg18-Atg2 complex is recruited to autophagic membranes via phosphatidylinositol 3-phosphate and exerts an essential function. *The Journal of Biological Chemistry*, *283*(35), 23972–23980. https://doi.org/10.1074/JBC.M803180200

Ogawa, M., Yoshikawa, Y., Kobayashi, T., Mimuro, H., Fukumatsu, M., Kiga, K., Piao, Z., Ashida, H., Yoshida, M., Kakuta, S., Koyama, T., Goto, Y., Nagatake, T., Nagai, S., Kiyono, H., Kawalec, M., Reichhart, J. M., & Sasakawa, C. (2011). A Tecpr1-dependent selective autophagy pathway targets bacterial pathogens. *Cell Host & Microbe*, *9*(5), 376–389. https://doi.org/10.1016/J.CHOM.2011.04.010

Osawa, T., Ishii, Y., & Noda, N. N. (2020). Human ATG2B possesses a lipid transfer activity which is accelerated by negatively charged lipids and WIPI4. *Genes to Cells : Devoted to Molecular & Cellular Mechanisms*, *25*(1), 65–70. https://doi.org/10.1111/GTC.12733

Osawa, T., Kotani, T., Kawaoka, T., Hirata, E., Suzuki, K., Nakatogawa, H., Ohsumi, Y., & Noda, N. N. (2019). Atg2 mediates direct lipid transfer between membranes for autophagosome formation. *Nature Structural & Molecular Biology*, *26*(4), 281–288. https://doi.org/10.1038/S41594-019-0203-4

Pircs, K., Nagy, P., Varga, A., Venkei, Z., Erdi, B., Hegedus, K., & Juhasz, G. (2012). Advantages and limitations of different p62-based assays for estimating autophagic activity in *Drosophila*. *PloS One*, *7*(8). https://doi.org/10.1371/JOURNAL.PONE.0044214

Proikas-Cezanne, T., & Robenek, H. (2011). Freeze-fracture replica immunolabelling reveals human WIPI-1 and WIPI-2 as membrane proteins of autophagosomes. *Journal of Cellular and Molecular Medicine*, *15*(9), 2007–2010. https://doi.org/10.1111/J.1582-4934.2011.01339.X

Reiter, L. T., Potocki, L., Chien, S., Gribskov, M., & Bier, E. (2001). A systematic analysis of human disease-associated gene sequences in *Drosophila* melanogaster. *Genome Research*, *11*(6), 1114–1125. https://doi.org/10.1101/GR.169101

Reunanen, H., Punnonen, E. L., & Hirsimäki, P. (1985). Studies on vinblastine-induced autophagocytosis in mouse liver. V. A cytochemical study on the origin of membranes. *Histochemistry*, *83*(6), 513–517. https://doi.org/10.1007/BF00492453

Rim, B., Yarong, S., Emilie, V., Marion, M. G., Nada, T. M., Sandrine, V., Cécile, F., Estelle, R., Philippe, N., Sophie, L., Michael, M., Galya, S., & Isabel, D. A. (2023). The impact of lipid polyunsaturation on the physical and mechanical properties of lipid membranes. *BBA Biomembranes*, *1865*(2), 184084. https://doi.org/10.1016/j.bbamem.2022.184084

Romanov, J., Walczak, M., Ibiricu, I., Schüchner, S., Ogris, E., Kraft, C., & Martens, S. (2012). Mechanism and functions of membrane binding by the Atg5-Atg12/Atg16 complex during autophagosome formation. *The EMBO Journal*, *31*(22), 4304–4317. https://doi.org/10.1038/EMBOJ.2012.278

Rong, Y., Zhang, S., Nandi, N., Wu, Z., Li, L., Liu, Y., Wei, Y., Zhao, Y., Yuan, W., Zhou, C., Xiao, G., Levine, B., Yan, N., Mou, S., Deng, L., Tang, Z., Liu, X., Kramer, H., & Zhong, Q. (2022). STING controls energy stress-induced autophagy and energy metabolism via STX17. *The Journal of Cell Biology*, *221*(7). https://doi.org/10.1083/JCB.202202060

Rusten, T. E., Vaccari, T., Lindmo, K., Rodahl, L. M. W., Nezis, I. P., Sem-Jacobsen, C., Wendler, F., Vincent, J. P., Brech, A., Bilder, D., & Stenmark, H. (2007). ESCRTs and Fab1 regulate distinct steps of autophagy. *Current Biology : CB*, *17*(20), 1817–1825. https://doi.org/10.1016/J.CUB.2007.09.032

Sader, J. E., Sanelli, J. A., Adamson, B. D., Monty, J. P., Wei, X., Crawford, S. A., Friend, J. R., Marusic, I., Mulvaney, P., & Bieske, E. J. (2012). Spring constant calibration of atomic force microscope cantilevers of arbitrary shape. *The Review of Scientific Instruments*, *83*(10). https://doi.org/10.1063/1.4757398

Schade, S. D., Shey, L., & Eaton, R. P. (2020). Cholesterol Review: A Metabolically Important Molecule. *Endocrine Practice*, *26*(12), 1514–1523. https://doi: 10.4158/EP-2020-0347

Schütter, M., Giavalisco, P., Brodesser, S., & Graef, M. (2020). Local Fatty Acid Channeling into Phospholipid Synthesis Drives Phagophore Expansion during Autophagy. *Cell*, *180*(1), 135-149. https://doi.org/10.1016/J.CELL.2019.12.005

Scott, R. C., Schuldiner, O., & Neufeld, T. P. (2004). Role and regulation of starvation-induced autophagy in the *Drosophila* fat body. *Developmental Cell*, *7*(2), 167–178. https://doi.org/10.1016/J.DEVCEL.2004.07.009

Sengupta, N., Jović, M., Barnaeva, E., Kim, D. W., Hu, X., Southall, N., Dejmek, M., Mejdrova, I., Nencka, R., Baumlova, A., Chalupska, D., Boura, E., Ferrer, M., Marugan, J., & Balla, T. (2019). A large scale high-throughput screen identifies chemical inhibitors of phosphatidylinositol 4-kinase type II alpha. *Journal of Lipid Research*, *60*(3), 683–693. https://doi.org/10.1194/JLR.D090159

Shpilka, T., Weidberg, H., Pietrokovski, S., & Elazar, Z. (2011). Atg8: an autophagy-related ubiquitin-like protein family. *Genome Biology*, *12*(7). https://doi.org/10.1186/GB-2011-12-7-226

Skowronska-Krawczyk, D., & Budin, I. (2020). Aging membranes: Unexplored functions for lipids in the lifespan of the central nervous system. *Experimental Gerontology*, *131*. https://doi.org/10.1016/J.EXGER.2019.110817

Sparkes, B. L., Slone, E. E. A., Roth, M., Welti, R., & Fleming, S. D. (2010). Intestinal lipid alterations occur prior to antibody-induced prostaglandin E2 production in a mouse model of

ischemia/reperfusion. *Biochimica et Biophysica Acta*, *1801*(4), 517–525. https://doi.org/10.1016/J.BBALIP.2010.01.004

Stapleton, M., Liao, G., Brokstein, P., Hong, L., Carninci, P., Shiraki, T., Hayashizaki, Y., Champe, M., Pacleb, J., Wan, K., Yu, C., Carlson, J., George, R., Celniker, S., & Rubin, G. M. (2002). The *Drosophila* gene collection: identification of putative full-length cDNAs for 70% of *Drosophila* genes. *Genome Research*, *12*(8), 1294–1300. https://doi.org/10.1101/GR.269102

Steegmaier, M., Oorschot, V., Klumperman, J., & Scheller, R. H. (2000). Syntaxin 17 is abundant in steroidogenic cells and implicated in smooth endoplasmic reticulum membrane dynamics. *Molecular Biology of the Cell*, *11*(8), 2719–2731. https://doi.org/10.1091/MBC.11.8.2719

Suetsugu, S., Kurisu, S., & Takenawa, T. (2014). Dynamic shaping of cellular membranes by phospholipids and membrane-deforming proteins. *Physiological Reviews*, *94*(4), 1219–1248. https://doi.org/10.1152/PHYSREV.00040.2013

Sun, H. Q., Chen, Y., Hedde, P. N., Mueller, J., Albanesi, J. P., & Yin, H. (2022). PI(4)P-Dependent Targeting of ATG14 to Mature Autophagosomes. *Biochemistry*, *61*(8), 722–729. https://doi.org/10.1021/ACS.BIOCHEM.1C00775

Suzek, B. E., Wang, Y., Huang, H., McGarvey, P. B., & Wu, C. H. (2015). UniRef clusters: a comprehensive and scalable alternative for improving sequence similarity searches. *Bioinformatics (Oxford, England)*, *31*(6), 926–932. https://doi.org/10.1093/BIOINFORMATICS/BTU739

Szegletes, Z., Végh, A. G., Nagy, K., Bálint, Z., Kerényi, Á., Rákhely, G., & Vár, G. (2011). Effect of antimicrobial peptide-amide: indolicidin on biological membranes. *Journal of Biomedicine & Biotechnology*, *2011*. https://doi.org/10.1155/2011/670589

Takahashi, Y., He, H., Tang, Z., Hattori, T., Liu, Y., Young, M. M., Serfass, J. M., Chen, L., Gebru, M., Chen, C., Wills, C. A., Atkinson, J. M., Chen, H., Abraham, T., & Wang, H. G. (2018). An autophagy assay reveals the ESCRT-III component CHMP2A as a regulator of phagophore closure. *Nature Communications*, *9*(1). https://doi.org/10.1038/S41467-018-05254-W

Takáts, S., & Juhász, G. (2013). A genetic model with specifically impaired autophagosome-lysosome fusion. *Autophagy*, *9*(8), 1251–1252. https://doi.org/10.4161/AUTO.25470

Takáts, S., Nagy, P., Varga, Á., Pircs, K., Kárpáti, M., Varga, K., Kovács, A. L., Hegedus, K., & Juhász, G. (2013). Autophagosomal Syntaxin 17-dependent lysosomal degradation maintains neuronal function in *Drosophila*. *The Journal of Cell Biology*, *201*(4), 531–539. https://doi.org/10.1083/JCB.201211160

Takáts, S., Pircs, K., Nagy, P., Varga, Á., Kárpáti, M., Hegedus, K., Kramer, H., Kovács, A. L., Sass, M., & Juhász, G. (2014). Interaction of the HOPS complex with Syntaxin 17 mediates autophagosome clearance in *Drosophila*. *Molecular Biology of the Cell*, *25*(8), 1338–1354. https://doi.org/10.1091/MBC.E13-08-0449

Tsuboyama, K., Koyama-Honda, I., Sakamaki, Y., Koike, M., Morishita, H., & Mizushima, N. (2016). The ATG conjugation systems are important for degradation of the inner autophagosomal membrane. *Science (New York, N.Y.)*, *354*(6315), 1036–1041. https://doi.org/10.1126/SCIENCE.AAF6136

Valverde, D. P., Yu, S., Boggavarapu, V., Kumar, N., Lees, J. A., Walz, T., Reinisch, K. M., & Melia, T. J. (2019). ATG2 transports lipids to promote autophagosome biogenesis. *The Journal of Cell Biology*, *218*(6), 1787–1798. https://doi.org/10.1083/JCB.201811139

Vance, J. E. (2015). Phospholipid synthesis and transport in mammalian cells. *Traffic (Copenhagen, Denmark)*, *16*(1), 1–18. https://doi.org/10.1111/TRA.12230

Varadi, M., Anyango, S., Deshpande, M., Nair, S., Natassia, C., Yordanova, G., Yuan, D., Stroe, O., Wood, G., Laydon, A., Zídek, A., Green, T., Tunyasuvunakool, K., Petersen, S., Jumper, J., Clancy, E., Green, R., Vora, A., Lutfi, M., & Velankar, S. (2022). AlphaFold Protein Structure Database: massively expanding the structural coverage of protein-sequence space with high-accuracy models. *Nucleic Acids Research*, *50*(D1), D439–D444. https://doi.org/10.1093/NAR/GKAB1061

Velázquez, A. P., Tatsuta, T., Ghillebert, R., Drescher, I., & Graef, M. (2016). Lipid droplet-mediated ER homeostasis regulates autophagy and cell survival during starvation. *The Journal of Cell Biology*, *212*(6), 621–631. https://doi.org/10.1083/JCB.201508102

Velikkakath, A. K. G., Nishimura, T., Oita, E., Ishihara, N., & Mizushima, N. (2012). Mammalian Atg2 proteins are essential for autophagosome formation and important for regulation of size and

distribution of lipid droplets. *Molecular Biology of the Cell*, *23*(5), 896–909. https://doi.org/10.1091/MBC.E11-09-0785

Wang, H., Sun, H. Q., Zhu, X., Zhang, L., Albanesi, J., Levine, B., & Yin, H. (2015). GABARAPs regulate PI(4)P-dependent autophagosome:lysosome fusion. *Proceedings of the National Academy of Sciences of the United States of America*, *112*(22), 7015–7020. https://doi.org/10.1073/PNAS.1507263112

Wang, L., Klionsky, D. J., & Shen, H. M. (2023). The emerging mechanisms and functions of microautophagy. *Nature Reviews Molecular Cell Biology*, *24*, 186–203.

Wang, Y., Que, H., Li, C., Wu, Z., Jian, F., Zhao, Y., Tang, H., Chen, Y., Gao, S., Wong, C. C. L., Li, Y., Zhao, C., & Rong, Y. (2023). ULK phosphorylation of STX17 controls autophagosome maturation via FLNA. *The Journal of Cell Biology*, *222*(8). https://doi.org/10.1083/JCB.202211025

Xia, Y., Li, K., Li, J., Wang, T., Gu, L., & Xun, L. (2019). T5 exonuclease-dependent assembly offers a low-cost method for efficient cloning and site-directed mutagenesis. *Nucleic Acids Research*, *47*(3). https://doi.org/10.1093/NAR/GKY1169

Yamamoto, H., Zhang, S., & Mizushima, N. (2023). Autophagy genes in biology and disease. *Nature Reviews. Genetics*, *24*(6), 382–400. https://doi.org/10.1038/S41576-022-00562-W

Ylä-Anttila, P., Vihinen, H., Jokitalo, E., & Eskelinen, E. L. (2009). 3D tomography reveals connections between the phagophore and endoplasmic reticulum. *Autophagy*, *5*(8), 1180–1185. https://doi.org/10.4161/AUTO.5.8.10274

Yu, L., Chen, Y., & Tooze, S. A. (2018). Autophagy pathway: Cellular and molecular mechanisms. *Autophagy*, *14*(2), 207–215. https://doi.org/10.1080/15548627.2017.1378838

Yu, Z. Q., Ni, T., Hong, B., Wang, H. Y., Jiang, F. J., Zou, S., Chen, Y., Zheng, X. L., Klionsky, D. J., Liang, Y., & Xie, Z. (2012). Dual roles of Atg8-PE deconjugation by Atg4 in autophagy. *Autophagy*, *8*(6), 883–892. https://doi.org/10.4161/AUTO.19652

Zhao, Y. G., & Zhang, H. (2019). Autophagosome maturation: An epic journey from the ER to lysosomes. *The Journal of Cell Biology*, *218*(3), 757–770. https://doi.org/10.1083/JCB.201810099

Zhao, Y., Zhang, W., & Kho, Y. (2004). Proteomic analysis of integral plasma membrane proteins. *Analytical Chemistry*, *76*(7), 1817–1823. https://doi.org/10.1021/AC0354037

Zhen, Y., Spangenberg, H., Munson, M. J., Brech, A., Schink, K. O., Tan, K. W., Sørensen, V., Wenzel, E. M., Radulovic, M., Engedal, N., Simonsen, A., Raiborg, C., & Stenmark, H. (2020). ESCRT-mediated phagophore sealing during mitophagy. *Autophagy*, *16*(5), 826–841. https://doi.org/10.1080/15548627.2019.1639301

Zhen, Y., & Stenmark, H. (2023). Autophagosome Biogenesis. *Cells*, *12*(4). https://doi.org/10.3390/CELLS12040668

Zheng, J. X., Li, Y., Ding, Y. H., Liu, J. J., Zhang, M. J., Dong, M. Q., Wang, H. W., & Yu, L. (2017). Architecture of the ATG2B-WDR45 complex and an aromatic Y/HF motif crucial for complex formation. *Autophagy*, *13*(11), 1870–1883. https://doi.org/10.1080/15548627.2017.1359381

Zhou, C., Wu, Z., Du, W., Que, H., Wang, Y., Ouyang, Q., Jian, F., Yuan, W., Zhao, Y., Tian, R., Li, Y., Chen, Y., Gao, S., Wong, C. C. L., & Rong, Y. (2022). Recycling of autophagosomal components from autolysosomes by the recycler complex. *Nature Cell Biology*, *24*(4), 497–512. https://doi.org/10.1038/S41556-022-00861-8

Zhou, F., Wu, Z., Zhao, M., Murtazina, R., Cai, J., Zhang, A., Li, R., Sun, D., Li, W., Zhao, L., Li, Q., Zhu, J., Cong, X., Zhou, Y., Xie, Z., Gyurkovska, V., Li, L., Huang, X., Xue, Y., & Segev, N. (2019). Rab5-dependent autophagosome closure by ESCRT. *The Journal of Cell Biology*, *218*(6), 1908–1927. https://doi.org/10.1083/JCB.201811173

Zhou, Z., Marepally, S. R., Nune, D. S., Pallakollu, P., Ragan, G., Roth, M. R., Wang, L., Lushington, G. H., Visvanathan, M., & Welti, R. (2011). LipidomeDB data calculation environment: online processing of direct-infusion mass spectral data for lipid profiles. *Lipids*, *46*(9), 879–884. https://doi.org/10.1007/S11745-011-3575-8.

8. SUMMARY

Autophagy is a process that is conserved throughout the evolution of eukaryotes. It is responsible for degrading various types of cargo, such as aggregate-prone proteins, pathogens, damaged organelles, and macromolecules, by delivering them to lysosomes. The process involves the formation of a double-membrane structure called an autophagosome, which engulfs the cargo that is destined for degradation. The contents of the autophagosome are then delivered to lysosomes by fusing with them. Autophagy is responsible for cellular homeostasis and cell survival. Misregulation of autophagy is associated with various neurodegenerative diseases, apoptosis, cancer, and ageing (Juhasz & Neufeld, 2006; Nezis et al., 2014). This conserved pathway relies on the de novo synthesis of double-membrane vesicles (Schütter et al., 2019). Therefore, lipids play a crucial role in various aspects of autophagy, contributing to the formation of autophagosomes and serving as a source of energy during this process. The autophagy pathway involves a core set of autophagy-related proteins (ATG proteins), so far 40 ATG proteins have been identified and extensively studied (Nishimura et al., 2020). Still, many questions remain unanswered in this emerging field. One among them is the "role of lipids during autophagy". Our research focuses on identifying the specific lipid molecules that interact with Syntaxin 17 (from both Drosophila and Homo sapiens) and facilitate its incorporation into the autophagosomal membrane, with a combination of *in vitro* and *in vivo* approaches. To perform these lipid-protein interaction studies it is important to know the lipids composing autophagic structures. Surprisingly, no research has been held to unravel the lipid profile of autophagic structures especially from *Drosophila*.

My PhD study was initiated by establishing a method to immunoprecipitate intact autophagic vesicles from *3xmCherry-Atg8a* reporter containing control and Atg2^{-} adult starved *Drosophila* flies and deciphering the phospholipid profiles of isolated autophagic membranes. The control flies were meant to be used to isolate collectively phagophores and autophagosomes. While Atg2^{-} flies were used specifically to isolate phagophores. This is because, in the absence of this protein phagophores become stalled, leading to their accumulation. It was later discovered that the Atg2 protein is a lipid transporter protein that is responsible for transporting lipids from the endoplasmic reticulum (ER) to phagophores. In general, autophagy works at the basal level and that can be induced by starvation that increases the number of autophagic structures. In this study, the flies

were starved to enrich the 3xmCherry-Atg8a positive structures. Atg8a is known as an autophagy marker protein that is present on phagophores and autophagosomes. However, these proteins are deconjugated from the autolysosomes after the autophagosome-lysosome fusion step. The intact autophagic vesicles were pulled down by binding the pre-cleared cryohomogenized fly lysate containing enriched 3xmCherry-Atg8a positive membranes with anti-mCherry magnetic agarose beads for 1 h. The isolated fractions were validated by western blot screened for autophagy marker proteins such as GABARAP (Atg8 homolog), Atg5-Atg12 (early autophagy marker that associates with phagophores), and for several other organelle marker proteins to show the presence of desired structures and their degree of high purity respectively. Further, the isolated intact vesicles were visualized by fluorescent microscopy and atomic force microscopy. The average size of the isolated vesicles was 400-600 nm in diameter which corresponds well to the literature data. The size of the isolated vesicles from $Atg2^{-}$ flies was smaller than those from the control (in the range of 400 nm in diameter). This correlates with previous studies that showed a decrease in the size of accumulated structures during Atg2 loss of function. Following successful validation steps that confirmed the presence of intact autophagic vesicles in the eluted fractions, the lipids were extracted from these vesicles and analyzed by mass spectrometry. Briefly, the phospholipid profile of autophagic structures isolated from the control is following: PE (67 %) + PC (15 %) + PI (10 %) + PA (5 %) + PS (3 %) and for the $Atg2^{-}$ samples: PI (40 %) + PA (21 %) + PS (15 %) + PE (14 %) + PC (10 %). While shorter fatty acyl chains are dominant in the control autophagic membranes, the longer fatty acyl chain lengths are abundant in $Atg2^{-}$. Although the degree of unsaturation was higher in the membranes isolated from the control flies (63.4%), it was even higher in the $Atg2^{-}$ samples (86%). The striking differences in the lipid patterns reflect the potential role of Atg2 lipid transporter protein and also the lipid dynamic characteristics causing remodelling effects during phagophores maturation and closure of autophagosomes. The autophagosomes have specific requirements for membrane curvature and fusion ability which are determined by unique phospholipid composition. The findings and reasonings of the lipidomics data correlate with recently published data on lipid profiling of autophagic structures from yeast and human cell lines (Schütter et al, 2019; Schmitt et al, 2022).

Characterization of the lipid composition of autophagic membranes from the control flies supported the understanding of lipid-protein interactions during autophagy by focusing on the

recruitment of Syntaxin 17 to the autophagosomes. In line with this, further *in vitro* reconstitution experiments were performed using recombinant *Drosophila* Syntaxin 17 (Syx17) and human Syntaxin 17 (STX17) and we generated liposomes of 100 nm in diameter. The most reliable biochemical method to study the lipid-protein interactions used in this study was liposome flotation assay. The well-known autophagy protein named Atg3 is involved in Atg8-PE lipidation and is known as a membrane-associating autophagy protein (Nath et al., 2014), its homolog *Drosophila* Atg3 served as positive control and GST (known as a globular protein which is not membrane associated) as a negative control. The *in vitro* reconstitution experiments showed the direct membrane binding of Syntaxin 17 to the mimicked autophagosomes. Further liposomes were generated from the total lipid of *Drosophila* and human cultured cells. The Syx17 showed species-specific interaction by efficiently interacting with its own species' total lipid in both Drosophila and human cells.Whereas the liposomes composed from total lipid extracts of human cultured cells and neutral lipids could not recruit the Syntaxin 17.

Our lipidomics analysis revealed that autophagic membranes are enriched in negatively charged lipids. Moreover, our *in vitro* lipid-protein interaction assays corroborated the role of negatively charged lipids in STX17 recruitment. We tested this by analyzing its interaction with synthetic membranes (liposomes) containing various compositions of negatively charged lipids. Subsequently, the negative charge of the generated liposomes was ensured by zeta potential measurements. An increase in the negative charge of the liposomes resulted in enhanced efficiency of Syntaxin 17 association with the membrane. We know from previous studies that the soluble cytosolic form of Syntaxin 17 is recruited not to the phagophores but to the closed autophagosomes by a conformational switch between its two transmembrane domains (Itakura et al., 2012). Previously it has been shown the role of LC3/Atg8 proteins in the autophagosomal recruitment of Syntaxin17 proteins (citation). Elucidating the primary cue for Syntaxin 17 (STX17/Syx17) recruitment to autophagosomes *in vivo* may be linked to changes during autophagosome maturation, rather than solely to the presence of the Atg8 family proteins, which are also found in phagophores. While the interaction between IRGM, Atg8/LC3 family proteins, and the LIR motif in STX17's SNARE domain plays a role in its autophagosomal recruitment (Kumar et al., 2018), this pathway cannot be universal. This is because *Drosophila* lacks an IRGM homolog, and Syx17, unlike STX17, does not have a LIR binding motif. This suggests an alternative, evolutionarily

conserved mechanism involving negatively charged signaling lipids like PI(3)P, PI(4)P, and PI(3,5)P_2, which emerge on autophagosomes during their maturation (Rusten et al., 2007; Axe et al., 2008; Juhász et al., 2008; Wang et al., 2015), might recruit Syntaxin 17 despite their low abundance and the typically low affinity of phospholipid-binding domains for these lipids (Carlton et al., 2005). As expected, Syx17/STX17 was recruited by the addition of the above-mentioned PIPs to neutral lipid composition, suggesting the key role of PIPs in the autophagosomal Syntaxin 17 recruitment during autophagy.

Further, PI(4)P is the most localized with LC3 and STX17 positive structures in the 1 h starved HEK-293 cells compared to PI(3)P, PI(3,5)P_2. Reasoning that, PI4K2A generates PI(4)P during autophagosome maturation is indispensable for autophagosome-lysosome fusion (Wang et al., 2015). PI(3)P is generated by VPS34 lipid kinase (Axe et al., 2008; Juhász et al., 2008) and its dephosphorylation is the signal for the phagophore maturation (Cebollero et al., 2012). Lastly, PI(3,5)P_2 is present at a late stage, feasibly during or after lysosomal fusion (Rusten et al., 2007; Dong et al., 2010). The concomitant localization of PI(4)P and STX17 on LC3 positive autophagosomes was visualized by live imaging of starved U2OS cells and in fat cells of 4 h starved *Drosophila* larvae suggesting that PI(4)P can be a potential maturation player that signals the Syntaxin 17 to the autophagosomal bilayer.

Further inhibiting the PI(4)P synthesis on autophagosomes by generating stably expressing doxycycline-inducible shRNA for *PI4K2A* manifested the impairment of autophagosomal STX17 recruitment. To avoid the complications caused by long-term PI(4)P inhibition, the cells were treated with NC03 which could significantly reduce the PI(4)P levels on the autophagosomes and impair the STX17 recruitment to the LC3 positive puncta. Interestingly, this treatment did not affect STX17 recruitment to mitochondria, suggesting that PI(4)P plays a specific role in STX17 binding to autophagosomal membranes during autophagy, but not necessarily to other cellular membranes.

The other curious question was which part of Syntaxin 17 is indispensable for the PI(4)P binding of the autophagosomes? The molecular simulation analysis revealed the importance of basic amino acids such as Arginine and Lysine that are located on the C-terminal part of STX17 and before the transmembrane region of the Syx17 in PI(4)P binding and its autophagosomal recruitment. The

Alanine replacement of these residues revealed the impairment of Syntaxin 17 recruitment in the *in silico* model membranes and *in vivo* as well. The fusion defect of siRNA *STX17* was rescued by expression of siRNA-resistant wild type but not arginine and lysine substituted with alanine mutants of STX17, concluding the significance of basic amino acids located in the specific regions of Syntaxin 17 in PI(4)P binding on the autophagosomes.

Based on the findings of my PhD project, it is evident that the electrostatic interactions between negatively charged lipids on autophagosomes and positively charged amino acid residues located near the predicted transmembrane domains of fly Syntaxin 17 and the C-terminus regions of human Syntaxin 17 play a crucial role in recruiting soluble cytosolic forms of these proteins to the autophagosomal membranes. Additionally, the generation of PI(4)P on the mature autophagosome is essential for the recruitment of Syntaxin 17. This mechanism is likely an evolutionarily conserved process involved in the autophagosomal recruitment of Syntaxin 17, acting as a competence factor for subsequent vesicle fusion and lysosomal degradation in *Drosophila* and human cells.

9. ÖSSZEFOGLALÁS

Az autofágia egy olyan folyamat, amely az eukarióták evolúciója során konzerválódott. Ez felelős a különböző típusú anyagok, például az aggregációra hajlamos fehérjék, kórokozók, sérült organellumok és makromolekulák lebontásáért, a lizoszómákba való szállításukkal. A folyamat során egy autofágoszómának nevezett kettős membránréteg alakul ki, amely magába zárja a lebontandó anyagokat. Az autofagoszóma tartalma ezután a lizoszómákba kerül, azokkal összeolvadva. Az autofágia felelős a sejtek homeosztázisáért és a sejtek túléléséért. Az autofágia hibás szabályozása összefüggésbe hozható különböző neurodegeneratív betegségekkel, apoptózissal, rákos megbetegedésekkel és öregedéssel (Juhasz & Neufeld, 2006; Nezis és mtsai., 2014). Ez a konzervált útvonal a kettős membránnal rendelkező vezikulák de novo szintézisén alapul (Schütter és mtsai., 2019). A lipidek tehát döntő szerepet játszanak az autofágia különböző vonatkozásaiban, hiszen hozzájárulnak az autofágoszómák kialakulásához, és energiaforrásként szolgálnak e folyamat során. Az autofágia útvonalában az autofágiával kapcsolatos fehérjék (ATG-fehérjék) központi készlete vesz részt, eddig 40 ATG-fehérjét azonosítottak és vizsgáltak széles körben (Nishimura és mtsai., 2020). Még mindig sok kérdés megválaszolatlan maradt ezen a fejlődő területen. Az egyik ezek közül a "lipidek szerepe az autofágia során". Kutatásaink olyan specifikus lipidmolekulák azonosítására irányulnak, amelyek kölcsönhatásba lépnek a Syntaxin 17 nevezetű fehérjével (mind a *Drosophila*, mind a Homo sapiens esetében), és elősegítik annak beépülését az autofagoszómális membránba. E lipid-fehérje kölcsönhatási vizsgálatokhoz, amelyeket *in vitro* és *in vivo* módszerekkel valósítottunk meg, fontos ismerni az autofág struktúrákat alkotó lipideket. Meglepő módon eddig nem folytak olyan kutatások, amelyek a *Drosophila* autofág struktúrák lipidösszetételének feltárására irányultak volna.

Éppen ezért, első lépésként kidolgoztunk egy olyan módszert, amelynek segítségével sikerült a *Drosophila* melanogaster felnőtt egyedeiből autofág struktúrákat izolálni és meghatározni membránjaik lipidösszetételét. Ez egy immunoprecipitáción alapuló módszer, ennek segítségével sikerült izolálni a 3xmCherry-Atg8a-val jelölt autofág vezikulákat a kontroll és Atg2- mutáns legyekből. A kontroll legyekből fagofórok és autofágoszómák együttesét izoláltuk. Míg az Atg2-legyeket kifejezetten a fagofórok izolálására használtuk. Ennek az az oka, hogy e fehérje hiányában a fagofórok nem tudnak bezárulni (így autofagoszómává alakulni), ami azok felhalmozódásához vezet. Később felfedezték, hogy az Atg2 fehérje felelős a lipidek szállításáért

is az endoplazmatikus retikulum (ER) és a fagofórok között. Általában az autofágia a sejtekben alapszinten működik, de fokozható éhezéssel, így ezáltal növelhetjük az autofág struktúrák számát. Vizsgálataink során a legyeket éheztettük, hogy a 3xmCherry-Atg8a pozitív struktúrák feldúsuljanak. Az Atg8a autofágia-markerfehérjeként ismert, mivel kovalensen kötődik a fagofórok és az autofágoszómák membránjaihoz. Ezek a fehérjék azonban az autolizoszómákról leválnak az autofagoszóma-lizoszóma fúziós lépése után. ezért nagy valószínüséggel az autolizoszómák kizárhatók az izolálás folyamatából. Az intakt autofág vezikulákat úgy kaptuk meg, hogy a kriohomogenizált légy lizátumot (amely dúsított 3xmCherry-Atg8a pozitív membrán-struktúrákat tartalmazott), mCherry-taget felismerő mágneses agaróz gyöngyökre kötöttük egy órán keresztül. Az izolált struktúrákat western blot segítségével azonosítottuk, több autofágia markerfehérje, például GABARAP (Atg8 homológ), Atg5-Atg12 (korai autofág marker, amely a fagofórokhoz kapcsolódik) segítségével. Az izolált autofág struktúrák magas tisztasági fokának bizonyítására pedig más sejtszervecskék jellemző fehérjéit felismerő ellenanyagokat is használtunk. Továbbá az izolált intakt vezikulákat fluoreszcens- és AFM-mikroszkópiával vizualizáltuk. Az izolált vezikulák átlagos mérete 400-600 nm átmérőjű volt, ami megfelel az irodalmi adatoknak. Az Atg2- legyekből izolált vezikulák (főként fagofórok) 400 nm átmérőjűek voltak, kisebbek, mint a kontrollból izolált vezikulák, ami összhangban van a korábban közölt irodalmi adatokkal, amelyek arra utalnak, hogy Atg2-funkcióvesztés esetén a feldúsult autofág struktúrák mérete lecsökken. Miután bizonyítottuk, hogy autofág vezikulákat izoláltunk, azok membránjaiból kivontuk a lipideket és tömegspektrometria segítségével elemztük lipidösszetételüket. Röviden, a kontrollból izolált autofág struktúrák főbb foszfolipidjeinek aránya a következő: PE (67 %) + PC (15 %) + PI (10 %) + PA (5 %) + PS (3 %), az Atg2- minták esetében pedig: PI (40 %) + PA (21 %) + PS (15 %) + PE (14 %) + PC (10 %). Míg a kontroll autofág-membránokban a rövidebb zsírsavláncok dominálnak, addig az Atg2-ben a hosszabb zsírsavláncok nagyobb mennyiségben fordulnak elő. Bár a lipidek telítetlenségének mértéke eleve magas volt a kontroll legyekből izolált membránokban (63,4%), az Atg2- mintákban még ennél is magasabb volt (86%). A lipidmintázatok szembetűnő különbségei tükrözik az Atg2 fehérje lipidszállításban játszott szerepét, valamint a fagofórok érése és az autofagoszómák bezáródása során fellépő membrán dinamikai változásokat, lipid átépüléseket. Az autofágoszómáknak sajátos igényeik vannak a membrán görbületével és fúziós képességével kapcsolatban, amelyeket egyedi foszfolipid-összetételük határoz meg. A lipidomikai eredményeink összecsengenek a humán

sejtvonalból és élesztőből származó autofág struktúrák lipidprofiljának nemrégiben publikált adataival (Schmitt et al, 2022; Schütter et al, 2019).

A kontroll legyekből származó autofág-membránok lipidösszetételének megállapítása alapul szolgált az autofágia során fellépő lipid-fehérje kölcsönhatások jobb megértéséhez, amely hozzájárul ahhoz, hogy megismerjük milyen lipidek segíthetik a Syntaxin 17 fúziós fehérjének az autofágoszómák membránjába való beépülését. A fehérjetoborzás vizsgálata céljából továbbiakban *in vitro* rekonstitúciós kísérleteket végeztünk rekombináns *Drosophila* Syntaxin 17 (Syx17) és humán Syntaxin 17 (STX17), valamint 100 nm átmérőjű liposzómák segítségével, melyeket sikeresen előállítottunk. Egy megbízható biokémiai módszert, a liposzóma flotációs esszét alkalmaztuk ahhoz, hogy megállapítsuk milyen lipidek iránt mutat affinitást a Syntaxin 17 fehérje (lipid-fehérje kölcsönhatási vizsgálatok). Az Atg3 nevű jól ismert autofágiafehérje részt vesz az Atg8-PE lipidációjában, és membránasszociáló autofágiafehérjeként ismert (Nath és mtsai., 2014), homológja, a *Drosophila* Atg3 pozitív kontrollként, a GST (mint globuláris, nem membrán asszociáló fehérje) pedig negatív kontrollként szolgált. Az *in vitro* rekonstitúciós kísérleteink segítségével kimutattuk, hogy a Syntaxin 17 fehérje beépül a liposzómákba, amelyeket szintetikus lipidekből állítottunk elő. A liposzómák lipidösszetételét úgy terveztük meg, hogy hasonlóságot mutassanak az általunk izolált autofág strukturák lipidarányaival (ezek az un. autofagszóma utánzatok). További liposzómákat generáltunk *Drosophila* és humán tenyésztett sejtek összlipidjéből. A Syx17 fajspecifikus kölcsönhatást mutatott, mivel hatékonyan lépett kölcsönhatásba a fajához tartozó lipidekkel. Míg a humán tenyésztett sejtek összlipidkivonatából és a semleges lipidekből összeállított liposzómák nem tudták toborozni a Syntaxin 17-et.

Lipidomikai vizsgálataink alapján láthattuk, hogy az autofág membránok bővelkednek negatív töltésű lipidekben. Ezen negatív töltésű lipidek szerepét a Syx17/STX17 toborzásban tovább igazolták *in vitro* lipid-fehérje kölcsönhatási vizsgálataink. Ezt úgy tudtuk megvalósítani, hogy megvizsgáltuk a fehérje kölcsönhatását olyan liposzómákkal, amelyek eltérő arányban tartalmaztak változatos, negatív töltésű szintetikus lipideket. Ezt követően a létrehozott liposzómák negatív töltését zéta-potenciál mérésekkel is igazoltuk. Minél negatívabbak voltak a liposzómák, annál nagyobb hatékonysággal kötődtek hozzájuk a Syntaxin17 fehérjék. Korábbi irodalmi adatokból tudjuk, hogy a Syntaxin 17 fehérje nincs jelen a korai autofág struktúrákon, a fagofórokon, hanem a már bezárult autofágoszómákhoz toborzódik, mely feltételezhetően konformációs változás révén történik (Itakura és mtsai., 2012). Korábban kimutatták az LC3/Atg8

fehérjék szerepét a Syntaxin17 fehérjék autofagoszómális toborzásában (citation is needed). Úgy gondoljuk, hogy *in vivo* a Syntaxin 17 (STX17/Syx17) autofágoszómákhoz való toborzásának elsődleges oka lehet az autofágoszómák érése során bekövetkező változások, nem pedig kizárólag az Atg8 család fehérjéinek jelenléte, hiszen azok a fagofórokon is jelen vannak. Bár az IRGM, az Atg8/LC3 család fehérjéi és az STX17 SNARE-doménjében lévő LIR-motívum közötti kölcsönhatás szerepet játszik az autofágoszómális toborzásban (citation is needed), mégis feltételezzük, hogy ez az útvonal nem lehet univerzális. Ennek oka, hogy a *Drosophila* nem rendelkezik IRGM homológgal, és a Syx17 az STX17-től eltérően nem rendelkezik LIR kötőmotívummal. Ez arra utal, hogy a fehérje autofagoszómális kettősrétegekbe történő toborzása mögött egy alternatív, evolúciósan konzervált, eddig fel nem tárt mechanizmus áll. Ezzel összhangban, feltételezhetően az érés során az autofágoszómák membránjaiban szintetizálódott negatív töltésű lipidek, mint a PI(3)P, PI(4)P és PI(3,5)P2, amelyekről ismert, hogy megjelennek az autofág struktúrákon (Axe és mtsai., 2008; Juhász és mtsai., 2008; Wang és mtsai., 2015; Rusten és mtsai., 2007) elősegíthetik a Syntaxin 17 toborzását, annak ellenére, hogy nagyon kis százalékban vannak jelen a membránokban (Carlton és mtsai., 2005). A várakozásoknak megfelelően a Syx17/STX17 fehérjék beépültek a foszfatidilinozitol-foszfátokat (PIP-et) tartalmazó liposzómákba, amelyeket úgy állítottuk elő, hogy semleges lipidekhez adtuk ezeket a negatív töltésű PIP-et. Ez arra utal, hogy a PIP-ek kulcsszerepet játszanak a Syntaxin 17 autofagoszomális rekrutációjában az autofágia során.

Továbbá, az 1 órán át éheztetett HEK-293 sejtekben a PI(4)P kolokalizálódott a leginkább az LC3 struktúrákkal, amelyek STX17-re is pozitívak voltak, ellentétben a PI(3)P-vel és PI(3,5)P2-vel. Ez összhangban van azzal, hogy a PI4K2A lipdkináz az autofagoszóma érés során PI(4)P-t generál, ami nélkülözhetetlen az autofagoszóma-lizoszóma fúzióhoz (Wang és mtsai., 2015). A VPS34 kináz egy jól ismert PI(3)P-t termelő enzim (Axe és mtsai., 2008; Juhász és mtsai., 2008). A PI(3)P defoszforilációja a fagofórok érésének egyik jele (Cebollero és mtsai., 2012). Végül a PI(3,5)P2 egy késői szakaszban van jelen, valószínüleg a lizoszómális fúzió során vagy azt követően (Rusten et al., 2007; Dong et al., 2010). Éheztetett U2OS sejtekben sikerült kimutatni a PI(4)P-nek a kolokalizációját az LC3 és STX17 pozitív struktúrákkal. A humán sejtekhez hasonlóan az éheztetett *Drosophila* lárvák zsírtestében is megfigyeltük a PI(4)P kolokalizációját Atg8a és STX17 pozitív vezikulákkal. Ezen eredményeink arra utalnak, hogy a PI(4)P egy lehetséges jelző

molekula lehet, amely a Syntaxin 17-et az autofágoszómális membrán kettős lipidrétegébe toborozza.

A doxiciklin-indukálható shRNS-PI4K2A stabil vonal létrehozásával sikeresen megakadályoztuk a PI(4)P szintézisét az autofágoszómákon. Ezen lipid hiányában a STX17-nek az autofagoszómák membránjába való beépülése károsodást szenvedett. A hosszú távú PI(4)P-hiány okozta komplikációk elkerülése érdekében a sejteket egy PI4K2A kinázra specifikus kémiai inhibitorral gátoltuk, amely rövid idő alatt (10 perc) fejti ki hatását. Az inhibitor jelentősen csökkentette a PI(4)P-szintet az autofagoszómákon és károsította a STX17 toborzását az LC3 pozitív struktúrákra. Ez a kezelés azonban nem zavarta meg a STX17 mitokondriális toborzását, ami arra enged következtetni, hogy a PI(4)P a STX17 fehérjének kimondottan az autofagoszóma membránjába történő toborzásában vesz rész.

Kíváncsiak voltunk, hogy a Syntaxin 17 melyik része nélkülözhetetlen az autofagoszómák PI(4)P kötéséhez? Molekuláris szimulációs elemzéseink segítségével feltártuk olyan pozitív töltésű aminosavak, mint az arginin és lizin jelentőségét, amelyek a STX17 C-terminális régiójában és a Syx17 transzmembrán régiója előtt helyezkednek el, és szerepet jászhatnak a PI(4)P-el való kölcsönhatásban, ezáltal elősegítve a fehérje autofagoszómákra történő toborzását. Az *in silico* modellmembránokban és *in vivo* kísérleteinkben is ezen amonosavaknak alaninokkal való helyettesítése (aminosav mutáns) a Syntaxin17 rekrutációjának károsodásához vezetett. Az siRNS STX17 fúziós fenotípusát az siRNS-rezisztens vad típusú STX17 expressziója menekítette, viszont az siRNS-rezisztens aminosav mutáns STX17 esetében nem, ami arra enged következtetni, hogy a Syntaxin 17 specifikus régióiban található aminosavaknak fontos szerepük van abban, hogy az autofagoszómákon található PI(4)P-hez kötődjön.

PhD dolgozatom eredményei alapján nyilvánvaló, hogy a *Drosophila* Syntaxin 17 és a humán Syntaxin 17 fehérjék transzmembrán doménjeinek közelében található pozitív töltésű aminosavjai és a negatív töltésű autofagoszóma membránok között egy elektrosztatikus kölcsönhatás jön létre, amelynek segítségével a Syntaxin17 fehérje a citoszolból az autofagoszóma membránjába beépül. Emellett a PI(4)P szintézise az érett autofágoszómán elengedhetetlen a Syntaxin 17 toborzásához. Ez a mechanizmus valószínűleg egy evolúciósan konzervált folyamat a *Drosophila* és humán sejtekben egyaránt, amely részt vesz a Syntaxin 17 autofagoszómális toborzásában, és kompetencia faktorként működik a későbbi vezikuláris fúzióban és a lizoszomális degradációban.

10. MY CONTRIBUTION TO THIS WORK

- ✔ Establishing a method to isolate intact autophagic vesicles and their validation by immunoblots
- ✔ Sample preparation for fluorescent microscopy, AFM, mass spectrometry
- ✔ Isolation of lipids from autophagic membranes
- ✔ Cloning, protein expression and purification of Syx17 and STX17
- ✔ Validation of purified proteins
- ✔ Extraction of lipids
- ✔ Optimization and generation of liposomes and giant unilamellar vesicles
- ✔ Sample preparations for DLS and Zeta Sizer
- ✔ Investigation of lipid-protein interactions by liposome flotation assays, protein precipitations by TCA, western blots run and processing the blots
- ✔ Maintenance of cell cultures and Plasmid DNA isolation for cell culture experiments
- ✔ Triple transfection methods and PIPs subcellular localization experiments with mammalian cell culture
- ✔ PI(4)P depletion by NC03 treatment in HEK-293 cells
- ✔ Investigation of mitochondrial STX17 recruitment in HEK-293 cells
- ✔ Mammalian cell culture samples preparation for confocal microscopy
- ✔ Quantification of all the acquired images from the confocal microscopy
- ✔ Cloning and generation of plasmids for Syntaxin 17 mutagenesis and investigations in cell line
- ✔ Involvement in writing, reviewing, and illustrating graphical abstracts for the manuscripts regarding this study.